Final Report

Volume 2

Radar Studies of the Moon

18 April 1968

Prepared for the U.S. National Aeronautics and Space Administration under Contract NSR 22-009-196 by

Lincoln Laboratory

MASSACHUSETTS INSTITUTE OF TECHNOLOGY

Lexington, Massachusetts

Final Report

Volume 2

Radar Studies of the Moon

18 April 1968

Issued 13 June 1968

Prepared for the U.S. National Aeronautics and Space Administration under Contract NSR 22-009-106 by

Lincoln Laboratory

MASSACHUSETTS INSTITUTE OF TECHNOLOGY

Lexington, Massachusetts

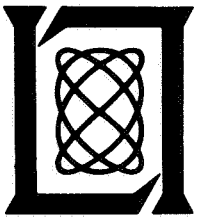

FOREWORD

This report has been prepared as part of the final report required under Contract NSR 22-009-106 between the National Aeronautics and Space Administration and M. I. T. Lincoln Laboratory. The measurements and analysis stipulated in the contract separate rather naturally into three parts: (1) the statistical scattering and polarization properties at several wavelengths of the mean lunar surface, (2) the local variations in these properties along the "Apollo belt" associated with different types of lunar surface, and (3) a comparative analysis of the results obtained under the present contract and those to be obtained at longer wavelengths under Grant NGR 33-010-024 between NASA and Cornell University.

In order to make results obtained under the present contract available as rapidly as possible, it has been decided to serialize the final report in three volumes corresponding to the areas of investigation described above. The first volume in the series has already been issued (31 August 1967). The present report constitutes Volume 2. Volume 3, a report to be prepared jointly with Cornell University, is in preparation.

CONTENTS

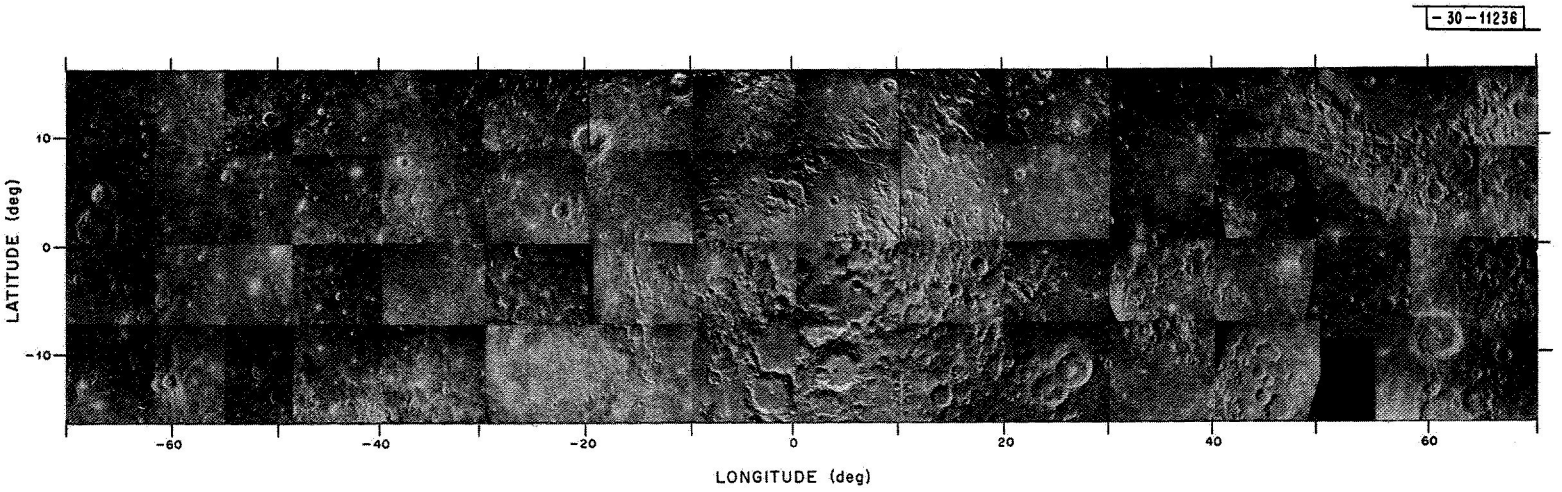

Radar map of 3.8-cm normalized lunar echo power.

RADAR STUDIES OF THE MOON

I. INTRODUCTION

Observations of the moon by radar, made shortly before the beginning of this decade [Pettengill (1960); Leadabrand, et al. (1960)], established the presence of a diffusely scattered echo component, which was interpreted as originating in wavelength-sized lunar surface structure. This conclusion was reinforced by later investigations using a variety of observing wavelengths and polarizations. Particularly significant was the discovery of anomalously strong scattering from the region of the crater Tycho [Pettengill and Henry (1962)], which was most easily accounted for on the assumption of a local increase in the amount of 70-cm-sized surface roughness. Ground-based telescopic observations of the moon, even under the best conditions of optical seeing, have yielded resolution of the lunar surface of no better than a few hundred meters. Lunar orbiting cameras have provided information on surface structure of the order of a meter in size, but only at considerable expense. Therefore, optical coverage at this high resolution has been limited to a relatively few selected areas. Since the diffusely scattered component of the radar echo has been shown to be directly related to the distribution of wavelength-sized irregularities across the lunar surface, its measurement at centimeter and decimeter wavelengths provides a comparatively inexpensive assessment of the local surface roughness in a size range of direct interest to a lunar landing system. With this in mind, NASA underwrote in late 1965 a program of radar observation of the moon, a portion of which is reported here.

The primary intent of the work under NASA Contract NSR 22-009-106 reported in this volume was to determine, using delay-doppler mapping techniques with as fine a resolution as possible, the distribution of radar scattering properties across the lunar surface at 3.8-cm wavelength. This investigation made use of the Haystack radar operated by M.I.T. Lincoln Laboratory. Because of limitation in budget and time, the observations were necessarily confined primarily to the lunar equatorial regions lying between 16° north and south latitude and 70° east and west longitude, as well as to a single component of received polarization. A similar set of observations at 70-cm wavelength has been carried out by Cornell University under NASA Grant NGR 33-010-024. Because of the longer wavelength, these latter observations were necessarily accomplished with poorer resolution. On the other hand, they encompass a larger fraction of the visible lunar surface and include observations in two orthogonal received polarization components. The radar observations at the two wavelengths will be compared with each other and with telescopic photographs of the lunar surface in a joint M.I.T. Lincoln Laboratory/Cornell University report to be issued at a later date. From the observed variations among the different sets of observations with respect to the lunar average, it should prove possible to deduce the surface distribution of wavelength-sized irregularities, as well as to locate regions having atypical local surface slopes.

In the course of carrying out the contracted research, a method of supersynthesis mapping [Thomson and Ponsonby (1968)] was investigated whose potential had not been recognized in the original contract proposal. This mapping permitted a determination of the distribution of the diffusely scattered echo component at 23 cm using the Millstone radar. Although the resolution of which this method is capable does not approach that yielded by the older delay-doppler mapping techniques as applied in the 3.8-cm work at the Haystack radar, it has the virtue of not requiring from the radar equipment any angular resolution of the lunar disk. Thus, it enabled mapping at 23 cm which would not otherwise have been possible.

The sections which follow first treat the theory involved in the two types of mapping: supersynthesis, and delay-doppler. Necessary ephemeris calculations are described. Next, the procedures employed and data obtained are separately presented for the two types of mapping. Discussion of the results is limited to only those features which are related directly to the data presented here. Placing of the results in a larger context will be done jointly with the longer wavelength measurements of Cornell University in a later volume.

II. RADAR MAPPING METHODS

Unlike the situation at optical wavelengths, where angular resolution of better than 1 arcsec can readily be obtained (even with small telescopes), straightforward attempts at angular resolution using currently available antenna beamwidths are limited to about 4 arcmin at radar wavelengths. While affording some resolution of the 30-arcmin-diameter lunar disk, this level of resolution does not permit fine-grained comparison between local radar and optical surface scattering characteristics. One could conceive of an interferometric observing system which would offer resolution approaching a few seconds of arc; because of the complex source distribution represented by the lunar disk, however, a large number of effective baselines (spatial Fourier components) would be required to determine the distribution unambiguously.

As a rigid body, the moon maintains an exact positional relationship among its surface features. Thus, a known motion of the whole body implies a predictable motion for each of its components. For example, because of the apparent lunar rotation as viewed from the radar, there will be a calculable locus of surface points which possess the same doppler-shifted echo frequency. Thus, frequency analysis with adequate resolution will select that component of the echo which originates from a known strip on the lunar surface.

An alternative way of looking at the phenomenon is to visualize the wavefront of the echo as it arrives at the surface of the earth. Since all elements of the lunar scattering surface are maintaining their relative alignment, rotation of the moon will serve only to sweep a fixed wavefront pattern past the antenna. Thus, sequential sampling of the received signal is equivalent to a simultaneous sampling of the original waveform over the dimension swept out by the antenna during the time interval of observation. In this way, one uses the coherence in time of the echo wavefront to synthesize a very much larger aperture than is available for simultaneous observation, and thus to obtain a vastly improved effective angular resolution. In the radar case, of course, the location of the illuminating wavefront with respect to the lunar surface is also being varied with time. The effects of this variation are straightforward, however, and can be allowed for in the analysis.

Over a short interval of time, the extension of aperture described above will proceed only in one dimension. Thus, only a one-dimensional strip distribution of the source will be obtained.

Over longer periods of time (typically several hours), however, the direction will change significantly. By combining data taken over relatively long intervals, such as significant fractions of a day, useful two-dimensional resolution may be obtained. The name generally applied to the latter analysis is "supersynthesis"; its mathematical foundations are given in Sec. A below.

An approach which combines short-term coherent analysis with resolution in delay, obtained by pulsing the illuminating radiation, has received the name "delay-doppler" mapping. The senior of the two methods employed in the work reported here, this technique is somewhat easier to visualize in detail and to analyze than is supersynthesis. While generally capable of far greater surface resolution for comparable observation times, the delay-doppler technique has intrinsic weakness in certain areas of application. In Sec. B below, the method is outlined in some detail together with its limits of applicability.

A. Supersynthesis Mapping Technique

1. Basic Principles

Let the power scattered per unit projected surface area of the moon be denoted by $f(\xi;\eta)$, where the coordinates ξ and η are related to the lunar surface as shown in Fig. 1. The power arising from a strip making an angle φ with the η-axis, which is at a distance r from the origin and has a width Δx, is given by

$$W(r,\varphi) = \int_{r-(\Delta x/2)}^{r+(\Delta x/2)} dx \int_{-\infty}^{+\infty} dy\, f(x\cos\varphi + y\sin\varphi;\ y\cos\varphi - x\sin\varphi) \qquad (1)$$

For the sake of these introductory arguments, we shall assume that by measurement we can derive the quantity (corresponding to infinitesimally fine resolution)

$$U(r,\varphi) = \lim_{\Delta x\to 0}\left[\frac{W(r,\varphi)}{\Delta x}\right] = \int_{-\infty}^{+\infty} dy\, f(r\cos\varphi + y\sin\varphi;\ y\cos\varphi - r\sin\varphi) \qquad (2)$$

The two-dimensional power distribution over the surface $f(\xi;\eta)$ may be derived from $U(r,\varphi)$ as follows: Assume that $f(\xi;\eta)$ may be represented as a double Fourier integral

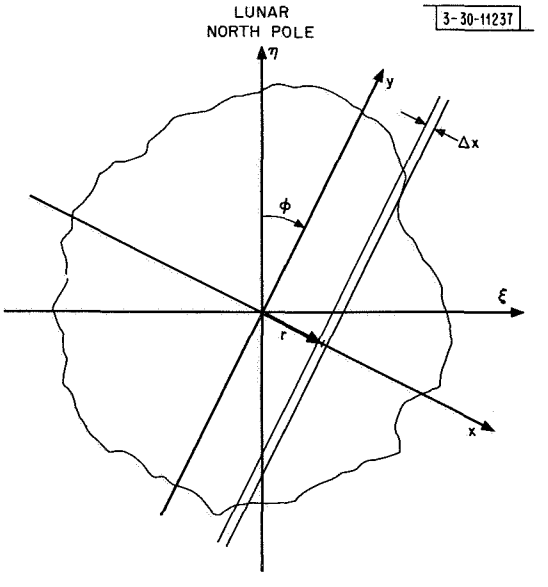

Fig. 1. Schematic of geometry used in supersynthesis radar mapping.

$$f(\xi;\eta) = \iint R(u;v)\,\exp[+2\pi i(u\xi + v\eta)]\,du\,dv \tag{3}$$

Substituting Eq. (3) into Eq. (2) and performing the integration over y give

$$U(r,\varphi) = \iint du\,dv\,R(u;v)\,\exp[+2\pi i(u\cos\varphi - v\sin\varphi)\,r]\,\delta(v\cos\varphi + u\sin\varphi) \tag{4}$$

where δ is Dirac's delta function. Integration over v and substitution of $t = u/\cos\varphi$ gives

$$U(r,\varphi) = \int dt\,R(t\cos\varphi;\ -t\sin\varphi)\,e^{2\pi irt} \tag{5}$$

Simple Fourier inversion of this gives

$$R(t\cos\varphi;\ -t\sin\varphi) = \int dr\,U(r,\varphi)\,e^{-2\pi irt} \tag{6}$$

Since Eq. (6) determines R(u; v) in the whole of the (u, v) plane, the power distribution $f(\xi;\eta)$ can be found by simple substitution into Eq. (3). In so doing, it is convenient to change the variables of integration to polar coordinates first:

$$f(\xi;\eta) = \iint R(t\cos\varphi;\ -t\sin\varphi)\,t\,\exp[2\pi it(\xi\cos\varphi - \eta\sin\varphi)]\,dt\,d\varphi$$

$$= \int_0^{2\pi} d\varphi \int_0^{\infty} t\,dt\,\exp[2\pi it(\xi\cos\varphi - \eta\sin\varphi)] \int_{-\infty}^{+\infty} dr\,U(r,\varphi)\,e^{-2\pi irt} \tag{7}$$

which solves the original problem. The function R(u; v) which was introduced is shown elsewhere to be related to the two-dimensional correlation function of the diffraction pattern of the source [Bracewell (1962)]. As such, it may be measured directly by spaced antennas or by a single antenna, provided in the latter case that the diffraction pattern moves over the antenna without change.

In the application of these ideas to lunar radar mapping, we have to measure strip distributions with finite resolution, and not necessarily with the rectangular filter indicated in Eq. (1). Let us assume that the power spectral response of the filter actually used is denoted by g(r). This means that Eq. (1) is replaced by

$$W(r,\varphi) = \iint_{-\infty}^{+\infty} g(x'-r)\,f(x'\cos\varphi + y'\sin\varphi;\ y'\cos\varphi - x'\sin\varphi)\,dx'\,dy' \tag{1a}$$

and it is not possible to pass to the limit of infinitely narrow filters in practice.

Suppose that we use Eq. (7) with $W(r,\varphi)$ rather than with $U(r,\varphi)$. The resulting power density, which we now denote by $P(\xi;\eta)$, must be some sort of smoothed average of $f(\xi;\eta)$. We now derive the relationship between the smoothing and filter functions. Substitution of Eq. (1a) into Eq. (7) and transformation of the integration variable give

$$P(\xi;\eta) = \int_0^{2\pi} d\varphi \int_0^{\infty} t\, dt \exp[2\pi i t(\xi \cos\varphi - \eta \sin\varphi)] \int_{-\infty}^{+\infty} dr\, e^{-2\pi i r t}$$

$$\iint_{-\infty}^{+\infty} g(x' - r)\, f(x' \cos\varphi + y' \sin\varphi;\ y' \cos\varphi - x' \sin\varphi)\, dx'\, dy'$$

$$= \iint_{-\infty}^{+\infty} dx\, dy\, f(x, y)\, G(x - \xi,\ y - \eta) \tag{8}$$

where $G(x, y)$ is a two-dimensional smoothing function defined by

$$G(x, y) = 2\pi \int_0^{\infty} r\, dr \int_{-\infty}^{+\infty} d\rho\, g(\rho)\, J_0\left(2\pi r\sqrt{x^2 + y^2}\right) e^{2\pi i r \rho} \tag{9}$$

where J_0 is a zero-order Bessel function. As an example, consider the case corresponding to Eq. (1), or

$$g(\rho) = 1 \quad , \quad |\rho| < \Delta x/2$$

$$= 0 \quad , \quad \text{otherwise}$$

which yields

$$G(x, y) = \frac{1}{\tau}\left[(\Delta x/2)^2 - (x^2 + y^2)\right]^{-1/2} \quad , \quad x^2 + y^2 < (\Delta x/2)^2$$

$$= 0 \quad , \quad \text{otherwise} \tag{10}$$

This smoothing function is unsatisfactory since it weights points removed from the origin more heavily than those near the origin. As another example, consider the case

$$g(\rho) = \exp[-\rho^2/2\Delta x^2] \tag{11a}$$

which gives

$$G(x, y) = [1/(2\pi\Delta x^2)] \exp[-(x^2 + y^2)/2\Delta x^2] \tag{11b}$$

This smoothing function appears to be satisfactory. The $g(\rho)$ actually used in the analysis of data below is of the intermediate form $[(\sin\alpha\rho)/\alpha\rho]^2$ but, unfortunately, an analytical expression for the corresponding $G(x, y)$ has not yet been found.

Having explored the effect of filtering the strip distribution, we must next turn our attention to the effect of not knowing $W(r, \varphi)$ for all φ but only for a discrete set of values, since this is all one can hope to measure in an actual experimental situation. Even a strictly discrete set of values for φ cannot be obtained in the case of lunar radar observations, since the direction φ is changing continuously during a run and an averaging over a certain sector of angles φ will automatically be made.

In the case of a discrete set of equally spaced angles φ_i, one can express the effect of the discrete angle sampling as a smoothing, as in Eq. (8). The smoothing function $G(x, y)$ now, however, is of the form

$$G(x, y) = \frac{1}{4\pi^2} \sum_{i=1}^{N} \frac{1}{(x \cos\varphi_i - y \sin\varphi_i)^2} \tag{12}$$

It follows that the sidelobe level is inversely proportional to the number of runs N combined to produce the map.

2. Application to Lunar Radar Studies

In lunar radar observations, the filtered strip distribution corresponding to $W(r, \varphi)$ of Eq. (1a) is obtained by coherently processing successive echoes of "long" radar pulses transmitted to the moon. The analysis program computes the frequency spectrum of a sequence of samples of the complex received waveform, the duration T of this sequence being determined by the required filter width of the smoothing function g(x); that is, $\Delta f \cong 1/T$. Since all the samples are weighted equally, the corresponding g(r) is a $(\sin r/r)^2$ frequency response. A number of spectra obtained from such sequences are then added incoherently to reduce the intrinsic noiselike fluctuations. The angle φ in the lunar observations corresponds to the angle between the projection of the lunar meridian through the subradar point and the instantaneous axis of apparent librational rotation. The libration axis is defined here as the locus of points across the lunar disk which have the same doppler frequency shift as the center of the moon. The subradar point (where a line from the radar to the center of the moon intersects the surface) in the course of time will move across the disk of the moon as a result of both optical librations and because of the change in parallax resulting from the diurnal motion of the observer. The instantaneous libration axis will always be normal to this curve. If the orientation of the instantaneous libration axis with respect to selenographic coordinates rotates by at least 180° in the course of a day's observation, then a completely unambiguous map can be produced. The maximum rotation of the libration axis may be expected when the moon is at a high declination, since the moon is then the longest above the horizon, and, in fact, days may be found (at northerly latitudes) when more than 180° of rotation occurs.

The motion of the subradar point across the surface of the moon causes the radar appearance of the moon to change somewhat in the course of an observation. If the average reflectivity does not change too rapidly with the orientation of the observer with respect to the surface, this is not serious. However, the specularly reflected component of the echo has a very bright highlight near the subradar point where reflection occurs at near normal incidence, and this highlight does not move with the surface, but remains fixed with respect to the subradar point. In order to avoid this difficulty, most observations have been carried out using a sense of received polarization which largely rejects the specular component. This sense, which in the case of circularly polarized transmission corresponds to reception in the same polarized sense, is called depolarized.

Since the maximum center-to-limb doppler-frequency difference changes with time, the coherent integration time T should be varied in inverse proportion to the center-to-limb doppler shift for the run under consideration in order to retain a fixed resolution with respect to the lunar surface. Thus, Δf will always remain a fixed fraction of the total limb-to-limb doppler spread across the moon, and surface resolution obtained in successive runs will remain constant.

The effects of quantizing and finite-length sampling intervals on the data are treated in Sec. I, "Systematic Errors," of Appendix A. The effects of fluctuations, caused both by fading in the echo as well as by additive system noise, are treated in Sec. II, "Random Errors," of the same Appendix.

B. Delay-Doppler Mapping Technique

If measurements of the distribution of echo power in delay are simultaneously available with measurements of the frequency distribution, a mapping of the origin of the echo power across the lunar surface is possible as shown in Fig. 2. A coordinate system in which it is convenient

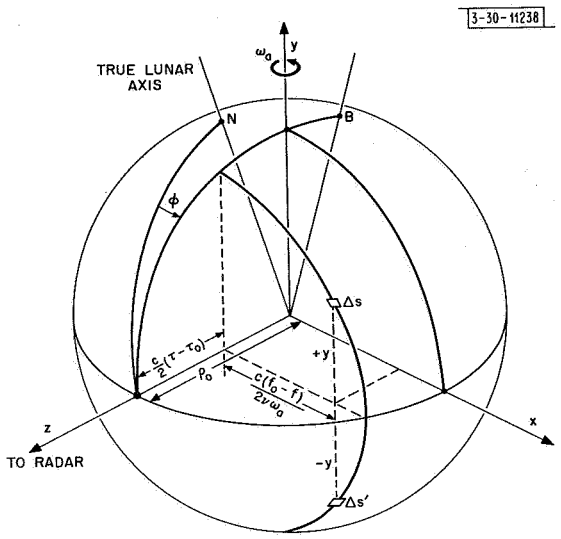

Fig. 2. Definition of delay-doppler mapping coordinates, and illustration of two areas of ambiguity (Δs and $\Delta s'$).

to express these measurements is given by the Cartesian set of direction cosines x, y, and z, similar to that defined in the preceding section, with origin at the lunar center-of-mass, where z is directed toward the radar, y is directed at right angles to z in the plane containing the apparent axis of rotation B, and x is chosen to complete a right-handed orthogonal set. In terms of the absolute delay τ and doppler f,

$$X = \frac{c(f_o - f)}{2\nu\omega_a} \tag{13}$$

$$Z = \rho_o - \frac{c}{2}(\tau - \tau_o) \tag{14}$$

where ρ_o is the lunar radius at the subradar point, τ_o and f_o are the absolute delay and doppler corresponding to this point, c is the velocity of light, ν is the radar carrier frequency, and ω_a is the apparent lunar rotation projected in the x-y plane. Thus, the basic mapping for data taken in delay-doppler coordinates occurs in the x-z plane. In the absence of any further information concerning the shape of the moon, a projection in this plane would be all that could be obtained, just as in the case of supersynthesis mapping previously described, only the projection in the x-y (ξ-η) plane was directly yielded.

If we let ρ equal the radius of the surface (which may vary over the moon), then the direction cosines for points on the surface become

$$x = \frac{X}{\rho} = \frac{c(f_o - f)}{2\rho\nu\omega_a} = \frac{f_o - f}{f_{c\ell}} \quad , \quad f_{c\ell} = 2\rho\nu\omega_a/c \tag{15}$$

$$z = \frac{Z}{\rho} = \frac{1}{\rho}\left[\rho_o - \frac{c}{2}(\tau - \tau_o)\right] \tag{16}$$

$$y = \pm(1 - x^2 - z^2)^{1/2} \tag{17}$$

where the two branches of y reflect an actual ambiguity as may be seen from Fig. 2.

In order to proceed further with the mapping, it is necessary to isolate the two branches of Eq. (17). If we are willing to exclude from consideration regions of large z (i.e., near the subradar point) and small y, the two branches of y will correspond to positions on the lunar surface which differ by a substantial fraction of the lunar radius, and thus in favorable cases may be distinguished using the angular resolution of the antenna beamwidth. Assuming that this has been accomplished, then, the analysis reduces to a reconstruction onto a near-spherical surface from a projection in the x-z plane. Because the deviations of the surface are small, we shall treat them as perturbations from a sphere of constant radius.

The mapping transformation consists first of a normalization to account for the projection of unit area on the sphere on to the x-z plane, since we wish to reduce the observed scattered power to unit lunar surface area. If P(x, z) is the observed two-dimensional density distribution in the x-z plane, then the corresponding density distribution on the spherical surface becomes

$$P'(x, y, z)\, dS = |y| P(x, z)\, dx\, dz \tag{18}$$

Strictly speaking, Eq. (18) holds only for truly differential areas, whereas radar measurements imply finite resolution in delay and doppler. As mentioned above and as discussed more fully in the section dealing with the actual measurements (Sec. V), however, the mapping reported here is carried out under conditions where the use of the differential limit leads to no significant error.

Following this normalization, three coordinate rotations are required to express the observed density in terms of standard selenographic coordinates. First, one seeks the transformation from the x, y, z system (called "radar" coordinates) to the ξ, η, z system (called "observer" coordinates) as defined in Figs. 1 and 2.

$$\begin{aligned} \xi &= x \cos\varphi + y \sin\varphi \\ \eta &= -x \sin\varphi + y \cos\varphi \end{aligned} \tag{19}$$

with its inverse

$$\begin{aligned} x &= \xi \cos\varphi - \eta \sin\varphi \\ y &= \xi \sin\varphi + \eta \cos\varphi \end{aligned} \tag{20}$$

The angle φ (the doppler angle) is measured positively in the clockwise direction from the lunar meridian passing through the subradar point to the great circle arc connecting the subradar point and the positive direction of the apparent rotation vector.

Next, two rotations are necessary to transform from the system of observer coordinates centered on the subradar point to the standard Cartesian selenographic grid aligned with the lunar equator and prime meridian as shown in Fig. 3.

$$\begin{aligned} x_s &= \cos\delta \sin\lambda = \xi \cos\lambda_o - \eta \sin\delta_o \sin\lambda_o + z \cos\delta_o \sin\lambda_o \\ y_s &= \sin\delta = \eta \cos\delta_o + z \sin\delta_o \\ z_s &= \cos\delta \cos\lambda = -\xi \sin\lambda_o - \eta \sin\delta_o \cos\lambda_o + z \cos\delta_o \cos\lambda_o \end{aligned} \tag{21}$$

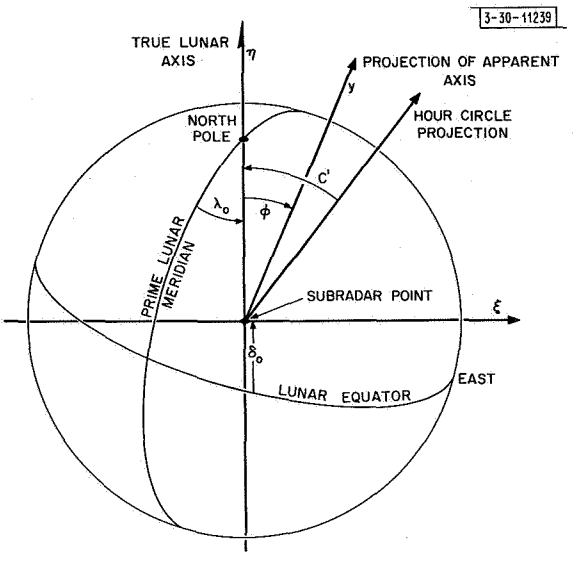

Fig. 3. Definition of angles calculated in lunar ephemeris, showing positive direction and origin.

where

$$\delta = \arcsin(y_s)$$

$$\lambda = \arctan(x_s/z_s) \tag{22}$$

are the usual selenographic latitude δ and longitude λ, and where δ_o and λ_o are the corresponding coordinates of the subradar point. A useful inverse relation is

$$\xi = \cos\delta \sin(\lambda - \lambda_o)$$

$$\eta = \sin\delta \cos\delta_o - \cos\delta \sin\delta_o \cos(\lambda - \lambda_o) \quad . \tag{23}$$

Thus, the observed reflected power density may be related to the specific scattering of an element of area on the lunar surface through Eqs. (18), (19), and (21).

The area resolution ΔS of the lunar surface resulting from a choice of pulse width $\Delta\tau$ and frequency filter width Δf is given by

$$\Delta S = \frac{c^2}{4\nu\omega_a} \cdot \frac{\Delta\tau\Delta f}{|y|} = \frac{c\rho}{2f_{c\ell}} \cdot \frac{\Delta\tau\Delta f}{|y|} \tag{24}$$

where the constants are as defined previously and y may be obtained from Eqs. (20) and (23). The shape of ΔS, of course, will vary even for constant y, depending on the other coordinates.

The effects of local variations in the lunar radius are treated in Appendix B. Provided features observed telescopically and by radar can be adequately correlated, the different projections in the two cases offer a means of deducing variations in topographic height.

In setting up the radar coordinate system, it was assumed that the radar line of sight remained parallel over the surface of the moon, i.e., that parallax was negligible. This is, of course, not quite true, since the lunar disk subtends approximately 0.5° at the radar. Because of the relatively small antenna beamwidth (0.05°) used in the work reported here, the mapping of a given run was restricted to a small area over which this parallax could be assumed to remain constant. The effect of parallax is included, however, in the ephemeris calculations relating to the position of the center of the beam (see Sec. III).

The chief advantage of the delay-doppler mapping method lies in its extremely high potential for resolution. This is due in part to the fact that modern radars are not signal limited in viewing the moon. Thus, the delay and doppler resolutions are restricted almost entirely by system stability and data processing constraints. Because the apparent lunar rotation is relatively slow, the doppler spread across the region illuminated by the radar beam, even at high microwave frequencies, is small compared with the reciprocal of the delay spread across the same region (and, in fact, is small compared with the reciprocal of the total delay spread corresponding to the lunar radius). Thus, aliasing resulting from constraints on the repetitive sampling of a given region can be simultaneously avoided in both delay and doppler. The doppler resolution may be made arbitrarily small (at least to the point where oscillator stability and atmospheric propagation limitations enter) by increasing the duration over which coherent observations are made. For a given total duration of observations, however, increasing this interval will correspondingly reduce the total number of such coherent intervals. The accuracy of the estimate of the mean of the fluctuating scattering to be identified with a given lunar surface element depends on the square root of the number of these independent intervals. Thus, increasing the doppler resolution will automatically degrade the intensity resolution. Nevertheless, in respect to the product of these resolutions, the delay-doppler method offers considerable advantage in those areas of the surface where the radar coordinate y [see Eq. (24)] is not unreasonably small.

Because the doppler angle φ for the moon varies over so large a range – a fact which makes possible supersynthesis mapping in the first place – judicious selection of observing times permits all portions of the lunar surface to be mapped under conditions where y will be relatively large. An exception is the region near the center of the lunar disk. Here, however, libration offers relief, since the awkward region will migrate sufficiently during the course of a month to permit even the center of the disk to be mapped with adequate resolution. Thus, the chief application for the supersynthesis approach lies in those radar systems lacking sufficient angular resolution to separate the ambiguities inherent in Eq. (17).

III. LUNAR EPHEMERIS

A. Ephemeris Requirements

To enable mapping by radar, a number of quantities concerning the location and orientation of the moon must be calculated. As input, the standard astronomical quantities as tabulated in the American Ephemeris and Nautical Almanac [United States Naval Observatory (1965)] have been assumed except where noted. These exceptions comprise the use of values for the horizontal parallax, and the geocentric right ascension and declination obtained from an improved lunar ephemeris supplied by the Jet Propulsion Laboratory [Mulholland and Block (1967)].

The calculations separate naturally into two parts. The first attacks the problem of deriving the absolute time of flight and doppler shift for transmissions from the radar to the subradar point on the lunar surface. The second derives the displacements in these parameters which are associated with other locations on the surface. For the delay-doppler mapping at 3.8 cm, these ephemeris predictions have been based on a relative accuracy requirement of 500 m in distance (equivalent to about 3 μsec in time delay), and a relative accuracy requirement of 1 mm/sec in the component of velocity along the radar line of sight (equivalent to about 0.05 Hz in doppler frequency). Since the actual values for the subradar point were measured at intervals during the observing period, equivalent precision in the absolute delay and doppler was not

required. In fact, substantial discrepancies were discovered between these observed values and those obtained from the ephemeris as described in Sec. VII-B.

The requirements for angular tracking of the antenna beam were less severe. With a two-way, half-power beamwidth of 3 arcmin, a calculated angular precision of 0.1 arcmin (about one-half the error contributed by the antenna system) was thought adequate. This error is equivalent to about 10 km when referred to the lunar surface.

The topocentric position of the moon is obtained from the tabulated geocentric positions and orientations using standard equations outlined in Appendix C. In addition to the apparent right ascension, declination, and distance of the moon's center, the position angle of the lunar axis and the selenographic coordinates of the subradar point are desired. For most of these quantities, it is also convenient to calculate analytic expressions for their rates of change as functions of the basic inputs.

Selenographic coordinate systems will be used as described in Sec. II, and as illustrated in Figs. 2 and 3. There are three basic sets of Cartesian coordinates, specified in terms of direction cosines of a hypothetical sphere of unit radius concentric with the moon: (1) radar coordinates x, y, z; (2) observer coordinates ξ, η, z; (3) selenographic coordinates x_s, y_s, z_s. The relations among them are given in Eqs. (19) through (23). A spherical coordinate system yielding the standard selenographic latitudes and longitudes based on the direction cosines x_s, y_s, and z_s is also defined [see Eq. (22)].

B. Calculation of Distance and Its Time Rate of Change

We now attack the problem of deriving the distance D and its time rate of change $\dot{D}$ for any arbitrary point on the lunar surface, given the distance to the lunar center R and its rate of change $\dot{R}$. The geometry of the radar and lunar surface in the ξ, η, z (observer) coordinate system is shown in Fig. 4. Here the radar is on the z-axis at a distance R from the center of the moon. The point on the lunar surface has been placed in the plane of the paper. The distance D to this point is given by the law of cosines as

$$D = (R^2 + \rho^2 - 2\rho R \cos\Theta)^{1/2}$$
$$= (R^2 + \rho^2 - 2\rho z R)^{1/2} \qquad (25)$$

where z is the coordinate of the surface point as defined in Eq. (16). The time derivative of D is

$$\dot{D} = \frac{1}{D}\left[(R - \rho z)\,\dot{R} - \rho R \dot{z}\right] \quad . \qquad (26)$$

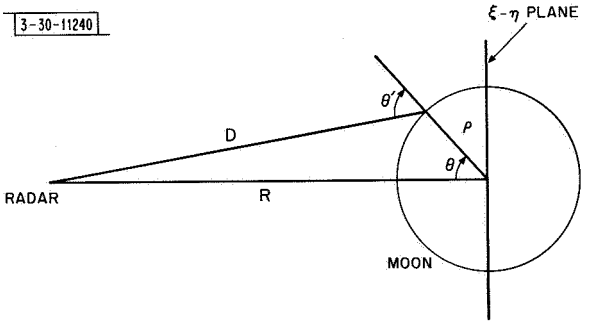

Fig. 4. Geometry for computation of distance D between radar and point on lunar surface. Note that angle of incidence of radar beam θ' cannot differ from parallel-ray approximation θ by more than angular radius of moon, approximately 0.25°.

The distance and its time derivative are related to the echo round-trip time delay τ and doppler frequency f (to second order in $\dot{D}$) by

$$\tau = \frac{2}{c} D \tag{27}$$

$$f = -\frac{2\nu\dot{D}}{c}\left(1 - \frac{\dot{D}}{2c}\right) \tag{28}$$

where c is the velocity of light, ν is the radar carrier frequency, and D and its derivatives are to be calculated at the instant of reflection ($\tau/2$ later than transmission, $\tau/2$ earlier than reception).

In Eq. (26), the term in $\dot{R}$ accounts for the motion of the center of the moon with respect to the radar, while the additional factor $(R - \rho z)/D$ corrects for the parallax. The term in $\dot{z}$ arises from the apparent rotation of the moon with respect to the radar. The apparent motion of the moon results in part from the changing parallax of the observer as the earth rotates, and in part from the changing geocentric libration. Thus, the selenographic coordinates δ_o and λ_o of the subradar point are constantly changing.

Differentiation of z yields

$$\dot{z} = \eta\dot{\delta}_o + \xi \cos\delta_o\dot{\lambda}_o \quad . \tag{29}$$

The term in $\dot{\delta}_o$ describes the apparent rotation about the ξ-axis, and the term in $\dot{\lambda}_o$ about the η-axis. The rotation about the z-axis does not induce a velocity component toward the radar. The total apparent rotation thus has a component ω_a when projected in the ξ-η plane which lies at the angle φ from the selenographic meridian of the subradar point (see Fig. 3). These quantities are derived from Eq. (29) as

$$\varphi = \arctan\left[\frac{-\dot{\delta}_o}{\dot{\lambda}_o \cos\delta_o}\right] \tag{30}$$

$$\omega_a = (\dot{\delta}_o^2 + \dot{\lambda}_o^2 \cos^2\delta_o)^{1/2} \quad . \tag{31}$$

signs in the argument of the arctangent were chosen in agreement with the definitions for φ shown in Figs. 1, 2, and 3. Equation (29) may be rewritten

$$\dot{z} = \omega_a(-\xi \cos\varphi + \eta \sin\varphi) = -\omega_a x \tag{32}$$

where the latter follows from Eq. (20).

The calculation of the time delay τ and doppler shift f, to an arbitrary point on the lunar surface specified in selenographic coordinates, may now be performed through successive applications of Eqs. (23), (30) through (32), recollection that

$$z = (1 - \xi^2 - \eta^2)^{1/2} \tag{33}$$

and Eqs. (25) through (28). The epoch for these calculations is the instant of reflection from the lunar surface. If it is desired to relate τ and f to the instant of transmission or reception, the epoch may be shifted appropriately by $\tau/2$.

C. Topocentric Celestial Coordinates of a Lunar Position

In order to properly aim the antenna, it is necessary to find the apparent right ascension and declination of the desired point on the lunar surface. First, the right ascension and declination

of the center of the moon are found using the computations outlined in Appendix C. Then, the offset in these coordinates is determined for the desired position on the lunar surface.

As viewed from the radar, the moon subtends a small angle, so that the contours of right ascension and declination projected onto the lunar disk form a nearly orthogonal grid. In fact, in this projection the two contours cannot depart from orthogonality by more than 2 seconds of arc. The orientation of these contours with respect to the ξ and η axes is given by C', the position angle of the optical axis, as defined in Appendix C (see also Fig. 3). The differences in topocentric right ascension $\Delta\alpha'$ and declination $\Delta\beta'$, measured from the center of the lunar disk, are determined by a rotation of the ξ-η plane about the z-axis through the angle C'. Thus,

$$\Delta\alpha' = [\xi \cos(C') - \eta \sin(C')] \, S \cos(\beta')$$

$$\Delta\beta' = [\xi \sin(C') + \eta \cos(C')] \, S \qquad (34)$$

where S = angular semi-diameter of the moon = $\arctan(\rho/R)$.

IV. APPLICATION OF SUPERSYNTHESIS TECHNIQUE AT 23 CM

Observations of the moon at 23 cm using the Millstone radar for coherent mapping purposes were made on four different occasions. The parameters of the radar system are given in Table I, and some particulars of the observations in Table II. The three successful runs have been analyzed and it was found that the depolarized reflectivity maps were very similar, although the last set of runs appears to give maps which are less noisy than the previous runs. Probably, this is primarily due to the greater number of runs in the December observation, but it is also due to the better rejection of the specular component in the last observations because of a better adjustment in the system hardware. Therefore, the analysis of the December data will be singled out for detailed discussion below.

A. Observational Procedure and Frequency Analysis

The date 27-28 December 1966 was chosen because of the favorable inclinations of the instantaneous libration axis available. The computation of the doppler angle, which corresponds to the angle φ in the analysis in Sec. II-A, was derived from the standard ephemeris program available on-site (see Sec. III). Figure 5 shows the variation of this angle with time during the December runs. Also shown in the diagram is the magnitude of the center-limb doppler spread and the altitude of the moon.

During a given run, sequences of 1-msec pulses were transmitted at an interpulse period of either 30, 36, or 48 msec, depending on the center-limb doppler spread and on the range of the target (so that the echo would be received during the interpulse period). The local oscillators of the receivers were steered according to ephemeris predictions to compensate for the doppler shift of the center of the moon. The transmission was right circularly polarized, and both senses of circular polarization were simultaneously received. In both polarization channels, the in-phase and quadrature outputs of coherent detectors were sampled, each at a rate of 1 kHz during a "window" of the interpulse period 18 msec wide. The position of this "window" was matched to the motion of the echo on the time base as the range to the moon varied. Of the 18 samples, 12 contained signal while the remaining 6 consisted of noise alone. No calibration pulse was inserted on the time base, since the mapping program did not retain absolute signal levels. The samples were digitized to 6-bit length and stored on magnetic tape. The duration of each run

TABLE I

MILLSTONE L-BAND RADAR PARAMETERS

Frequency	1295.0 MHz
Antenna	84-ft parabola with Cassegrainian feed
Antenna gain (one-way)	47.3 db
Polarization	Right circular transmitted; right and left circular separately received
Beamwidth (one-way)	0.6° between half-power points
Transmitter power	Variable, 5-MW peak maximum (continuously monitored)
Pulse length	Variable, pulses 10 to 1000 μsec long were employed in these observations
Receiver bandwidth	100- or 50-kHz predetector; postdetector filter matched to 10-μsec pulses for 10-μsec pulse transmissions, matched to 20-μsec pulses for all other transmissions
System noise temperature	~150°K (continuously monitored)
Overall feed-line and other losses	2.1 db

TABLE II

SUMMARY OF 23-CM OBSERVATIONS

GMT Date (1966)	No. Runs	Transmitter Polarization	Receiver Polarization	Comment
21 June	18	Right circular	Right circular (depolarized received component)	Successful
3 October	18	Right circular	Right circular	Unsuccessful
5 November	17	Right circular	Both right and left circular	Successful
27-28 December	27	Right circular	Both right and left circular	Successful

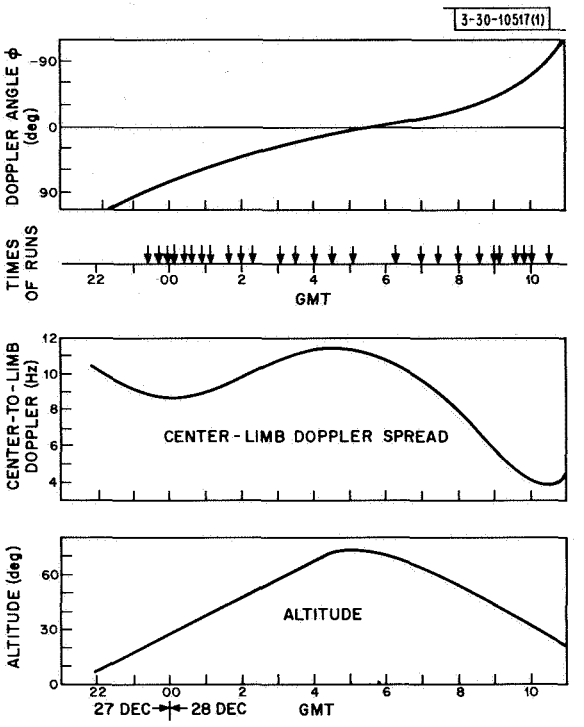

Fig. 5. Variation of doppler angle, center-limb doppler spread, and altitude vs time during runs of 27-28 December 1966.

was 5 minutes. During this time interval, the doppler axis rotated in the worst case by as much as 4°. In the great majority of runs, the rotation was less than 2°. This was not considered serious, since only relatively coarse resolution was possible in any event. For finer resolution, each 5-minute run would have to be subdivided, with each subdivision treated as a separate run.

Because of the way in which the data were taken, the computation of spectra was done relative to the subradar point and not with reference to a point fixed on the lunar surface. As a result, some blurring of the data occurred. In order to determine the severity of this effect, the motion of the subradar point in selenographic latitude and longitude during the observational period is shown in Fig. 6. As can be seen, the amount of change did not exceed 1.5° in selenographic

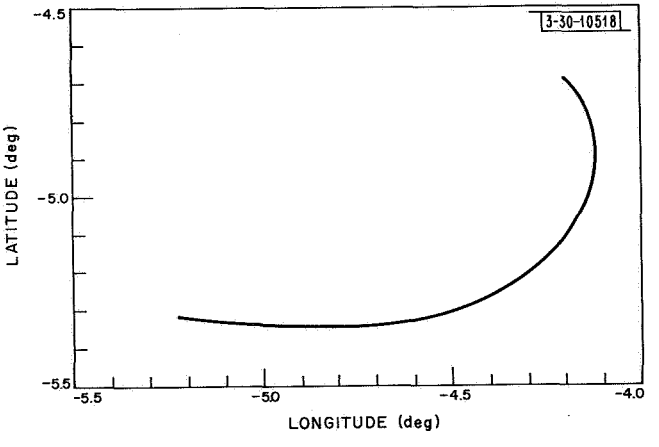

Fig. 6. Variation of coordinates of subradar point during runs of 27-28 December 1966.

TABLE III

PARAMETERS RELATING TO 27-28 DECEMBER 1966 MOON RUNS

Run No.	Time (GMT)	Doppler Angle (deg)	Center-to-Limb Doppler (Hz)	Filter Spacing (Hz)	Starting Frequency (Hz)	Interpulse Period (msec)	No. of Pulses Coherently Integrated
1	2325	+90.695	8.783	0.3520	−10.55	36	79
2	2340	+85.306	8.683	0.3475	−10.42	36	80
3	2350	+79.871	8.636	0.3455	−10.35	36	80
4	0005	+76.256	8.633	0.3455	−10.35	48	60
5	0020	+70.897	8.669	0.3470	−10.40	48	60
6	0035	+65.671	8.751	0.3505	−10.49	48	59
7	0050	+60.631	8.874	0.3550	−10.64	48	59
8	0105	+55.812	9.031	0.3610	−10.83	48	58
9	0140	+45.548	9.494	0.3795	−11.38	30	88
10	0155	+41.581	9.717	0.3890	−11.65	30	86
11	0215	+36.674	10.020	0.408	−12.23	30	82
12	0305	+26.094	10.721	0.4290	−12.87	36	65
13	0330	+21.536	10.998	0.440	−13.19	36	63
14	0400	+16.550	11.232	0.449	−13.48	36	62
15	0430	+11.963	11.336	0.454	−13.62	36	61
16	0505	+6.947	11.274	0.452	−13.53	36	62
17	0620	−3.445	10.423	0.417	−12.50	36	67
18	0655	−8.594	9.694	0.388	−11.63	36	72
19	0725	−13.475	8.919	0.3563	−10.69	36	78
20	0750	−18.919	8.182	0.3272	−9.82	36	85
21	0835	−28.653	6.712	0.2685	−8.06	48	78
22	0850	−33.181	6.202	0.2485	−7.45	48	83
23	0905	−38.458	5.702	0.2285	−6.85	48	84
24	0940	−54.861	4.645	0.1863	−5.58	48	112
25	0955	−64.141	4.291	0.1720	−5.16	48	121
26	1005	−71.136	4.109	0.1643	−4.93	48	127
27	1030	−90.76	3.903	0.1565	−4.69	48	133

latitude or longitude, corresponding to less than about 45 km on the surface, about one-half the finest resolution used.

The 18 range samples, for each of the 27 runs taken on 27-28 December 1966, were frequency analyzed into 61 equally spaced frequencies so chosen that 51 of them just spanned the limb-limb doppler spread. The width of the $(\sin x/x)^2$ filter resolution function was chosen so that the first zero on either side of the center of the filter coincided with the centers of the neighboring filters. Table III lists in detail the parameters of the 27 runs. The column listed as "Starting Frequency" refers to the frequency offset of the lowest frequency filter with respect to the subradar point, while the last column lists the number of data samples (separated by the interpulse period) which were strung together coherently to form the analyzing filter.

B. Run Combination and Mapping Display

The two-dimensional mapping procedure can be carried out in the following steps. First, collect a number M of frequency spectra:

$$W(f_\ell, \varphi_m)$$

where

$\ell = 1 \rightarrow N$

N = number of filters

$m = 1 \rightarrow M$

φ_m = doppler angle for run m.

An estimate of the weighted correlation function for run m is

$$R_W(\tau, \varphi_m) = \sum_{\ell=1}^{N} W(f_\ell, \varphi_m) \exp[-2\pi i \tau (f_\ell - f_{om})] \tag{35}$$

where f_{om} is the doppler frequency offset of the feature we are interested in during run m, and

$$f_\ell = \ell \cdot \Delta f \quad . \tag{36}$$

Note that $R_W(\tau, \varphi_m)$ is periodic in τ with period $\tau_P = 1/\Delta f$. Therefore, the correlation function should <u>not</u> be estimated from Eq. (35) for $\tau > \tau_{max} = 1/2\Delta f$.

Since the procedure used in computing the frequency spectra $W(f_\ell, \varphi_m)$ implies a triangular weighting of the correlation function, we should "unweight" Eq. (35) by a ramp function:

$$R_{est}(\tau, \varphi_m) = \frac{1}{1 - |2\tau| \cdot \Delta f} \sum_{\ell=1}^{N} W(\ell \cdot \Delta f, \varphi_m) \exp[-2\pi i (\ell \Delta f - f_{om})\, \tau] \quad . \tag{37}$$

Since the limb-to-limb doppler shift is varying from run to run, we normalize so that they all have the same equivalent width by introducing

$$\Theta = \tau \cdot f_{Lm} \tag{38}$$

where f_{Lm} is the center-to-limb doppler offset for run m there results

$$R_{est}(\Theta, \varphi_m) = \frac{1}{1 - |2\Theta| \cdot \Delta f/f_{Lm}} \sum_{\ell=1}^{N} W(\ell\Delta f, \varphi_m)$$

$$\exp[-2\pi i\Theta(\ell\Delta f - f_{om})/f_{Lm}] \tag{39}$$

Finally, in order to reduce noise in the final map, it is necessary to filter the data by applying a ramp function which is narrower than the original ramp

$$R_f = \frac{1 - \text{Filt} \cdot |\Theta|}{1 - 2|\Theta|\ \Delta f/f_{Lm}} \sum_{\ell=1}^{N} W(\ell\Delta f, \varphi_m) \exp[-2\pi i\Theta(\ell\Delta f - f_{om})/f_{Lm}] \tag{40}$$

where the filtering factor must satisfy

$$\text{Filt} > 2\Delta f/f_{Lm}$$

With this estimate of $R_f(\Theta, \varphi_m)$, the two-dimensional distribution of power may be calculated over the lunar disk area of interest:

$$P(\xi, \eta) = \int_o^{1/\text{Filt}} \Theta d\Theta \int_o^{2\pi} d\varphi_m \frac{1 - \text{Filt} \cdot |\Theta|}{1 - 2|\Theta|\ \Delta f/f_{Lm}} \cdot \sum_{\ell=1}^{N} W(\ell\Delta f, \varphi_m)$$

$$\cdot \exp[-2\pi i\Theta(\ell\Delta f - f_{om})/f_{Lm}] \cdot \exp[2\pi i\Theta(\xi \cos\varphi_m - \eta \sin\varphi_m)]$$

$$= \int_o^{1/\text{Filt}} \Theta d\Theta \int_o^{\pi} d\varphi_m \{\text{Re}(R_f) \cos[2\pi\Theta(\xi \cos\varphi_m - \eta \sin\varphi_m)]$$

$$-\text{Im}(R_f) \sin[2\pi\Theta(\xi \cos\varphi_m - \eta \sin\varphi_m)]\} \quad . \tag{41}$$

The program is basically divided into two parts: the first part computing and storing the smoothed correlation function R_f, and the second part computing the reflectivity $P(\xi, \eta)$ as a function of the coordinates ξ and η from the reflectivity matrix.

Consider the first part of the analysis program. For each run characterized by a certain doppler angle φ, 18 frequency spectra (each containing 61 frequencies) are read in from magnetic tape previously generated by the spectral analysis program. The mean power at each frequency due to noise alone is computed from the 6 positions of range sampling which do not contain an echo. This mean noise level is subtracted from the signal-containing range samples. For the depolarized (diffusely scattered) component which represents the results reported here, all the signal-containing frequency spectra corresponding to different ranges were added. For the polarized (specularly reflected) components, the "glare" from the subradar point can be avoided by omitting one or two of the first range boxes. In other cases, we may want to consider only a single range ring, as will be explained below. The ranges of interest can be freely specified in the analysis program.

The averaged frequency spectra obtained in Sec. IV-A above were used to compute the complex autocorrelation R_f for each run. The smoothing factor "Filt" of Eq. (41) was chosen to be equal to 0.25 on the basis of experimentation. This value corresponds approximately to trebling the filter widths of the frequency spectra in order to reduce noise. Hence, in the final output for this choice, there will be only the equivalent of 17 filter widths along the diameter of the

moon. This first part of the program also requires, as an input for each run, the center-to-limb doppler frequency as well as the doppler offset of the particular feature wanted at the center of the displayed map, that is, at $\xi = \eta = 0$. In the present case, this was chosen to be the subradar point. The computed complex correlation functions are stored on magnetic tape in order of increasing doppler angle φ

Part two of the program first reads the complex correlation functions for all the runs into core memory of the computer, together with the associated doppler angles φ_m. The program must also be given information about the extreme values of ξ and η, and the steps by which ξ and η are to be incremented. The integrations over Θ and φ are made using a simple trapezoidal method, and the resulting matrix of powers $P(\xi, \eta)$ is stored on magnetic tape. The final step in the procedure is to correct for the antenna beam weighting and to produce a contour map by means of a standard contour display program. The results for 27-28 December with Filt = 0.25 are given in Fig. 7, with a selenographic grid overlaid.

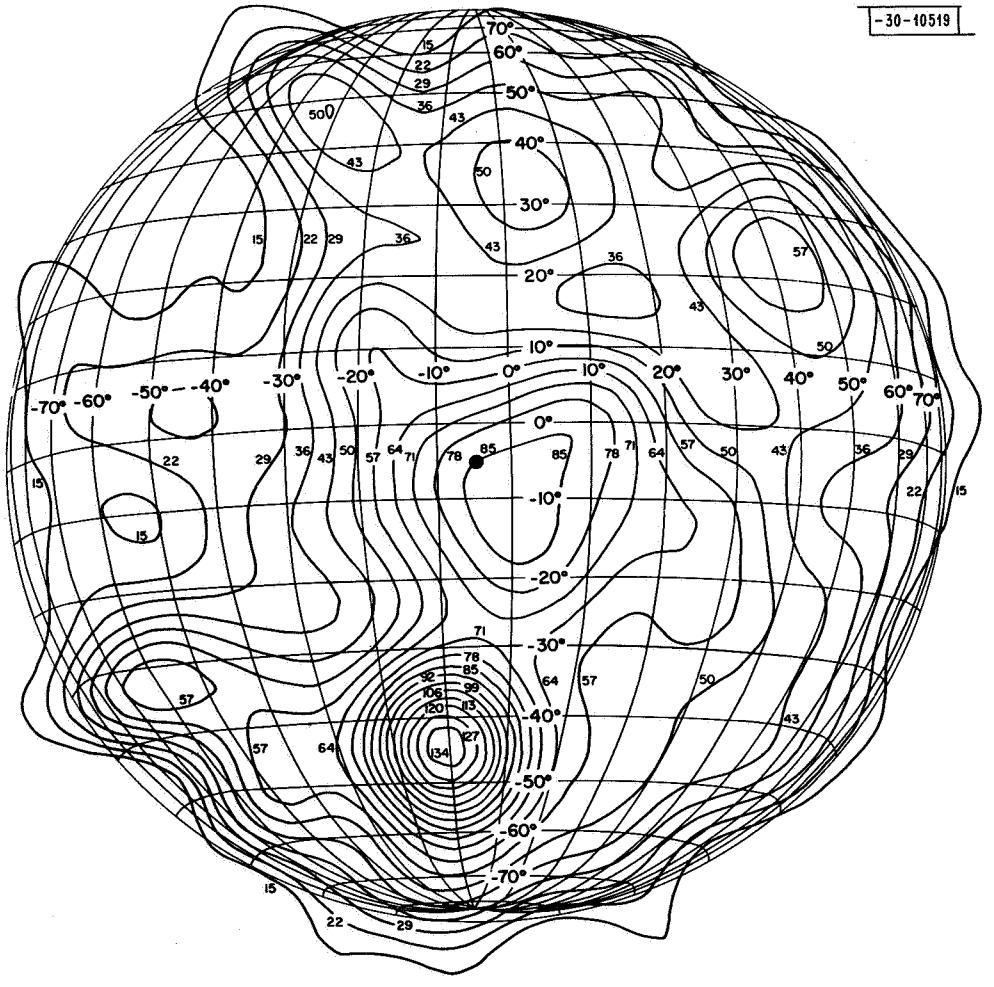

Fig. 7. Contour map of 23-cm lunar scattering for depolarized circular received component. Contours labeled in relative power; Filt = 0.25. Subradar point during these observations (27-28 December 1966) is shown by small central spot.

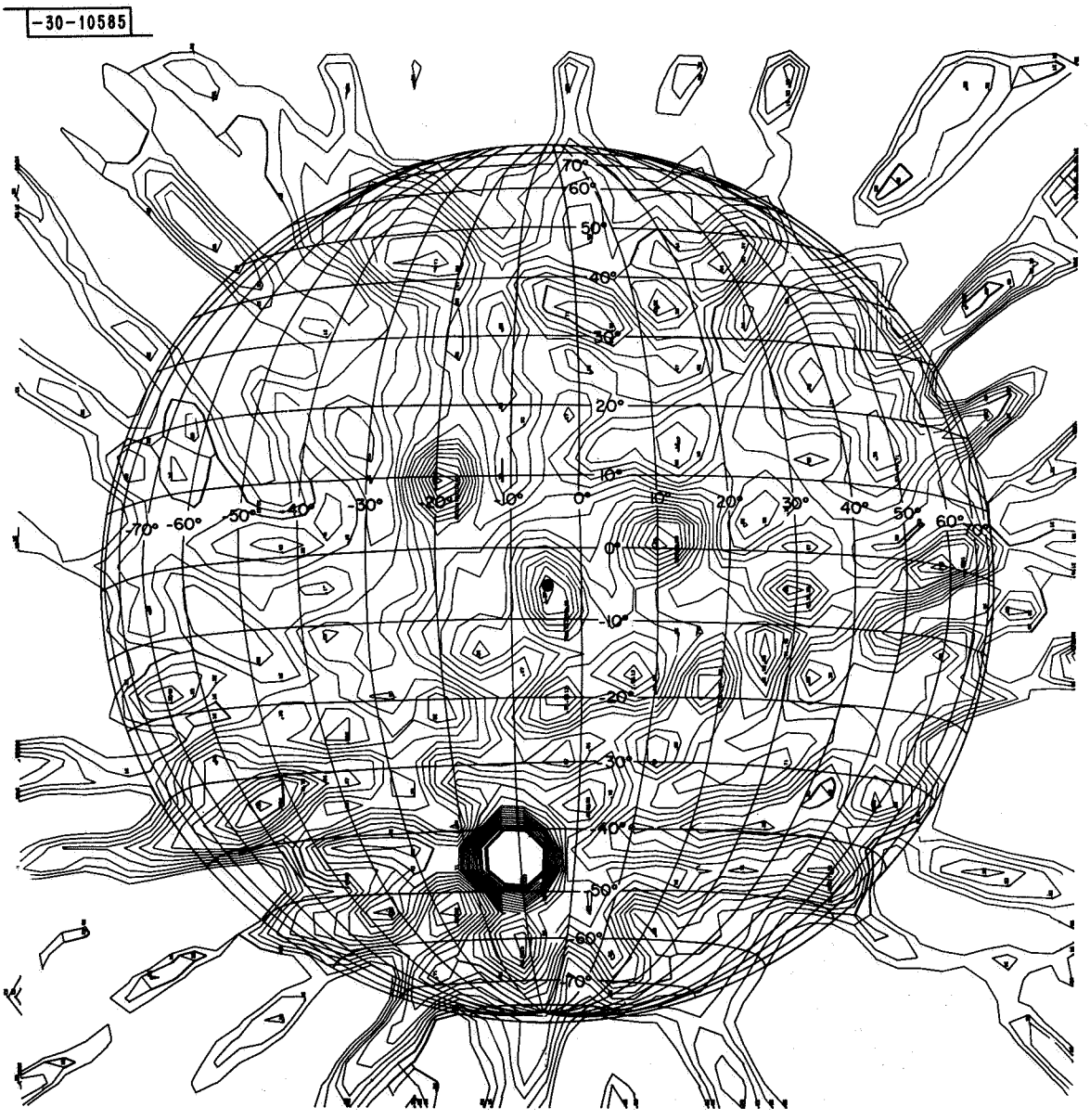

Fig. 8. Same data as shown in Fig. 7, but with filtering constant Filt reduced to 0.132 to improve surface resolution at cost of higher sidelobe level. Peak intensity of Tycho (−44° latitude) has been clipped in this presentation.

For the interval of φ_m chosen in the data of 27-28 December, the resolution shown in Fig. 7 near the edge of the lunar disk represents a near-optimal tradeoff between resolution and sidelobes as discussed in Appendix A. This is not the case near the center of the disk, where the linear separation associated with adjacent values of φ_m is very much less. To improve the resolution in this central region and to appreciate the severity of the sidelobes produced near the edge of the disk, the same data were processed a second time with Filt = 0.132, which corresponds to a reduction of only 50 percent in the number of degrees of freedom contained in the original data set during their transformation to the ξ, η plane. The results of this processing are given in Fig. 8, where a substantial improvement in resolution as compared with Fig. 7 may be seen, along with the cost in terms of considerable peripheral sidelobes. Appendix A contains a discussion of these constraints as well as those imposed by random noise.

C. Discussion of 23-cm Results

In order to identify some of the features in the maps, the selenographic coordinate system was superimposed on the rectangular ξ, η grid system by making use of the transformation formulas given in Eq. (23). The coordinates of the subradar point were assumed to remain fixed at $\delta_o = 5.3°S$ and $\lambda_o = 4.8°W$ throughout the observations presented here.

The most striking feature on the maps, not unexpectedly, is the crater Tycho at approximately 43°S, 11°W. In depolarized radiation at 23 cm, this area appears significantly brighter than the subradar point. Even with the relatively coarse resolution of Fig. 7, the peak of the reflection at the crater Tycho is ten times higher than in the regions of Mare Imbrium. Another feature of interest is the asymmetry in the contours near the subradar point, where they appear to be displaced toward the south-southeast. From an optical picture of the moon, it appears that the area to the south of Sinus Medii is more mountainous than that to the north. The crater Copernicus (10°N, 20°W) is quite prominent, especially in Fig. 8, as also is (but to a lesser extent) the crater Theophilus (12°S, 27°E).

It is also obvious that some of the marial regions appear quite dark, notably Serenitatis, Tranquilitatis, Imbrium, and Procellarum. Other generalizations include an association of high reflectivity with Sinus Iridium or possibly with the Jura Mountains immediately to the north of it. The reflectivity in the southern hemisphere is higher in the western part than in the eastern part. The depolarized scattering from the areas to the southwest of Mare Humorum is particularly strong, although there are no spectacular craters in this region.

On the whole, we conclude that there is good correlation between strong depolarized scattering and optically bright mountainous regions, as also between low scattering and dark marial regions. In its present form, the supersynthesis mapping technique finds its most important application in situations such as with the Millstone radar at 23 cm, where no alternative method of mapping exists. It also appears more efficient at the task of providing a relatively quick survey at low but uniform resolution of the scattering from the entire lunar disk.

V. DELAY-DOPPLER SYSTEMS AND PROCEDURES AT 3.8 CM

A. General Description

The delay-doppler mapping observations were carried out using the Haystack Microwave Radar Facility located in Tyngsboro, Massachusetts. The radar operating parameters for this system are given in Table IV, with the major elements shown as a block diagram in Fig. 9. Two

TABLE IV

HAYSTACK OPERATING PARAMETERS

Radar location:	
Latitude (geodetic)	42°37'24"N
Longitude	71°29'19"W
Height above MSL	145 m
Operating frequency	7840 MHz
Operating wavelength	3.8 cm
Antenna:	
Configuration	120-ft steerable paraboloid with Cassegrainian feed
Gain (one-way)	66 db
Beamwidth (half-power, one-way)	4 arcmin
Transmitter:	
Peak power	200 kW
Average power	15 to 100 W
Polarization	Right circular
Pulse length	5 or 10 μsec
Receiving system:	
Temperature on moon	200°K
Polarization	Left circular
Bandwidth	Matched to transmitted pulse
Feed-line losses (two-way)	0.5 db

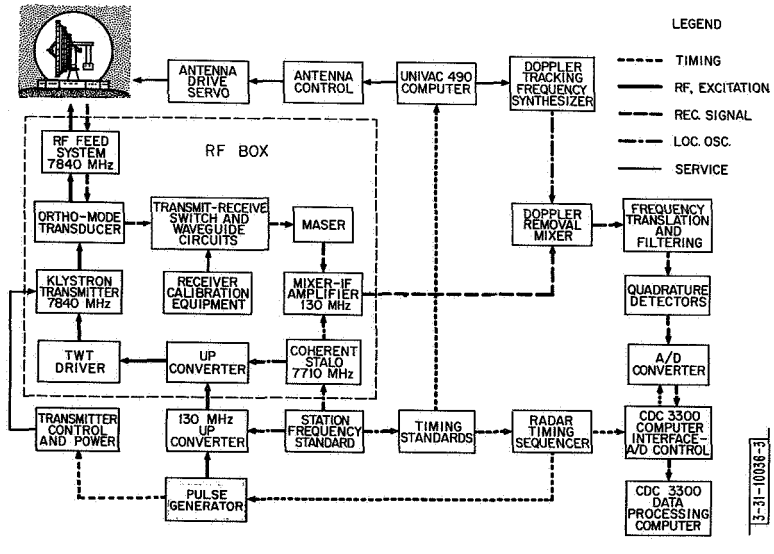

Fig. 9. Block diagram of radar system used in 3.8-cm wavelength, delay-doppler mapping observations at Haystack radar.

digital computers are an integral part of the observing system. The Univac 490 is responsible for on-line ephemeris calculations necessary to point the antenna and to remove the effects of the doppler shift in the received signal. The CDC 3300, on the other hand, is concerned exclusively (during the actual observations) with sorting and storing the digitalized data, and with performing a few checking calculations to monitor their quality.

The U-490 requires as input, in addition to its programmed instructions, smoothed data on the lunar orbit and libration. From these, it calculates both the antenna pointing and the expected doppler frequency for a desired selenographic position. The calculated doppler, in digital form, is used to control the synthesis of a frequency appropriately displaced from 100 MHz. In addition to its use in the removal of most of the doppler shift, this frequency is effectively heterodyned to the equivalent received RF value and then divided by the operating frequency in megahertz (7840) to obtain a doppler-shifted 1-MHz reference from which the sampling timing is derived. Thus, the progressive change in range arising from the apparent motion of the moon is automatically accounted for.

The CDC 3300 computer is used to reduce the data. In the actual data-taking phase, it sorts and stores the incoming data on magnetic tape and calculates a "quick look" of the mean power received as a function of delay. The latter is plotted immediately following a run and can be used to check the operation of the data-taking procedures. The CDC 3300 is also used subsequent to the run for spectrum analyzing and mapping, as described below.

Transmitted pulse widths of either 5 or 10 μsec were employed. The use of shorter pulses than these was not possible due to limitations on the sampling rate set by the computer interface. In general, the longer pulse width was found to provide adequate resolution except when mapping regions near the subradar point, where the shorter pulse was used. The over-all accuracy of the system (excluding errors associated with the ephemeris) was better than 1 μsec in delay and 0.05 Hz in frequency.

A pair of synchronous detectors are located at the end of the IF receiver chain, driven by a pair of local oscillators of the same frequency but 90° apart in phase. The output from these detectors is at video frequencies with DC corresponding to components of the received signal at the frequency of the doppler correction. Each detector is followed by a low-pass filter matched to the transmitted pulse width. Thus, the pair of quadrature outputs contains complete fine-scale information on both the delay and frequency behavior of the echo. Digital sampling of the output is performed at intervals of the pulse width in each channel.

In the more detailed description which follows, the procedures are broken down into five successive steps:

(1) Preparation for a run,
(2) Making observations,
(3) Spectrum analysis,
(4) Computer mapping,
(5) Display of results.

Each of these is treated separately in the following sections.

B. Preparation for a Run

In planning for a run, the first step was to consult the American Ephemeris and Nautical Almanac [U. S. Naval Observatory (1965)] to locate the selenographic position of the sub-earth

point (which will approximate the subradar point). Based on this information, a selection of possible areas lying further than 7° (selenographic) from this point was made. The second step required the preparation of a planning ephemeris for the dates selected which gave, at 5-minute intervals, a list of areas which passed certain tests. The tests consisted first of a check to make sure that the region conjugate, in delay-doppler coordinates (see Sec. II-B), to the desired region would be separable by the angular resolution available from the antenna. Second, it was required that the delay and doppler contours passing through the center of the desired region on the lunar surface not depart by more than 30° from orthogonality. The angle of this departure is called the local doppler angle.

For convenience, an area code was devised based on the numbering of the Lunar Aeronautical Charts (LAC). Charts numbered 57 through 61 and 75 through 79, covering the region between 50° east and west longitude and 16° north and south latitude, were each broken up into four equal subareas, designated by a decimal and a digit following the respective LAC number. Placed with north up, these subunits were numbered counter-clockwise within the LAC area, starting in the upper right-hand corner. Because of the higher resolution afforded, LAC Nos. 56, 62, 74, and 80 were broken up into six subareas defined in a manner similar to the others. The location of these areas is shown more precisely in the figures of Sec. VI-A. Altogether, 64 LAC subareas were observed.

For each subarea which passed the tests above, the planning ephemeris listed the surface resolution in kilometers corresponding to representative values of delay and doppler resolution. Based on these calculations, an operations schedule was drawn up in which it was usually possible to take data at periods when the local doppler angle was less than 10° (for the center of the observed subarea). The pulse length for a given run was chosen (i.e., either at 10 or 5 μsec) to optimize surface resolution while retaining adequate coverage of the subarea, since a maximum of only 190 samples in delay could be taken in a given run (see Sec. V-C below).

Following the fixing of the surface resolution corresponding to the delay coordinate, an attempt was made to match this resolution in the frequency direction. In the analysis program (see Sec. V-D below), the frequency resolution was fixed at 1/256 times the radar pulse repetition frequency (PRF) used, because of program constraints. Thus, the only parameter left free was the PRF. However, if this variable divided by the center-limb doppler spread (f_{cl}) is smaller than the angular response of the antenna divided by the angular radius of the lunar disk, significant observable frequency aliasing will occur. In general, a PRF just above this minimum was used, unless a larger value provided a better match to the delay resolution.

Measurements of the echo power from the subradar point were scheduled at convenient intervals interspersed among the mapping runs. These observations provided a convenient opportunity to check the lunar ephemeris predictions of delay and doppler, as well as to standardize the received power and test the general performance of the entire radar system. In addition to these observations (called "leading-edge" runs), a closed-loop ("sync check") measurement of the system response to a small amount of transmitter leakage was scheduled for the beginning and end of a day's operations.

Once a reasonably firm schedule of operations had been arrived at, an ephemeris spanning the expected duration of observation was run off using the CDC 3300 computer for the center (aiming point) of each area to be observed. Thus, it was possible to spot check independently the values calculated by the U-490 during the actual observations. In addition, a complete

ephemeris for the subradar point was calculated which, in addition to elevation, azimuth, delay, and doppler, contained supplementary data on the subradar position coordinates, the center-limb doppler frequency $f_{c\ell}$, the doppler angle φ, and several other parameters.

C. Making Observations

In making the observations, it was necessary to follow the planned schedule rather closely (within about 5 minutes, typically) because, for the observing conditions appropriate for mapping at high equatorial longitudes, the doppler angle changes very rapidly. Prior to a given run, the round-trip echo delay appropriate to the selected starting time was manually loaded into the radar timing sequencer (see Fig. 9). This delay was obtained from the ephemeris which had been precomputed for the desired area. The starting time was also entered, with synchronization and start-up of the run automatically enabled when that time arrived. Also set into the sequencer were the desired relative positioning of the data sampling (typically the total string of samples was centered on the entered flight time), as well as the number and spacing of the samples to be taken. A related timer controlled the transmitted pulse width and interpulse period.

Prior to the start of a run, it was necessary to enter into the U-490 computer the selenographic coordinates of the center of the area to be mapped. These coordinates could be stated in several ways: as standard selenographic, either in latitude and longitude or in direction cosines; as "observer" coordinates (see Sec. II-B); or in terms of the apparent offset in right-ascension and declination compared with the coordinates for the lunar center. The first of these options generally proved most convenient, and was entered via a teletypewriter connected to the computer. The subsequent positioning of the antenna, as well as the doppler frequency generated, was compared against the precomputed ephemeris at intervals during the observations, as a check.

The data-taking program in the CDC 3300 permitted the recording of 200 quadrature pairs of data samples per interpulse interval. Of these, 10 were positioned at an instant in the interval known to contain no lunar echo power, and served to establish the noise level for that particular run. The remaining 190 sets of samples were positioned to span the desired area as described above. Since the interpulse interval typically lay between about 30 and 80 msec, and the intersampling interval was chosen to equal the transmitted pulse width (either 5 or 10 μsec), it can be seen that only a small fraction of the interpulse interval was actually sampled. In addition to storing these samples on magnetic tape for subsequent frequency analysis, a running sum was kept, for each relative delay position, of the sums of the squares of the two quadrature components. Thus, at the conclusion of the run, a statement of the mean received power at each sampling position within the interpulse was available. From this, a signal-to-noise ratio could be estimated and, for the runs aimed at the subradar point, an indication of the position of the leading edge of the echo could be deduced for comparison with the ephemeris.

The duration of the runs was chosen to provide a sufficient number of independent measurements of returned power so that local variations in scattering effectiveness could be distinguished from the statistical fluctuations associated with measurement. In general, it was possible to obtain between 50 and 100 independent samples of power from a resolved element of surface with an observing time of between 10 and 20 minutes. Thus, the rms of the intensity fluctuations associated with the scattering measurements lay between 10 and 15 percent (see Sec. VII for a graphic display of these fluctuations).

At intervals during the radar operation, the effective noise temperature of the receiving system was measured using a calibrated noise source with the antenna directed both at the moon

and at "cold" sky. Against the cold sky, typical values of 60°K were obtained, while 200°K was normal when looking at the moon. From these measurements, it was possible to calibrate the series of noise samples taken with each run in terms of effective temperature, and thus to obtain a measure of the absolute power response of the receiving system. Knowing the transmitted power (typically 200 kW, see Table IV), it was possible to relate the measurements directly to cross section. Occasional measurements of the subradar point provided an additional reference point.

The results of each observing run lasting 10 to 20 minutes were stored on slightly less than one full 2400-foot reel (at 800 lines per inch) of digital recording tape. Between 5 and 10 such runs plus a number of leading-edge runs constituted a day's or night's operation. The total of 67 subareas whose radar maps are presented in Sec. VI-A required about 10 scheduled "days" of operations.

D. Spectrum Analysis

Following the recording of "raw" data as described above, the first step in the digestion process was to perform a Fourier frequency analysis of the phase-coherent, time-sequential data. A time series of complex samples of the waveform corresponding to an echo from a region of fixed relative delay on the lunar surface was formed by selecting the appropriate quadrature pair from the data for each interpulse period. The duration of the time series was set by processing constraints (described below) at 256 interpulse intervals; this duration is called the coherent integration period (CIP). Thus, 200 such time series were formed over each CIP, corresponding to the 200 sample pairs taken within each interpulse period. Discrete Fourier analysis using the Cooley-Tukey algorithm was performed on each time series, yielding 256 complex Fourier components. The resulting frequency resolution, of course, was approximately 1/CIP.

Much of the actual programming complexity arises from the need to conserve processing time and interim data storage. The full data matrix for one CIP consists of 200 by 256 words; each 24-bit word contains the imaginary component of the complex waveform in the left-hand 12 bits, and the real component in the remainder. Such a matrix is too large to be held in normal internal core storage, and must be transferred to an external disk, with portions read back as needed.

The use of the Cooley-Tukey "Fast Fourier Transform" (see Appendix D) permits a processing speedup of about 30 times in the present program, compared with straightforward summing of successive products for each frequency component. The only limitations in its application are that one must solve for the complete set of independent output coefficients (one for each input element in the time series, or 256, here) and that these must be a number equal to an integral power of 2. The processing time for a given series of n elements is proportional to $n \log_2 n$ instead of to n^2 as in conventional programming approaches.

Following the application of the Cooley-Tukey algorithm, each of the words in the 200 by 256 output matrix of complex Fourier coefficients for one CIP had its real and imaginary parts squared and summed to obtain an estimate of the scattered power corresponding to that element. In the final mapping, discussed below, the results from all the CIP's for a given surface element were drawn together so that the final estimate of scattered power underwent significant statistical improvement. In the output of the spectral phase of the processing, however, the squared modulus of each Fourier coefficient was preserved for each delay in each CIP. Thus, the output

tape contains exactly as many data words as the input "raw" data tape. (Although the input data were complex, the real and imaginary components were packed into one word.)

In addition to the output digital magnetic tape, the estimates of power obtained at each frequency and delay were maintained in a running sum as each subsequent CIP was processed, and were printed out at the conclusion of processing. The results for delays corresponding to system noise only (see Sec. V-C above) yielded an estimate of the mean system noise, as well as of the DC detector level. The latter may differ from the mean system noise if the synchronous detectors are not perfectly balanced; the zero-frequency noise results obtained in this phase of the analysis are summed and used to obtain a correction for DC level. The other frequency components of the noise were summed to provide a background for subsequent subtraction from the mapping data. The summed data from the leading-edge runs were used to obtain corrections to the ephemeris in delay and doppler.

E. Computer Mapping

The spectral analysis described in the previous section produces a number of independent sets of samples of the scattered power resolved in delay and frequency. The primary task of the computer mapping described in this section is to assemble these sets into a map of the mean observed power distribution expressed in standard lunar coordinates. In the process of transformation, corrections and normalizations are applied to the data in order to account for background noise and variations in system sensitivity, antenna beamwidth, and the mean lunar scattering law. Thus, what is actually obtained is a surface map of the proportional departure from the mean scattering behavior at 3.8 cm.

Since the sampling of the radar waveform occurs at discrete intervals related to the available resolution, the mapping transformation is similarly discrete. But, because the transformation is changing with time during the course of a run (primarily through changes in the center-limb frequency $f_{c\ell}$ and in the doppler angle φ), the mapped result appears relatively smooth in most cases, even though the surface resolution must reflect the basic input sampling interval in delay and frequency.

A block diagram of the mapping program is given in Fig. 10, and a Fortran listing appears in Appendix E. From Fig. 10, it can be seen that there are five main phases in the processing:

(1) SETUP, in which the program is initialized and the validity of the specified input constants are checked.

(2) SELEN, in which the selenographic coordinates of each element in the output map are calculated.

(3) READIN, in which the transformation matrix elements connecting the radar and selenographic coordinates are calculated for each CIP, and in which the delay-doppler power distributions obtained from the spectrum analysis previously described are read into storage. Corresponding samples of power from consecutive sets are summed over an interval chosen so that a given transformation will not cause appreciable smearing.

(4) NORMAL, in which normalizations of several kinds are applied to the observed power.

(5) READOUT, in which the observed powers are tagged with the appropriate selenographic labels and accumulated. The final result is written on magnetic tape or optionally printed out in decimal form.

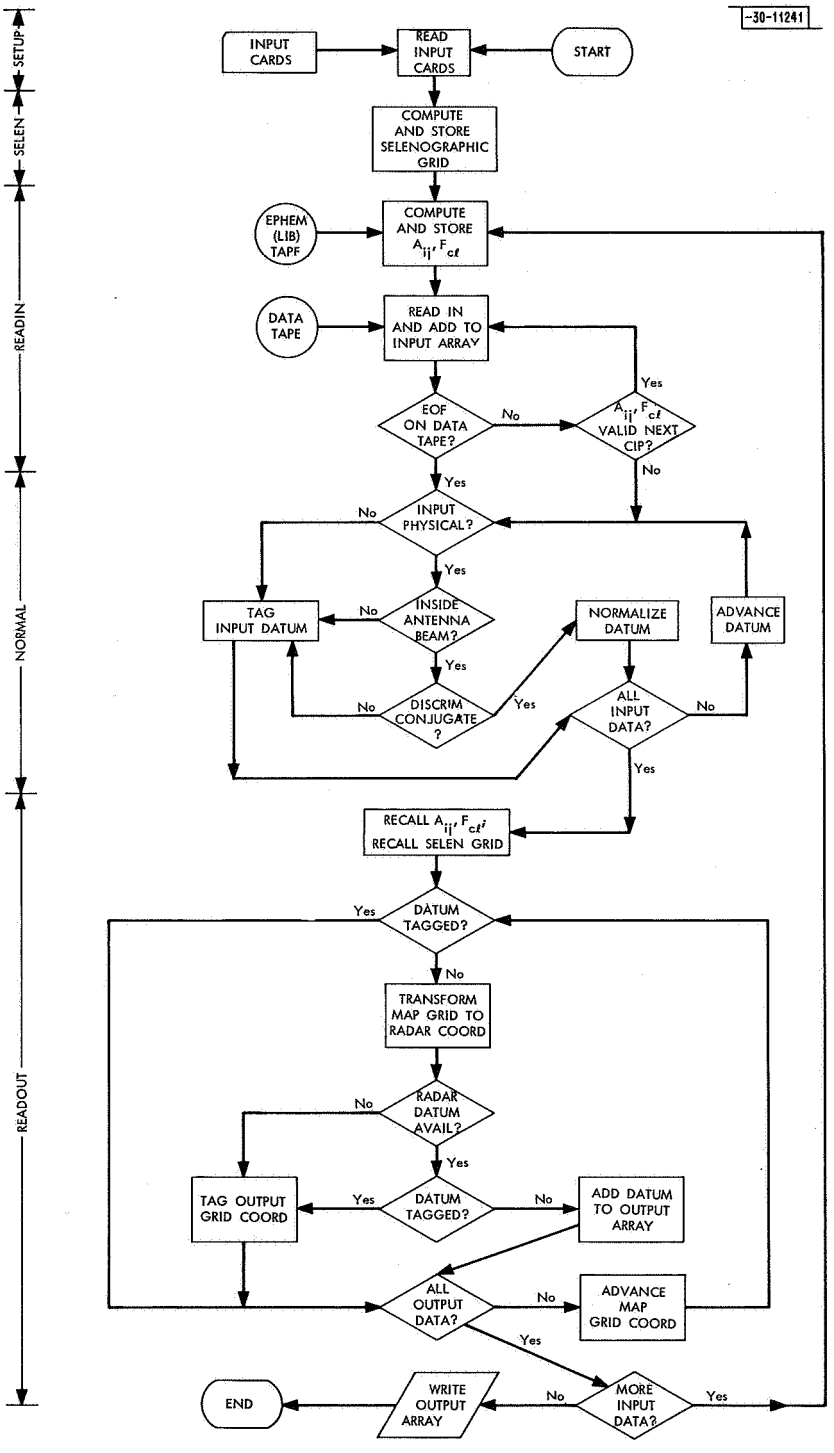

Fig. 10. Flow chart for digital computer program used in delay-doppler mapping of 3.8-cm data.

The subprograms listed above are organized and called by the master program SUPER, together with a sub-supervisory program MAIN. MAIN, followed by the five programs listed above, form overlay (1) (see Appendix E). The oscillographic display program to be described in Sec. V-F is also organized by SUPER and contained as overlay (3). In the paragraphs immediately below, the operation of the five subprograms listed above is described in some detail. Reference to Fig. 10 and Appendix E may be helpful in following the discussion.

1. SETUP

This subprogram serves to define constants used in subsequent programs and to initialize the operating conditions. It reads in, from punched cards, information which is additional to that contained on the data and ephemeris magnetic tapes. It also positions these latter tapes correctly for reading by the subsequent programs. Finally, it calculates the selenographic coordinates corresponding to the four corners of the map, and prepares a heading for the final mapped data output.

2. SELEN

This subprogram, together with its subroutine PROJECTN, calculates the Cartesian selenographic coordinates x_s, y_s, and z_s relative to the corresponding coordinates of the center of the map for each data point to be established in the output. The map, consisting of 201 by 201 resolution cells, is produced in either Mercator or orthographic projection. The type of map as well as its scale and positioning on the moon are specified through the card inputs. Obviously, it must be located within the region for which valid data exist; if portions of the specified mapping area fall outside the observed region, or fail to be adequately resolved from their conjugates by the antenna beam, they are detected and left blank by the subsequent programs.

The relationship between the location of a given cell (i, j) on the map, in Mercator projection, and the corresponding latitude β_j is

$$\beta_j = 2 \arctan \left[e^{\Delta y (j-1)} \tan (\beta_o/2 + \pi/4) \right] - \pi/2 \qquad (42)$$

where Δy is the specified cell separation at the equator, and β_o is the latitude corresponding to $j = 1$ (i.e., the southernmost). This latitude has already been calculated in SETUP such that the center of the map coincides with the desired position.

3. READIN

This subprogram first reads in from magnetic tape one set of delay-doppler radar data (corresponding to the results for one CIP) and stores this in the computer disk memory. Provision is made for storage of up to 200 by 256 values. Then, with the help of subroutine LIBREAD, it reads from the special ephemeris tape a set of values for: longitude λ_o and latitude δ_o of the subradar point, center-limb doppler frequency $f_{c\ell}$, doppler angle φ, and total echo delay to the center of the moon. The first four values are used in calculating the transformation between radar and selenographic coordinates (see below), while the total echo delay is used to normalize the power to a standard distance and to determine the angular semi-diameter of the lunar disk, needed later. These values have been prepared in advance as part of the pre-run ephemeris calculations, and are written on a special ephemeris tape (called "libration tape") specifically for use in this phase of the data reduction. Interpolation is performed in LIBREAD as necessary, to refer these values to the precise time corresponding to the delay-doppler data record.

From the ephemeris quantities, the program then proceeds to calculate the matrix elements of the transformation from selenographic to radar coordinates according to Eqs. (19) and (21), which reduce to

$$\left.\begin{aligned} A_{11} &= \cos\varphi\ \cos\lambda_o + \sin\varphi\ \sin\lambda_o\ \sin\delta_o \\ A_{12} &= -\sin\varphi\ \cos\delta_o \\ A_{13} &= -\cos\varphi\ \sin\lambda_o + \sin\varphi\ \cos\lambda_o\ \sin\delta_o \end{aligned}\right\} \tag{43a}$$

$$\left.\begin{aligned} A_{21} &= \sin\varphi\ \cos\lambda_o - \cos\varphi\ \sin\lambda_o\ \sin\delta_o \\ A_{22} &= \cos\varphi\ \cos\delta_o \\ A_{23} &= -\sin\varphi\ \sin\lambda_o - \cos\varphi\ \cos\lambda_o\ \sin\delta_o \end{aligned}\right\} \tag{43b}$$

$$\left.\begin{aligned} A_{31} &= \sin\lambda_o\ \cos\delta_o \\ A_{32} &= \sin\delta_o \\ A_{33} &= \cos\lambda_o\ \cos\delta_o \end{aligned}\right\} \tag{43c}$$

Matrix elements of Eqs. (43a) and (43c) are dimensioned into their respective units of frequency and delay by multiplying A_{1j} by $f_{c\ell}$, and A_{3j} by $2\rho_a/c$, where ρ_a is the average lunar radius (1738 km). (A_{2j} are required in the normalization calculations of Sec. V-E-4 below.) Use of the average radius here (it is also implied in $f_{c\ell}$) does not introduce significant error since only displacements from the map center are being considered, and the individual maps represent only a small fraction of the lunar surface. Variations in the lunar radius over the map compared with the map center will, of course, lead to apparent errors in position as discussed in Appendix B. Similarly, changes in parallax over the region being mapped may be ignored (parallel-ray approximation). Thus, the requirements for high accuracy are shifted into the pre-run ephemeris, which calculates the delay and doppler shift for the center of the region being mapped.

Following the calculation of the transformation matrix, the delay and doppler values corresponding to the center of the map are calculated. Differences are computed from these values for the four corners of the map. For the first set of radar data read in from tape, these differences are simply stored. The program then sums in a second set of radar data (corresponding to the next CIP) on top of the first set of data, and reads in a new set of ephemeris values appropriate for this later time. Again, it calculates the delay and doppler differences that now exist between the four map corners and the center for this later time. Then, each of these differences is compared against the corresponding difference calculated for the first CIP, and if none of the new differences departs from the former by more than the delay or doppler resolution of the input data, the program returns for a third set of radar data.

This process continues until finally a set of radar data is read in for which the selenographic-radar transformation has changed sufficiently to cause the above test to fail.* In this event, control reverts to MAIN which then calls NORMAL. The reason for summing as many successive

* Logically, this test should be performed before the new data are summed in, and this was the original intention. However, the situation described here occurred from programming oversight and, since it contributed negligible error in the present mapping work, was allowed to remain.

sets of radar data as possible, subject to negligible loss of resolution, is to reduce the number of times it is necessary to pass through the succeeding time-consuming routines: NORMAL and READOUT.

4. NORMAL

This subprogram applies a series of corrections to the delay-doppler radar measurements which have been summed in READIN. First, the average AC and DC noise background is subtracted from all data, as appropriate, followed by normalizations to account for changes in system gain, operating power levels, delay and frequency resolution, and distance to the moon. The coordinates of each delay-doppler datum are checked to make sure that (a) it corresponds to an actual location on the lunar surface, (b) it lies within an area where the two-way antenna response is down by no more than 5.5 db compared with beam center, and (c) the point corresponding to the conjugate branch of the radar coordinate y [see Eq. (17)] is suppressed by at least 6 db. Any datum which fails to pass these tests has its measured power replaced by a flag which prevents its later use in the mapping.

Next, a correction is applied to remove the average lunar scattering law. The scattering law for the polarized case is derived from measurements made at Haystack previously and reported in Vol. 1 of this Final Report. The empirical formulas used to provide an analytic approximation to the (polarized) scattering law take the forms

$$P(\Theta) \propto \frac{\cos\Theta}{(\cos\Theta + \sin\Theta/\alpha)^3} \quad , \quad 0 \leqslant \Theta \leqslant 60^\circ \tag{44a}$$

$$P(\Theta) \propto \frac{\cos\Theta}{(\cos^2\Theta + \sin^2\Theta/\alpha^2)^{3/2}} \quad , \quad 60^\circ < \Theta \leqslant 90^\circ \tag{44b}$$

In Eq. (44a), α is best fit by 0.35, while in Eq. (44b) the best fit to the measurements occurs for $\alpha = 0.295$. Over the range of angles $13^\circ < \Theta < 71^\circ$, these formulas fit the measured data to within 0.2 db. Outside this range, errors of up to 1 db may exist. Very little of the lunar surface mapped in the work reported here falls outside the 0.2-db error region. In the case of the depolarized scattering mode, an assumption of $P(\Theta) \propto \cos\Theta$ has been programmed, based on measurements at 23- and 68-cm wavelength. The actual law for 3.8 cm, however, has not yet been measured. Note that the angle of incidence Θ to the local mean surface is easily related to the radar coordinate z, through $z = \cos\Theta$.

As discussed in Sec. II-B [Eqs. (18) and (24)], a correction to account for the change in projected surface area as a function of the radar coordinate y and the center-to-limb doppler spread $f_{c\ell}$ is required. In all the mapping reported here, the local doppler angle (see Sec. V-B above) was very low and, therefore, the resolved surface element Δs was nearly rectangular in shape. In these circumstances, since $\Delta\tau \ll 2\rho/c$, and $\Delta f \ll f_{c\ell}$, Eq. (24) is applicable with negligible error.

Finally, a correction is applied for antenna beam response according to $\exp[1.3863(\Theta/\Theta_o)^2]$, where Θ is the angular departure of the position of the datum, as viewed by the radar from the center of the antenna beam, and $2\Theta_o$ is the one-way, 3-db antenna beamwidth. For Haystack, Θ_o has been chosen as 2.20 arcmin. The criterion (b) above corresponds to $\Theta = 0.95\Theta_o$, or about 2 arcmin. The Gaussian function approximates the actual beam shape to within 0.1 db over this range.

5. READOUT

This subprogram takes the normalized delay-doppler power density data resulting from the previous subprogram and assigns it to the appropriate selenographic coordinates in the output map. In detail, the coordinates of each cell of the output map, calculated above in SELEN, are first recalled from disk memory. Then, the transformation matrix calculated in READIN (for the first CIP of the summed sequence) is used to calculate the corresponding radar (delay-doppler) coordinates of each cell. If no input datum exists for the radar coordinates calculated, or if the datum has been flagged as not meeting all the criteria (a), (b), and (c) in subprogram NORMAL, that cell is assigned zero intensity. Once a cell has been so marked, it is excluded from the map even though at a later (or earlier) time the transformation had been such as to permit that cell to pass the above criteria.

Since the cell size of the output map is generally chosen to retain the resolution inherent in the radar mapping, adjacent map cells will frequently be assigned the same normalized radar datum. In the final mapping, some interpolative smoothing is performed at the boundaries of the discrete steps which result when a new radar datum is called. Nevertheless, particularly for those areas near the subradar point where the radar resolution is relatively coarse, the shape of the basic delay-doppler area resolution may sometimes be seen. This artificial appearance has been retained, since it was feared that any attempt to smooth these regions might compromise the information content of other areas in the same map.

At the conclusion of the coordinate transformation, control is returned to MAIN and the program goes to READIN to repeat the earlier incoherent summation process. The next time through READOUT, the transformed data are summed on top of the previously generated map. Thus, the statistical fluctuations in the observed scattered power are reduced inversely as the square root of the total number of CIP's available. This process continues until the entire tape of spectrum data is exhausted or until the program is stopped for other reasons. The final map, consisting of 201 by 201 cells, is written on magnetic tape preparatory to display.

F. Display of Results

The mapped data may be displayed in several ways. For detailed examination, a "power profile" which plots the measured, normalized intensity along a coordinate line is likely to be preferred. The large amount of data produced in the mapping reported here, however, calls for an additional type of display from which an overview can be obtained. The display which has been chosen for this purpose uses a computer-driven, photographed oscilloscope.

Intensity modulation is obtained by varying the display duration of each point. For this purpose, the range of intensities to be displayed is divided into 20 levels. A point having a value 10 on this scale, then, will be indicated by displaying a spot on the oscilloscope at the proper coordinate location for 10 unit intervals of time. In actuality, 20 rasters of data are displayed consecutively, with only those points which exceed a constantly increasing threshold appearing on each raster.

The oscilloscope is capable of positioning a matrix of 1000 by 1000 points. However, only about 500 by 500 positions are truly resolvable. Thus, the 201 by 201 output data matrix is interpolated (as shown in Fig. 11) to 500 by 500 points, with adjacent lines staggered by a part in 1000. In this way, the final photograph of the display appears to be continuous in texture.

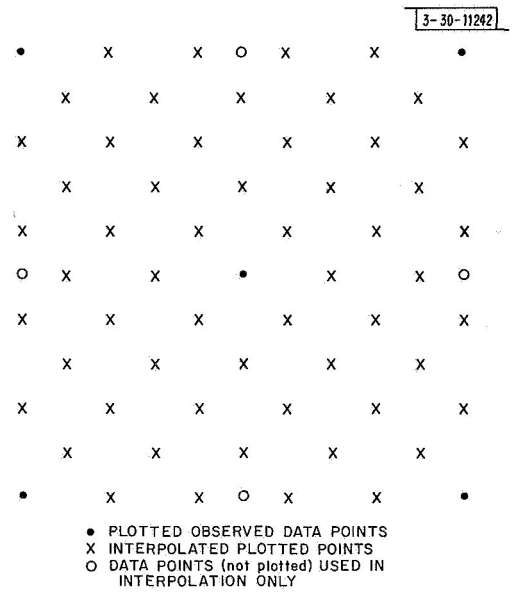

Fig. 11. Interpolation grid used in producing oscillographic display of mapped data.

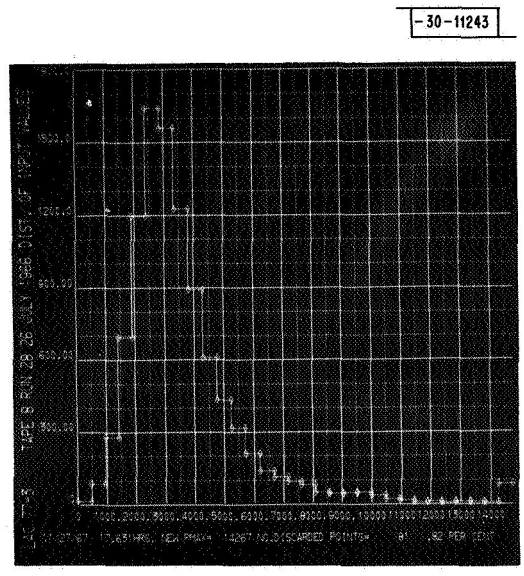

Fig. 12. Histogram showing typical intensity distribution obtained for mapped subarea. Here, intensity values above approximately 14,000 (arbitrary units) have been clipped and will all be assigned same maximum brightness in associated shaded plot.

The interpolation process serves to smooth the boundaries corresponding to the original delay-doppler resolution cells. However, because of the fineness of the plotting, no meaningful resolution is lost. The time required to produce and photograph the interpolated display varies between 60 and 100 sec on the CDC 3300 computer used, depending on the distribution of intensities.

In order to position and scale the quantized intensity levels properly, an intensity distribution of the mapped data points was first calculated and displayed, as shown in Fig. 12. In this calculation, 32 levels are linearly distributed between zero and the largest value found. If it is desired to clip some of the highest values in order to bring out detail at the lower levels, a light-gun signal will cause a new distribution to be calculated, using a maximum value which has been reduced to 80 percent of the original. This process is repeated until the desired distribution has been obtained. The final displays appeared best when the peak in the distribution was placed at about one-fourth the maximum value, for average lunar terrain. At this setting, less than 1 percent of the intensity levels are clipped. Figure 13 diagrams the steps required in producing a shaded plot of the mapped intensity.

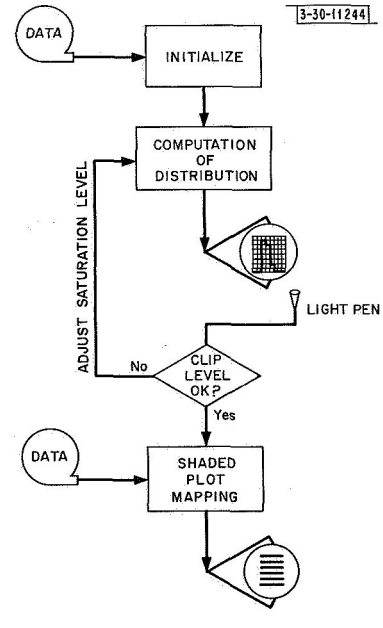

Fig. 13. Schematic flow diagram for shaded-plot program.

VI. DELAY-DOPPLER RESULTS AT 3.8 CM

A. Presentation of Maps and Description of Data Format

The delay-doppler results obtained under this contract are being reported in two ways: (1) as digital data contained on two reels of magnetic tape; (2) as photographs of computer-derived oscillographic displays. Details of the data presentation format are given below.

1. Digital Magnetic Tape Data

The data making up a map for each Lunar Aeronautical Chart (LAC) subarea, derived from a single radar run, are contained within a single file on the tape. Altogether, there are 64 files of data corresponding to the LAC subareas described in Sec. V-B (LAC 80.40 failed to process correctly and is not included, while an additional area, LAC 61.35, was found necessary to properly display the results for that region). Within each file, the first 2 records are assigned to a heading containing the information detailed in Table V (in BCD format), most of which is

TABLE V
TITLE FORMAT FOR MAGNETIC TAPE DATA
(Title Records are in BCD)

First Record		
Parameter Description	Fortran Format (BCD)	Example
Title (LAC subarea)	F5.2	56.10
Second Record		
West limit longitude of map (deg) (east longitude positive)	F5.1	−58.5
Center longitude of map (deg)	F5.1	−53.5
East limit longitude of map (deg)	F5.1	−48.5
North limit latitude of map (deg)	F7.3	+16.841
Center latitude of map (deg)	F7.3	+12.000
South limit latitude of map (deg)	F7.3	+07.071
Month/day/year of run	I6	022467
Universal Time of run (hr/min)	I4	0955
Surface resolution in delay (km)	F3.1	1.9
Surface resolution in doppler (km)	F3.1	3.9
Mean angle of incidence at map center (deg)	F5.2	52.67
Subradar selenographic longitude (deg)	F6.3	−3.476
Subradar selenographic latitude (deg)	F6.3	−5.316
Local doppler angle (see text, Sec. V-B) (deg)	F6.2	−8.32
Pulse width (μsec)	I2	10
Total CIP's in run	I2	76

necessary for interpreting the map. Following these are 201 records, each containing 201 sequential 24-bit binary words (2's complement) to express the full 201 by 201 mapped data matrix. Format is standard 7-track digital magnetic tape (6 binary data tracks plus 1 track for odd cross-tape parity) recorded at 556 bits per inch.

The data are stored with each record corresponding to a row of constant latitude, starting at the southernmost latitude and westernmost longitude (lower left-hand corner of the map). The latitudes and longitudes for each corner, as well as the center of the map, are given in the heading (see Table V). Note that selenographic coordinates are positive to the east and north. The latitudes corresponding to intermediate rows may be calculated from Eq. (42). Two sets of these tapes are being forwarded to the contracting agency (c/o the National Space Science Data Center, Goddard Space Flight Center, Greenbelt, Maryland) with this report.

2. Oscillographic Displays

Intensity displays of the 64 subareas have been prepared as described in Sec. V-F, and have been assembled into a mosaic of the equatorial region as shown in the frontispiece and in Figs. 14(a), 15(a), and 16(a). On the pages facing each of these figures are shown the approximate locations and identifications of each of the LAC subareas comprising the mosaic (labeled Figs. 14(b), 15(b), and 16(b), respectively). The relevant information for each of these subareas, contained in the magnetic tape headings (see Table V), is shown in Tables VI, VII, and VIII, corresponding to Figs. 14(b), 15(b), and 16(b), respectively.

Each subarea covers a region precisely ±5° in longitude about the map center. In latitude, because of the Mercator projection, the span is slightly less: for maps whose centers lie at ±12° latitude, the corresponding limits in latitude are ±7.071° and ±16.81°; for centers at ±4° latitude, the limits are ∓0.997° and ±8.966°. In many cases, adjacent subareas overlapped; this redundancy was useful in building up the mosaics shown. Small discrepancies between the nominal coordinates specified on the tape headings and actual locations as deduced from comparison against optical maps may be noted. In most cases, these discrepancies do not exceed 0.25°, although in a few instances, near the prime meridian, departures of up to 0.5° are seen. The discrepancies are probably related to difficulties in the accuracy of the basic mapping ephemeris, but may also depend in part on topography (see Appendix B).

Because of their special interest, several maps were also obtained for regions lying outside the basic "Apollo Zone." In order to test the applicability of the delay-doppler mapping technique near the lunar limb, Fig. 17 was prepared. Here, the resolution in longitude (delay) is about 0.05° or 1.5 km, and in latitude (frequency) about 0.1° or 3 km. Because of the reduced signal level for echoes from the limb, some noise may be seen in the regions of low intensity. Nevertheless, the resolution is substantially better than that available from the very best ground-based telescopic observations.

Figures 18 and 19 show the mapped (normalized) reflectivity in the vicinity of the crater Tycho using delay resolutions of 10 and 5 μsec, respectively. Tycho has long been known to scatter decimeter radiowaves considerably more effectively than the lunar average, and, because of the concentration of attention it has received, it serves as a point of reference for lunar scattering calibrations. In these maps, an orthographic projection system of coordinates has been used (see Sec. V-E), in order to compare better with telescopic photographs (no LAC for this area was available at the time of the measurements). Surface resolutions of about 2 and 1 km were obtained in Figs. 18 and 19, respectively.

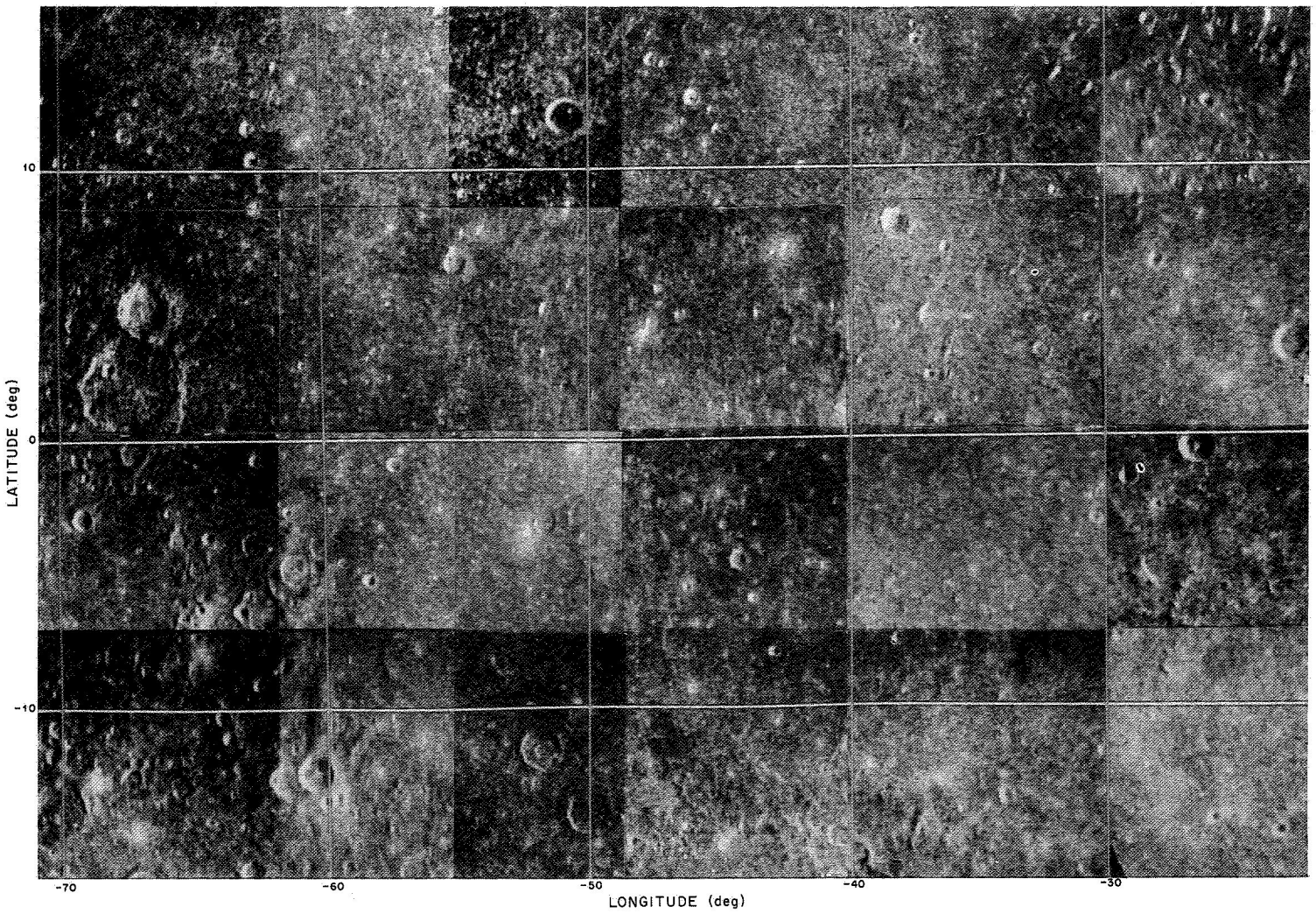

Fig. 14(a). Mosaic of 3.8-cm radar maps (polarized component) for equatorial longitude range −70° to −25°.

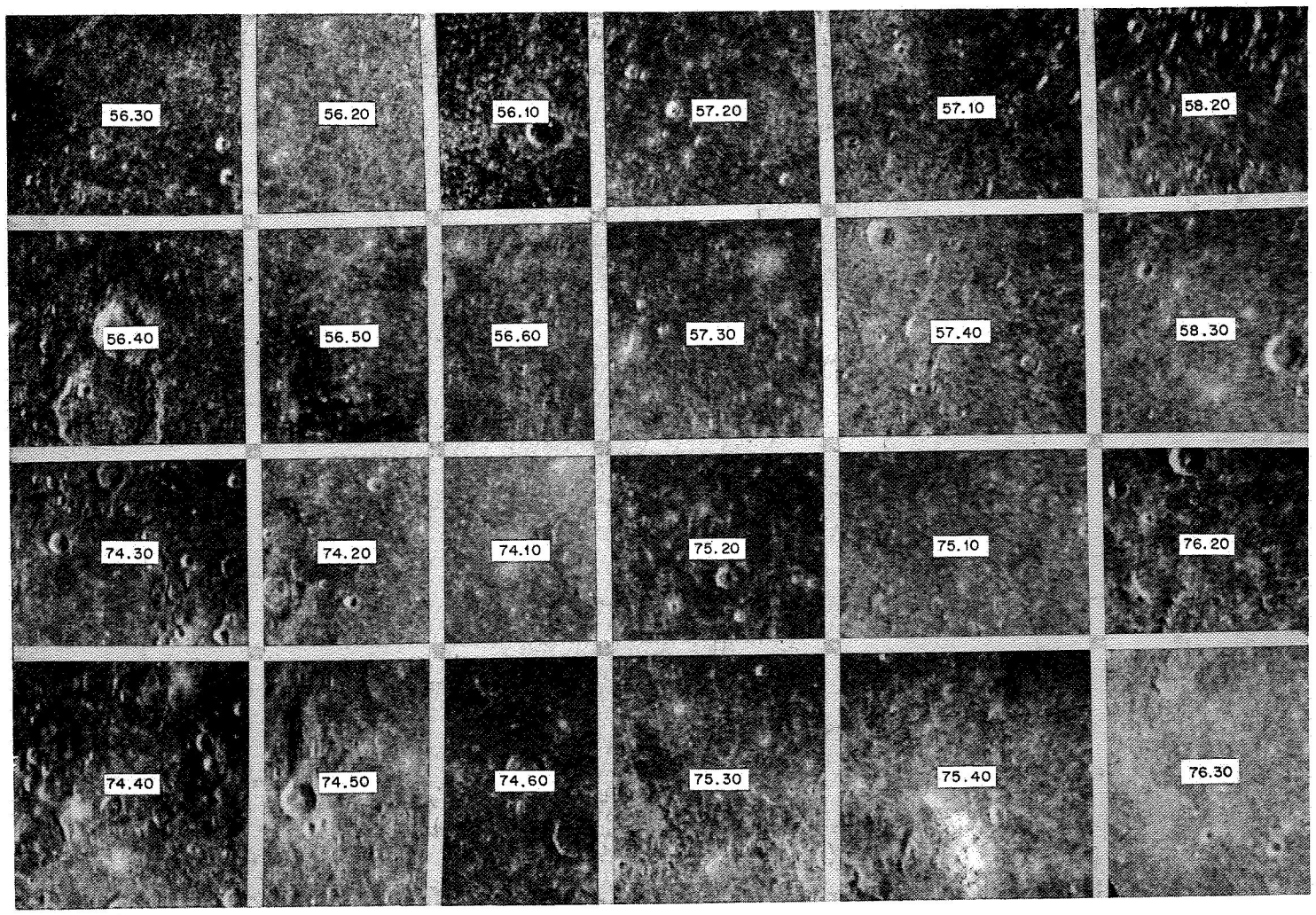

Fig. 14(b). Location key for identifying individual radar runs described in Table VI.

-30-11247

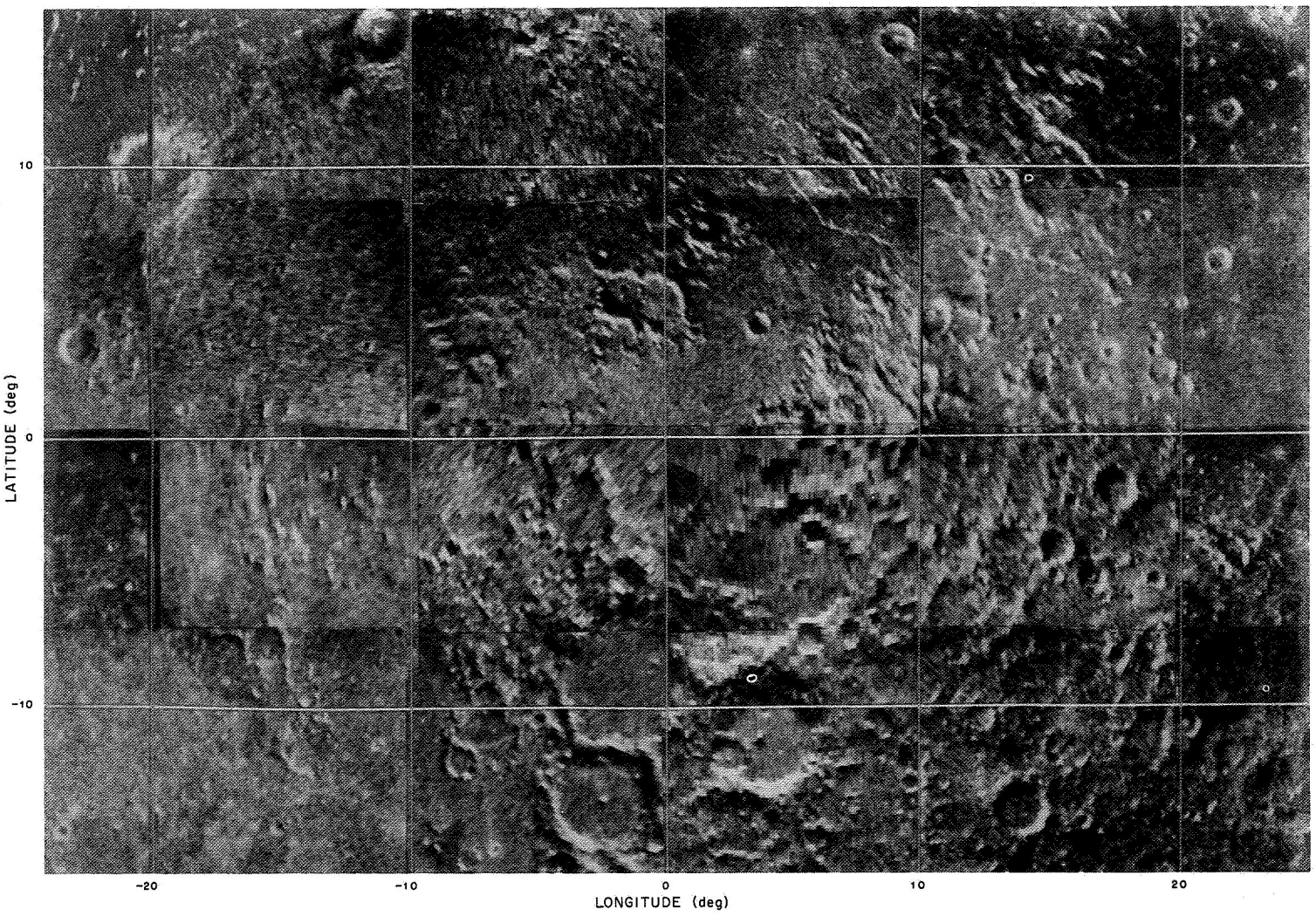

Fig. 15(a). Mosaic of 3.8-cm radar maps (polarized component) for equatorial longitude range −25° to +25°.

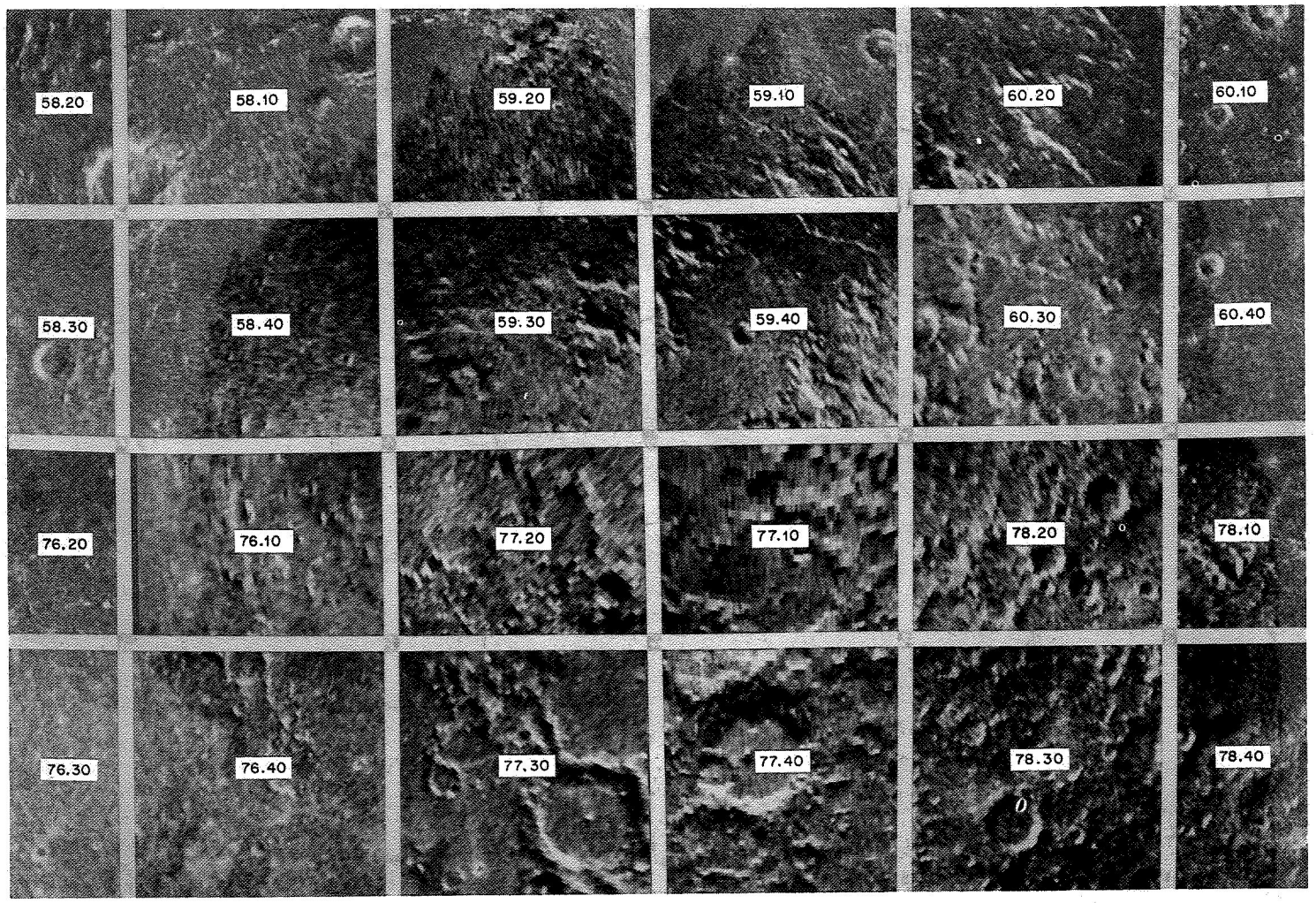

Fig. 15(b). Location key for identifying individual radar runs described in Table VII.

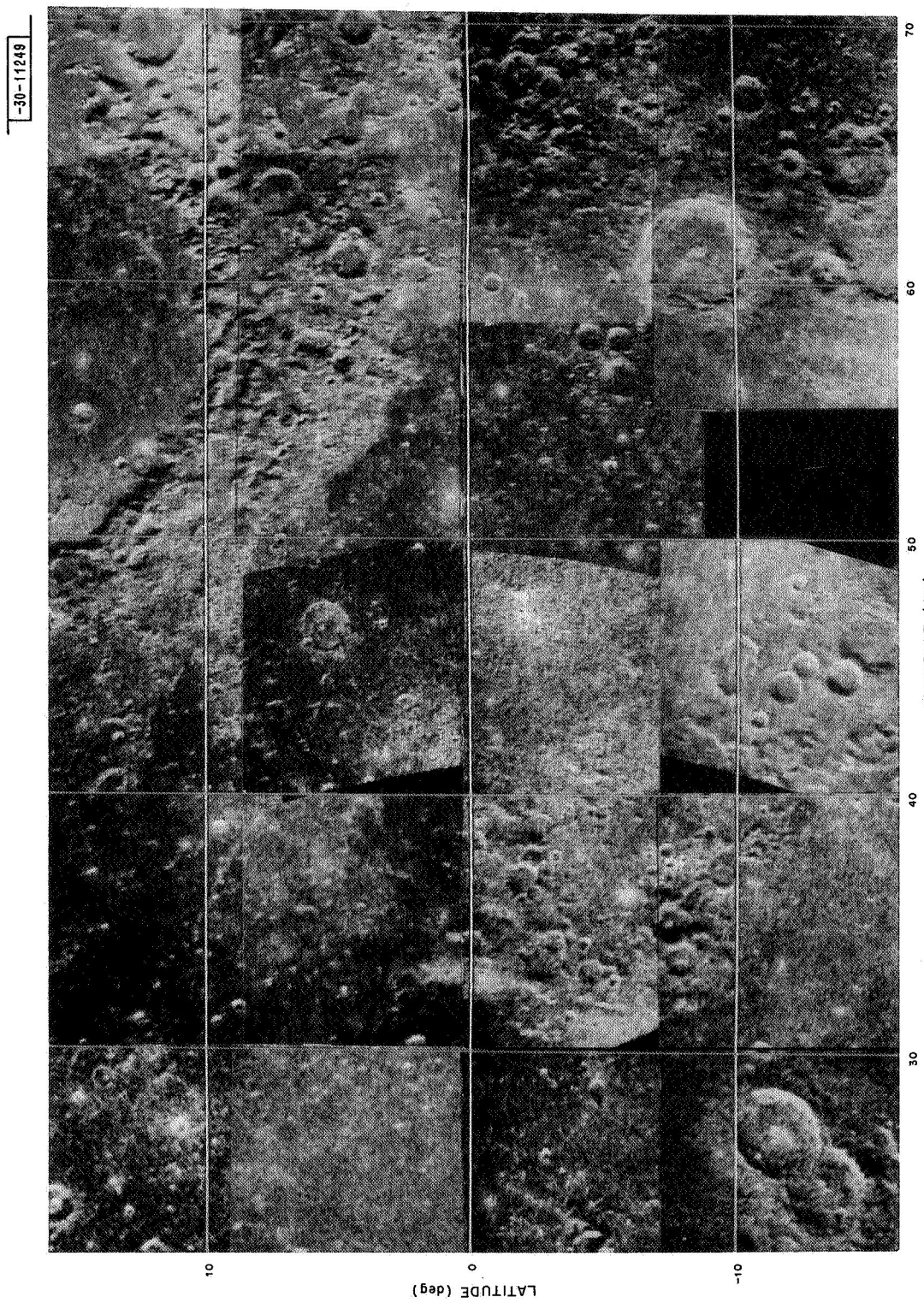

Fig. 16(a). Mosaic of 3.8-cm radar maps (polarized component) for equatorial longitude range +25° to +70°.

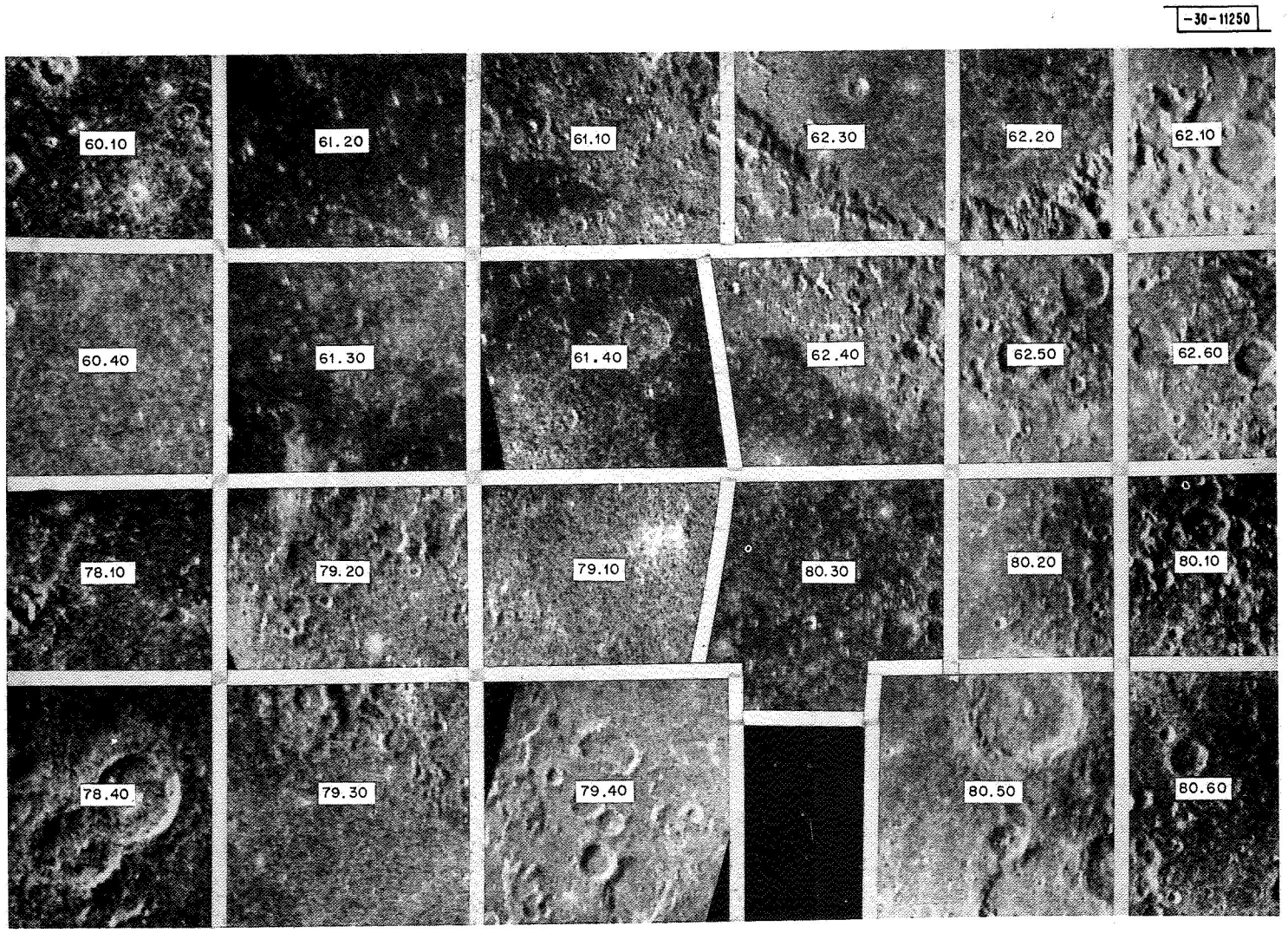

Fig. 16(b). Location key for identifying individual radar runs described in Table VIII.

TABLE VI

INFORMATION RELEVANT TO FIG. 14(b)

LAC Subarea	Map Center		Date of Run	Universal Time of Run	Surface Resolution		Incident Angle (deg)	Subradar		Local Doppler Angle (deg)	Pulse Width (μsec)	Total CIP's
	Longitude (deg)	Latitude (deg)			Delay (km)	Doppler (km)		Longitude (deg)	Latitude (deg)			
56.10	−53.5	+12.0	2/24/67	0955	1.9	3.9	52.67	−3.476	−5.316	−8.32	10	76
56.20	−60.0	+12.0	3/20/67	1915	1.8	3.8	55.43	−7.232	−5.893	−3.04	10	39
56.30	−66.5	+12.0	3/23/67	0725	1.7	4.1	62.49	−6.233	−5.739	−1.68	10	24
56.40	−66.5	+4.0	3/23/67	0708	1.7	4.1	60.96	−6.240	−5.765	−2.32	10	18
56.50	−60.0	+4.0	3/20/67	1850	1.9	3.9	53.62	−7.218	−5.852	−2.85	10	50
56.60	−53.5	+4.0	2/24/67	0905	1.9	4.0	50.81	−3.508	−5.393	−1.34	10	36
57.10	−35.0	+12.0	2/21/67	2235	2.7	4.3	34.04	−5.970	−6.044	−8.72	10	50
57.20	−45.0	+12.0	3/23/67	0750	2.2	4.0	42.44	−6.215	−5.702	−5.05	10	40
57.30	−45.0	+4.0	12/22/66	1855	2.2	4.3	42.12	−2.842	+2.303	−15.65	10	55
57.40	−35.0	+4.0	2/21/67	2145	2.9	4.5	30.70	−5.931	−5.981	−1.14	10	42
58.20	−25.0	+12.0	12/21/66	1955	3.6	3.2	24.47	−1.801	+3.549	−27.43	10	48
58.30	−25.0	+4.0	1/31/67	0435	3.0	4.0	29.67	+4.015	−2.287	+13.43	10	36
74.10	−53.5	−4.0	3/20/67	1825	2.1	3.7	46.14	−7.211	−5.809	−2.65	10	63
74.20	−60.0	−4.0	3/23/67	0635	1.9	4.1	53.57	−6.246	−5.818	+0.67	10	35
74.30	−66.5	−4.0	3/20/67	1750	1.7	3.6	59.07	−7.214	−5.747	+4.48	10	59
74.40	−66.5	−12.0	3/20/67	1725	1.8	3.5	58.81	−7.226	−5.701	+4.26	10	56
74.50	−60.0	−12.0	3/23/67	0535	1.9	3.6	53.39	−6.222	−5.919	+7.47	10	44
74.60	−53.5	−12.0	3/20/67	1705	2.1	3.3	46.09	−7.241	−5.665	+9.78	10	37
75.10	−35.0	−4.0	1/24/67	2240	3.0	3.8	30.09	−4.839	−5.447	−4.34	10	38
75.20	−45.0	−4.0	2/21/67	2055	2.4	4.1	38.97	−5.921	−5.907	+3.74	10	36
75.30	−45.0	−12.0	2/21/67	2010	2.4	3.6	39.04	−5.938	−5.833	+7.44	10	51
75.40	−35.0	−12.0	1/24/67	2105	3.0	3.1	30.50	−4.877	−5.301	+10.79	10	42
76.20	−25.0	−4.0	3/28/67	0420	3.0	3.0	29.53	+4.221	+0.429	+13.80	10	51
76.30	−25.0	−12.0	2/3/67	0925	2.7	3.0	34.17	+5.872	+3.027	+14.26	10	49

TABLE VII

INFORMATION RELEVANT TO FIG. 15(b)

LAC Subarea	Map Center		Date of Run	Universal Time of Run	Surface Resolution		Incident Angle (deg)	Subradar		Local Doppler Angle (deg)	Pulse Width (μsec)	Total CIP's
	Longitude (deg)	Latitude (deg)			Delay (km)	Doppler (km)		Longitude (deg)	Latitude (deg)			
58.10	−15.0	+12.0	2/21/67	2335	4.3	3.7	20.17	−6.051	−6.102	+0.06	10	39
58.20	−25.0	+12.0	12/21/66	1955	3.6	3.2	24.47	−1.801	+3.549	−27.43	10	48
58.30	−25.0	+4.0	1/31/67	0435	3.0	4.0	29.67	+4.015	−2.287	+13.43	10	36
58.40	−15.0	+4.0	1/31/67	0415	4.4	4.1	20.03	+4.015	−2.320	+12.53	10	24
59.10	+5.0	+12.0	3/21/67	0335	2.0	3.5	22.35	−8.309	−6.010	+2.02	5	45
59.20	−5.0	+12.0	2/22/67	0030	4.8	3.4	18.17	−6.151	−6.136	+15.24	10	28
59.30	−5.0	+4.0	3/21/67	0230	4.1	2.8	10.56	−8.187	−6.071	−3.65	5	43
59.40	+5.0	+4.0	3/21/67	0410	2.6	4.0	16.65	−8.357	−5.972	+9.41	5	33
60.10	+25.0	+12.0	2/24/67	0630	2.7	3.0	33.34	−3.432	−5.668	+1.25	10	36
60.20	+15.0	+12.0	2/24/67	0615	3.5	3.0	25.46	−3.413	−5.695	−7.23	10	54
60.30	+15.0	+4.0	1/24/67	2045	4.0	2.9	21.93	−4.899	−5.262	+7.37	10	42
60.40	+25.0	+4.0	1/24/67	2125	2.9	3.2	31.25	−4.859	−5.339	+3.77	10	42
76.10	−15.0	−4.0	3/28/67	0435	4.4	4.5	19.70	+4.203	+0.466	+12.92	10	86
76.20	−25.0	−4.0	3/28/67	0420	3.0	3.0	29.53	+4.221	+0.429	+13.80	10	51
76.30	−25.0	−12.0	2/3/67	0925	2.7	3.0	34.17	+5.872	+3.027	+14.26	10	49
76.40	−15.0	−12.0	2/3/67	0955	3.5	2.8	25.60	+5.806	+3.091	+10.47	10	47
77.10	+5.0	−4.0	2/7/67	1445	7.7	2.7	11.213	+4.785	+7.211	+0.06	10	58
77.20	−5.0	−4.0	2/3/67	0940	6.7	2.9	12.93	+5.840	+3.060	+12.62	10	42
77.30	−5.0	−12.0	2/3/67	1010	4.7	2.7	18.53	+5.771	+3.122	−4.59	10	78
77.40	+5.0	−12.0	2/7/67	1430	4.6	2.7	19.21	+4.833	+7.211	−0.97	10	54
78.10	+25.0	−4.0	2/24/67	0810	3.1	3.6	28.45	−3.509	−5.488	+6.54	10	44
78.20	+15.0	−4.0	12/22/66	2100	4.6	2.9	19.00	−3.014	+2.086	−26.79	10	27
78.30	+15.0	−12.0	12/22/66	2115	3.9	2.5	22.78	−3.045	+2.057	−9.03	10	28
78.40	+25.0	−12.0	12/22/66	2045	2.9	2.8	31.18	−2.984	+2.115	−15.12	10	26

TABLE VIII

INFORMATION RELEVANT TO FIG. 16(b)

LAC Subarea	Map Center		Date of Run	Universal Time of Run	Surface Resolution		Incident Angle (deg)	Subradar		Local Doppler Angle (deg)	Pulse Width (μsec)	Total CIP's
	Longitude (deg)	Latitude (deg)			Delay (km)	Doppler (km)		Longitude (deg)	Latitude (deg)			
60.10	+25.0	+12.0	2/24/67	0630	2.7	3.0	33.34	−3.432	−5.668	+1.25	10	36
60.40	+25.0	+4.0	1/24/67	2125	2.9	3.2	31.25	−4.859	−5.339	+3.77	10	42
61.10	+45.0	+12.0	2/21/67	1950	1.9	3.3	53.70	−5.954	−5.798	+4.94	10	30
61.20	+35.0	+12.0	2/21/67	1930	2.1	3.2	44.45	−5.975	−5.763	+6.99	10	70
61.30	+35.0	+4.0	1/24/27	2200	2.3	3.6	40.89	−4.841	−5.405	−2.46	10	66
61.35	+40.0	+4.0	2/24/67	0715	2.1	3.4	44.47	−3.478	−5.587	+9.36	10	56
61.40	+45.0	+4.0	1/24/67	2220	1.9	3.7	50.66	−4.838	−5.442	−5.16	10	30
62.10	+66.5	+12.0	3/29/67	0500	1.7	2.5	60.89	+5.799	+2.265	+7.56	10	35
62.20	+60.0	+12.0	3/23/67	0520	1.6	3.5	68.23	−6.210	−5.945	+4.38	10	37
62.30	+53.5	+12.0	2/24/67	0650	1.7	3.3	59.31	−3.454	−5.632	+6.36	10	50
62.40	+53.5	+4.0	3/23/67	0600	1.7	3.8	60.47	−6.237	−5.877	+3.50	10	68
62.50	+60.0	+4.0	3/28/67	0315	1.8	2.6	55.80	+4.276	+0.268	+4.10	10	62
62.60	+66.5	+4.0	3/29/67	0440	1.7	2.6	60.60	+5.823	+2.216	+10.42	10	54
78.10	+25.0	−4.0	2/24/67	0810	3.1	3.6	28.45	−3.509	−5.488	+6.54	10	44
78.40	+25.0	−12.0	12/22/66	2045	2.9	2.8	31.18	−2.984	+2.115	−15.12	10	26
79.10	+45.0	−4.0	12/21/66	1835	2.0	4.6	47.27	−1.677	+3.663	−23.50	10	40
79.20	+35.0	−4.0	12/21/66	1855	2.5	4.1	37.46	−1.701	+3.637	−27.58	10	36
79.30	+35.0	−12.0	2/21/67	2120	2.3	4.3	40.83	−5.922	−5.945	+2.96	10	35
79.40	+45.0	−12.0	12/21/66	1915	2.0	3.6	49.00	−1.730	+3.609	−19.25	10	70
80.10	+66.5	−4.0	3/29/67	0420	1.7	2.8	60.93	+5.843	+2.166	+13.02	10	59
80.20	+60.0	−4.0	3/29/67	0400	1.8	2.8	54.45	+5.858	+2.117	+12.88	10	60
80.30	+53.5	−4.0	2/24/67	0830	1.8	3.9	56.82	−3.513	−5.452	+1.85	10	51
80.40	+53.5	−12.0	—	—	—	—	—	—	—	—	—	—
80.50	+60.0	−12.0	3/28/67	0210	1.8	2.9	56.59	+4.286	+0.114	+4.80	10	56
80.60	+66.5	−12.0	3/29/67	0335	1.7	2.9	61.84	+5.871	+2.055	+11.58	10	70

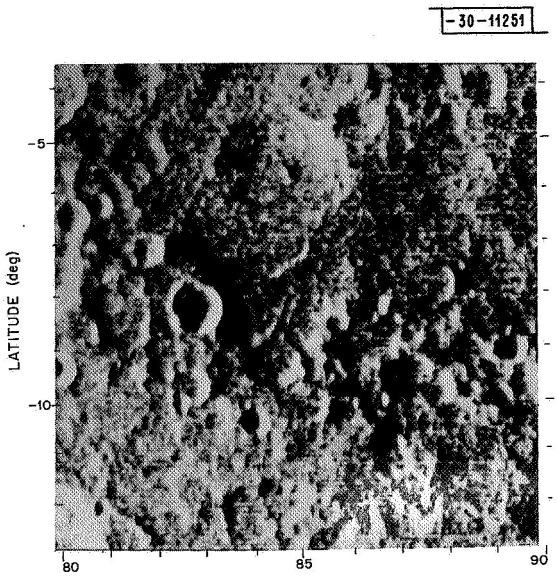

Fig. 17. Delay-doppler, 3.8-cm radar map (polarized component) for region near easterly limb of moon.

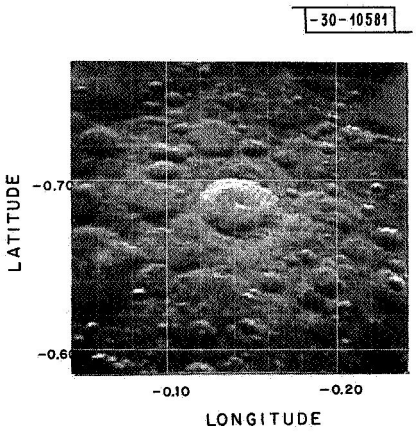

Fig. 18. Delay-doppler map at 3.8 cm (polarized component) for region surrounding crater Tycho (coordinates shown in orthographic direction cosines). Delay resolution was 10 μsec, corresponding to effective surface resolution of about 2 km.

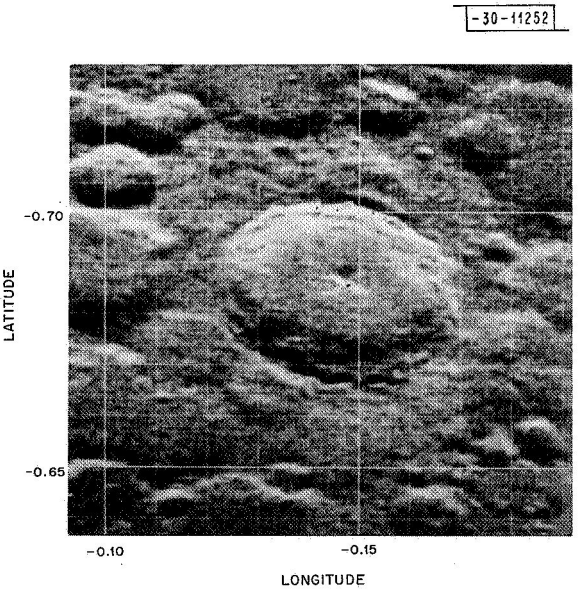

Fig. 19. Same region as shown in Fig. 18, but with delay resolution improved to 5 μsec (1-km surface resolution).

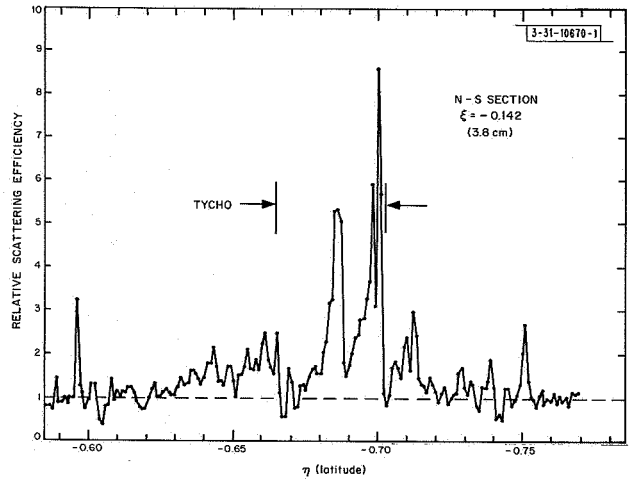

Fig. 20. Intensity profile of radar scattering shown in Fig. 18, taken along north-south line running through approximate center of Tycho. Large peaks correspond to regions where local surface normal is inclined toward radar, improving efficiency of quasi-specular scattering mechanism.

In order to show more quantitatively the variation from the mean scattered power, plots of the intensity data given in Fig. 18 have been made through the approximate center of Tycho along lines of constant latitude and longitude in Figs. 20 and 21, respectively. These plots show very clearly the enhancement in the echo associated with a localized, highly inclined slope facing the radar, such as is found in the near inner walls of recently formed craters, and in the central peak of Tycho. Also evident, particularly in Fig. 20, is a generalized increase in scattering thought to be associated with exceptional roughness in the Tycho area [Pettengill and Henry (1962); Pettengill and Thompson (1968)]. In these plots, the intensity scale has been normalized to unity at the level predicted by the mean lunar scattering law at each delay.

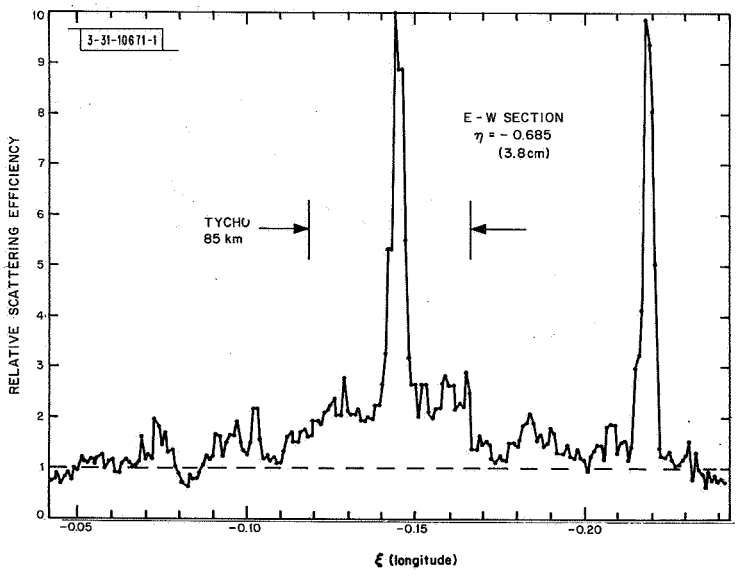

Fig. 21. Intensity profile of radar scattering shown in Fig. 18, taken along east-west line running through approximate center of Tycho. In addition to large quasi-specular peaks, note generalized enhancement associated with crater.

B. Tabulation of Measured Delays and Dopplers

As described in Sec. V, observations with the radar beam directed at the subradar point were made during the course of a day's operation. These measurements yielded a determination of the scattered power distribution in delay from which the absolute delay to the nearest portion of the lunar surface could be inferred. In order to reduce the biasing effects of contributions away from the subradar point, only the power densities contained in a narrow frequency interval centered on the scattered spectrum were considered. In fact, the limit to measurement accuracy in the determination of absolute delay was set by the finite data sampling interval. In most cases, interpolation was possible to about one-third the pulse width used. The results obtained are given in Table IX.

TABLE IX

OBSERVED ECHO DELAYS AND DOPPLER SHIFTS FOR LUNAR SURFACE HAYSTACK RADAR

Date	Universal Time (UTC)*	Observed Delay to Lunar Surface (msec)	Error (μsec)	Observed Doppler Shift at 7840 MHz (Hz)	Error (Hz)
21 December 1966	2050	2647.330	±3	+14,844.09	±0.15
	2200	2640.372	3	+10,965.50	
22 December 1966	1840	2648.483	3	+19,321.31	
	2130	2625.053	3	+15,309.03	
24 January 1967	2030	2475.930	3	+17,463.76	
	2300	2455.293	3	+17,487.49	
31 January 1967	0400	2436.890	3	+14,945.34	
	0515	2428.782	3	+13,042.38	
3 February 1967	1025	2499.457	3	+3,638.15	
7 February 1967	1500	2597.683	3	+864.79	
21 February 1967	1920	2468.909	5	+18,294.78	
	2050	2455.988	3	+18,850.47	
	2255	2438.975	5	+16,054.65	
24 February 1967	0735	2367.506	3	−9,879.90	
	1020	2384.089	3	−15,198.50	
20 March 1967	1815	2512.873	3	+19,078.20	
	1940	2500.685	3	+18,065.73	
21 March 1967	0010	2475.190	3	+4,677.06	
	0115	2473.913	2	+454.23	
	0245	2475.507	2	−4,925.99	
	0355	2479.089	2	−8,288.80	
23 March 1967	0505	2396.481	3	−7,546.42	
	0625	2402.283	3	−11,159.90	
	0815	2412.888	3	−13,480.27	
29 March 1967	0520	2405.355	3	+5,871.32	

*Referred to instant of reception of signals.

TABLE X

OBSERVED DOPPLER SHIFTS
FOR LUNAR SURFACE, 25-26 JULY 1966
HAYSTACK RADAR

Date (1966)	Universal Time (UTC)*	Observed Doppler Shift at 7840 MHz (Hz)	Error (Hz)
25 July	2018	+9414.65	±0.15
	2054	+7563.53	
	2104	+7004.21	
	2210	+2918.18	
	2314	−1471.97	
	2318	−1752.84	
26 July	0014	−5675.11	
	0058	−8646.39	
	0116	−9806.32	
	0120	−10058.61	
	0210	−13005.49	
	0214	−13222.57	
	0300	−15482.57	
	0304	−15656.85	

*Referred to instant of reception of signals.

The doppler shift associated with the motion of the lunar center of mass was inferred from the mean position of the sharply defined edges of a spectrum obtained at a delay which exceeded the delay to the subradar point. If the echo were free from noise and the moon a perfect sphere, this mean value would be identical to the frequency of the echo from the subradar point (and, assuming uniform mass density distribution, to the doppler shift to be associated with the lunar center of mass). Since these conditions are not perfectly satisfied, this frequency was obtained by averaging the results corresponding to about a dozen independent delays positioned substantially later than (i.e., "behind") the subradar point. An estimate of the error was obtained by observing the consistency between the results for different delays; in no case did variations occur which exceeded about 0.05 Hz. The results obtained are given in Tables IX and X, the latter containing 14 values spread over 7 hours of observation to investigate short-period ephemeris errors. The measurement errors quoted (0.15 Hz) were obtained by tripling the maximum internal inconsistency observed, and are felt to be conservative.

VII. DISCUSSION OF 3.8-CM RESULTS

A. Radar Maps

In the radar maps shown in Figs. 14 through 19, the visual aspect which most immediately strikes the eye is a close resemblance to telescopic photographs. This resemblance, insofar as it relates to localized inclined slopes on the lunar surface, is real. The detailed reflection properties which underlie the optical and radar maps, however, are quite different. In the radar case, where the illuminating and observing directions are coincident (i.e., the "full moon"),

systematic departures from the horizontal of the local surface are converted to variations in scattered intensity through the radar angular scattering law. Since a correction is being applied according to Eq. (44) for the scattering expected on the basis of a horizontal mean slope, departures will serve to increase the observed scattering if tilted to more nearly face the radar direction, and to decrease the scattering if tilted away. At optical wavelengths, where the backscattering is associated with an almost perfectly rough surface, almost no intensity variation corresponding to surface slopes occurs when observing at full moon. It is only when the illumination is sufficiently oblique to permit partial shadowing by the surface irregularities that the presence of local slope variations is seen.

Intensity variations related to surface inclinations can usually be distinguished by the proximity of enhanced and suppressed echoing regions which are a consequence of surface continuity. This association is most dramatically apparent in the geometrical regularity of a crater, but may also be seen, for example, in the mountainous region to the south of Mare Crisium (Fig. 16, +10° latitude, +50° to +65° longitude). A second type of scattering mechanism is related to a surface containing irregularities on the scale of the radar wavelength. This type of scattering, called diffuse, is characterized by only a very slight dependence on the angles of illumination and observation, and by a high degree of depolarization in the scattered power as compared with the "normal" or quasi-specular component of the scattering law (see Vol. 1 of this report). In the present series of observations, instrumental limitations prevented measurement of the amount of depolarization at 3.8 cm. Nevertheless, inspection of the results shown in Figs. 14 through 16 will disclose a number of instances of localized enhancement which do not appear to be related to local variations in surface slope. These tend to be more visible at high longitudes, where the scattering angles are large with respect to the mean surface normal and where, therefore, the diffuse scattering tends to predominate.

In attempting to locate these regions of increased local surface roughness, an estimate must be made first of the fluctuations in observed echo intensity which are a consequence of the observation statistics. Since the power sample obtained in a given delay-doppler measurement corresponding to one CIP is the resultant of a random addition in voltage of contributions from many, phase incoherent, small surface scattering elements distributed over the resolution cell, it represents only one sample from a (presumably) Gaussian distribution. As the number of independent power samples increases, their average represents more closely the mean scattering power from the resolved surface element, of course, with an uncertainty proportional to the inverse square root of their number. In order to help estimate the magnitude of this intrinsic fluctuation as a function of the number of CIP's employed, Fig. 22(a-d) has been prepared. The right-hand columns of Tables VI, VII, and VIII list the number of CIP's which have been used in the preparation of each LAC subarea; thus, reference to the relevant panel of Fig. 22 will give an indication of the intrinsic fluctuation to be expected in the results for each subarea.

Referring to Figs. 14, 15, and 16, we note a number of relatively small, light-colored regions which appear to result primarily from locally enhanced diffuse scattering. Most of these are probably associated with ejecta from relatively recent meteoric impacts. Table XI lists the coordinates of the more prominent of these. A quantitative investigation of their scattering properties is being left to a later joint effort comparing these results with those obtained at 70-cm wavelength by Cornell University. A search at the five locations chosen as prime Apollo landing sites (41°40'W, 1°40'N; 36°05'W, 3°30'S; 1°20'W, 0°25'N; 23°37'E, 0°45'N; and 34°00'E, 2°40'N) disclosed no unusual scattering in their vicinity.

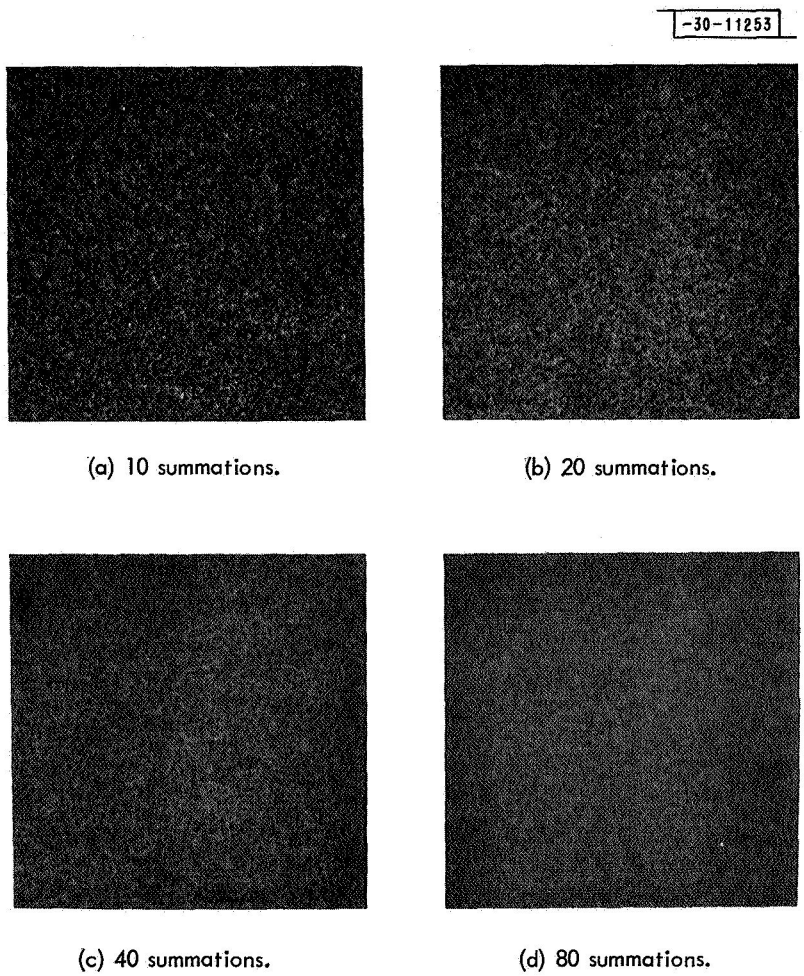

(a) 10 summations.

(b) 20 summations.

(c) 40 summations.

(d) 80 summations.

Fig. 22(a-d). Demonstration of intrinsic intensity fluctuations associated with finite number of spectra which have been incoherently summed to form a given map. These noise samples may be used, together with data of Tables VI, VII, and VIII, to estimate significance of fluctuations observed in mapped lunar data.

TABLE XI

LOCATION OF RELATIVELY LARGE REGIONS OF STRONGLY ENHANCED LOCAL ROUGHNESS

Identification	Longitude (deg)	Latitude (deg)	Approximate Diameter (km)
A	−68.7	−12.9	25
B	−67.0	−14.7	20
C	−64.7	−8.0	25
D	−59.8	−13.5	30
E	−52.3	−3.5	30
F	−50.5	−0.2	20
G	−48.0	+3.9	35 × 18
H	−44.9	−15.0	30 × 20
I	−42.3	+7.0	30
J	−40.3	+1.0	30 × 15
K	−36.8	−12.8	18
L	−25.8	+1.8	15
M	+32.8	0	100 × 30
N	+36.2	−6.0	18
O	+41.4	+3.1	15
P	+47.2	−2.0	50
Q	+51.7	+0.6	35
R	+53.3	+12.3	18

It is interesting to note that none of the regions listed in Table XI were located less than about 30° surface arc from the subradar point at the time of observation. According to a hypothesis which has been advanced by Pettengill and Thompson (1968), based on the observed mean scattering laws, one should not expect to see an enhancement caused by increased local surface roughness at distances less than about 23° from the subradar point. In fact, inside this zone the effect of increased local roughness, compared with the lunar average, should decrease the normalized radar scattering. A possible example of this phenomenon may be seen in the floor of crater Réamur about 3° south of the center of Fig. 15(a), although other explanations can, of course, be put forward. More definitive conclusions can be drawn concerning surface roughness, particularly near the subradar point, when depolarized observations become available at 3.8 cm.

B. Comparison of Observed and Theoretical Delays and Dopplers

Values for the time-of-flight and doppler frequency shift of radar echoes received from the lunar subradar point have been given in Tables IX and X of Sec. VI-B. Those values have been compared against the Brown lunar ephemeris, as corrected by Eckert [Eckert, Walker, and Eckert (1966); Mulholland and Block (1967)], using the additional constants listed in Table XII, to obtain the residuals shown in Table XIII and in Fig. 23. As may be seen, the residuals are in many cases, particularly for the doppler results, significantly larger than the corresponding errors of measurement.

A number of possible explanations for these residuals have been investigated. In addition to possible errors in the basic ephemeris, variations in surface topography – i.e., departures of the lunar radius from 1738 km at the subradar point – could obviously cause residuals in the observed echo delays. The data represented in Tables IX and XIII, unfortunately, do not cover the monthly track of the subradar point with sufficient redundancy to allow the two sources of error to be distinguished. Perhaps the closest match in subradar point is between the data of

TABLE XII

CONSTANTS USED
IN DERIVING LUNAR EPHEMERIS PREDICTIONS

Haystack operating frequency	7840.000 MHz
Haystack site coordinates (geocentric):	
Radius	6368.5504 km
Latitude	42.43157°N
Longitude	71.48869°W
Earth's equatorial radius (a'_e)	6378.1615 km
Velocity of light	299,792.5 km/sec
Lunar radius at subradar point	1738.0 km
Universal time "C" minus atomic time, and UTC minus UT-2 assumed as given in bulletins issued routinely by the U. S. Naval Observatory	
Atomic time minus ephemeris time taken as −32.2 sec	

TABLE XIII

RESIDUALS BETWEEN 3.8-CM LUNAR RADAR MEASUREMENTS AND ECKERT-CORRECTED BROWN THEORY

Date	UTC*	Selenographic Subradar Coordinates		Approximate Elevation Angle (deg)	Observed – Theory (DE-19) Residuals			
		Longitude (deg)	Latitude (deg)		Delay Residual (μsec)	Measurement Error (μsec)	Doppler Residual (Hz)	Measurement Error (Hz)
21 December 1966	2050	−1.93	+3.46	32	−0.6	±3	−0.51	±0.15
	2200	−2.12	+3.33	43	+0.1		−0.56	
22 December 1966	1840	−2.83	+2.33	6	−2.5		+0.13	
	2130	−3.08	+2.03	36	−1.9		−0.46	
24 January 1967	2030	−4.92	−5.23	5	−5.0		+0.64	
	2300	−4.85	−5.51	30	−7.8		−0.25	
31 January 1967	0400	+4.01	−2.34	4	−7.6		+0.27	
	0515	+4.00	−2.22	17	−4.6		+0.43	
3 February 1967	1025	+5.73	+3.15	21	+1.2		−0.30	
7 February 1967	1500	+4.74	+7.21	20	+1.8		−0.38	
21 February 1967	1920	−5.99	−5.75	6	−4.2	5	+0.44	
	2050	−5.92	−5.90	21	−8.7	3	−0.14	
	2255	−5.99	−6.07	43	−6.0	5	−0.43	
24 February 1967	0735	−3.49	−5.55	44	−3.5	3	−0.30	
	1020	−3.45	−5.28	15	−2.7		+0.05	
20 March 1967	1815	−7.21	−5.79	18	−3.9		−0.17	
	1940	−7.25	−5.93	33	−6.7		−0.42	
21 March 1967	0010	−7.83	−6.14	74	+1.4		−0.71	
	0115	−8.01	−6.12	71	−2.4	2	−1.04	
	0245	−8.22	−6.06	58	+2.1		−0.49	
	0355	−8.34	−5.99	45	+3.8		−0.34	
23 March 1967	0505	−6.20	−5.97	49	+0.5	3	−0.36	
	0625	−6.25	−5.83	34	+4.0		−0.08	
	0815	−6.19	−5.67	15	+3.1		+0.19	
29 March 1967	0520	+5.77	+2.31	20	−1.9		−0.79	

* Referred to instant of reception of signals.

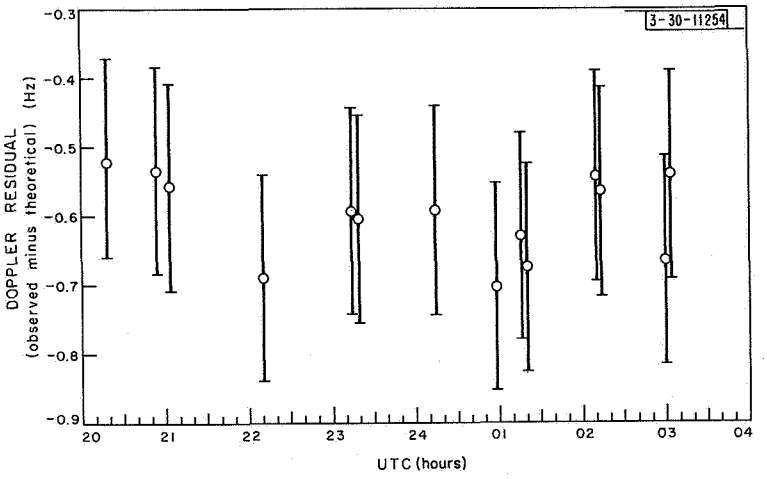

Fig. 23. Plot of doppler residuals resulting from comparison of observed data of 25-26 July 1966 with lunar orbital theory described in text.

21 February and 23 March 1967, where little agreement between the two groups of residuals appears to exist. Full comparison with the lunar topographical results reported by Shapiro, et al. (1967) has not yet been possible. Assuming 6378.1495 km for the earth's equatorial radius [as suggested by Mulholland and Block (1967)], rather than 6378.1615 km as used here, increases the delay residuals by about +5 μsec, but does not otherwise affect the results. (This change has negligible effect on the doppler residuals.)

For the doppler results, where the residuals (in terms of measurement error) are generally larger than for the delay results, other effects have been investigated [see Smith, et al. (1968)]. Because of the change in elevation angle of the radar beam during the course of an observation, the earth's atmosphere and ionosphere introduce systematic changes in the doppler shift (but do not significantly affect delay). Using a model ionosphere in which the integrated electron density in the zenith direction is $6 \times 10^{13}/cm^2$, we found that, even for the lowest elevation angles at which measurements were made, the effect on the doppler shift was always less than 10 percent of the estimated error, and thus was negligible. Except for the relatively few observations made at elevation angles less than about 10°, the correction for the neutral atmosphere, although larger than the ionospheric contribution, was substantially smaller than the quoted measurement error. The possible influence of clouds passing rapidly through the radar beam was considered as well. If conditions were to change within 10 sec from absolutely clear to cloudy, with a cloud thickness of 1 km, the concomitant effect on the doppler shift would be about 0.15 Hz; we conclude that the passage of clouds is unlikely to cause the observed discrepancies. Similar calculations of the effects of rapidly changing ionospheric conditions lead to the same conclusion.

Since the moon is ellipsoidal in shape, rather than spherical as was assumed in the calculations, the loci of constant time delay are not circular and the doppler shift inferred for the subradar point may therefore be in error. However, a simple calculation shows that the surface at the apparent lunar equator would require an ellipticity as great as 0.003 – about 15 times larger than currently believed – to induce an error in the doppler shift of even 0.1 Hz; hence, this possible source of error also is negligible. Doppler shifts attributable to polar motions and variations in the earth's rotation rate are lower by several orders of magnitude than the threshold of observability. To have an appreciable effect on the doppler shift, an error in the estimate of

the difference between universal and ephemeris time would have to exceed the published estimate of error (±0.1 sec) by a factor greater than 10.

The remaining aspect of the theoretical model to be investigated is the assumed location of the radar site. To check on possible errors in surveying (or modeling of the spheroid), we investigated the effects of variation in site coordinates. Since, for the observations under discussion, the effect of change in the station altitude could be almost exactly duplicated by a suitable change in its latitude, only variations in latitude and longitude were considered. The making of a weighted-least-mean-square fit to the raw residuals, for estimation of corrections to the latitude and longitude, led to changes of a few seconds of arc in these coordinates. The root-mean-square values of the after-fit residuals, although of course reduced, were still essentially double the estimated errors. Thus, even following this fit, residuals with absolute values averaging about 0.3 Hz remain, corresponding to unexplained average variations of nearly 0.6 cm/sec in the radial velocity between the Haystack site and the lunar subradar point.

These unexplained doppler residuals have complicated the problem of obtaining precise selenographic coordinates during the delay-doppler mapping. The problem was minimized, but not completely corrected, by making "leading-edge" runs before and after taking mapping data (see Sec. V-B). Efforts to understand the source of these residuals and, hopefully, to improve the lunar ephemeris are continuing.

VIII. SUMMARY

The successful application of two quite different techniques to the mapping of the radar echo power distribution across the lunar surface has been described in this report. In one of these methods, carried out at 23-cm wavelength using the L-band Millstone radar facility of M.I.T. Lincoln Laboratory, consecutive measurements of the CW lunar echo power spectrum were obtained over a period of many hours. During the interval of observation, the position angle of the apparent axis of lunar rotation, measured with respect to the projection of the lunar polar axis, varied through an angle of 180°. Combination of the spectral information obtained in this way (a procedure called "supersynthesis") yielded an effective resolution of about 100 km on the lunar surface.

Maps of the surface distribution of reflected power density were attempted in this way at 23 cm, using two orthogonal senses of receiving polarization, one of which was matched to the returned component corresponding to specular reflection. This latter "polarized" sense yielded a distribution which, as expected, showed an extremely strong quasi-specular highlight in the center of the observed disk (i.e., near-normal incidence to the lunar surface). Because of the limited dynamic range inherent in the supersynthesis procedure, little else could be seen in this polarization. The orthogonal "depolarized" sense, however, was sensitive primarily to the diffusely scattered echo component, whose distribution is fairly uniform, on average, over the visible lunar hemisphere. In this mode, a significant scattering variation over the surface was established which appeared to correspond quite closely to the distribution of visible features. In particular, large craters of relatively recent origin, such as Tycho and Copernicus, displayed a substantially enhanced scattering efficiency. Lesser enhancements were also noted as a property of the lunar highlands (see Fig. 8).

The second method of mapping required analysis of the returned echo power simultaneously in range as well as in frequency. This method, called "delay-doppler mapping," was relatively

efficient, yielding an estimate of the distribution of radar reflectivity with a fine-grained surface resolution of between 1 and 7 km after only about 15 minutes of operation. Because of the requirement for modest direct angular resolution by the observing antenna (i.e., sufficient to permit at least crude resolution of the lunar disk), only measurements at 3.8-cm wavelength, using the Haystack radar facility of M.I.T. Lincoln Laboratory, were possible. At this wavelength, maps of the surface distribution of echo power density in the polarized sense have been obtained over the region bounded by ±70° in longitude and ±16° in latitude, selenographic coordinates. Maps in the depolarized sense were not available because of limitations in the radar system used.

These maps, shown in the frontispiece and in Figs. 14 through 16, display the variation in surface backscattering compared with the lunar average. Two basic properties of the surface appear to be responsible for most of the observed variation: inclined slopes, and increased roughness. The radar variation arising from the effects of local surface inclinations toward or away from the line-of-sight leads to a pattern similar to that observed at optical wavelengths under oblique lighting conditions (large phase angles of solar illumination). Significantly increased local roughness at the scale of the radar wavelength (3.8 cm) is inferred for at least 18 regions of the mapped area (see Table XI). Further, the regions surrounding the five prime Apollo landing sites appear smooth and relatively free of anomalous roughness.

Measurements of the round-trip lunar echo time of flight and doppler frequency displacement were obtained in the course of the 3.8-cm mapping observations. These have been compared with the most recently available lunar orbital theory; significant residuals have been noted from the theoretical predictions of doppler shift. The source of these discrepancies is not fully understood, although a number of possibilities (lunar shape, terrestrial atmosphere, errors in site coordinates, errors in the specification of ephemeris time) have been investigated. An attempt to fit a new lunar orbit to combined radar and optical data is under way, but no results are yet available.

APPENDIX A
LIMITATIONS OF THE SUPERSYNTHESIS TECHNIQUE

I. SYSTEMATIC ERRORS

In Sec. II-A, it was shown that the filtering of the observed data with a power-frequency response g(x) and the subsequent combination of the data – observed for all angles φ between the apparent libration axis and the true lunar axis – could be interpreted as a two-dimensional convolution of the true distribution f(x, y) and a function G(x, y) as given in Eqs. (8) and (9), respectively. The use of finite-width filters in determining the strip distribution is equivalent to multiplying the correlation function by a weight function which de-emphasizes the values for large arguments $\sqrt{u^2 + v^2}$. Let us denote the weight function by h(s) and determine its relation to the smoothing function G(x, y). The modified correlation function is $\rho_a(s \cos\varphi;\ s \sin\varphi) = \rho(s \cos\varphi;\ s \sin\varphi)\, h(s)$ and yields an expression identical to Eq. (8) except that the smoothing function is now of the form

$$G(x, y) = 2\pi \int_0^\infty r\, dr\, J_0\left(2\pi r \sqrt{x^2 + y^2}\right) h(r) \quad . \tag{A-1}$$

Comparison of Eqs. (9) and (A-1) shows that the multiplying function h(r) is the Fourier transform of the filter function $g(\rho)$.

In mapping the lunar surface, the filter function actually used is given by

$$g(\rho) = \left\{ \frac{\sin[\pi(\rho/\Delta_f)]}{\pi(\rho/\Delta_f)} \right\}^2 \quad . \tag{A-2}$$

Unfortunately, we have not yet been able to determine an exact analytic expression for the corresponding G(x, y). Therefore, we have been forced to rely on a Gaussian approximation, as given in Eq. (11a) of Sec. II-A.

Next, it is necessary to further explore the effect of only knowing the strip distribution or the visibility function at discrete values of the angle φ. For this purpose, we imagine that the visibility is known at N equidistant values of φ, viz.,

$$\varphi_n = \frac{\pi}{N}\, n \quad , \quad n = 1, N \quad . \tag{A-3}$$

In addition, the complex visibility is de-emphasized at large arguments as just described. In the integral for the apparent power distribution Eq. (8), we therefore substitute a two-dimensional correlation function modified in the following manner:

$$\rho_a(s \cos\varphi;\ s \sin\varphi) = \sum_{n=0}^{N-1} \delta\left(\varphi - \frac{\pi}{N}\, n\right) h(s)\, \rho(s \cos\varphi;\ s \sin\varphi) \quad . \tag{A-4}$$

Substituting Eq. (A-4) into Eq. (8) gives

$$P_a(x, y) = \sum_{n=0}^{N-1} \int_0^\infty s\, ds \left\{ \rho(s \cos\varphi_n;\ -s \sin\varphi_n) \exp[2\pi i s(x \cos\varphi_n - y \sin\varphi_n)] \right.$$

$$\left. + \rho^*(s \cos\varphi_n;\ -s \sin\varphi_n) \exp[-2\pi i s(x \cos\varphi_n - y \sin\varphi_n)] \right\} h(s)$$

$$P_a(x, y) = \iint d\xi'\, d\eta'\, P(\xi', \eta') \sum_{n=0}^{N-1}$$

$$\times \int_o^\infty s\, ds\, h(s)\, 2 \cos\{2\pi s\, [(x - \xi') \cos\varphi_n - (y - \eta') \sin\varphi_n]\} \quad . \quad \text{(A-5)}$$

In this case, therefore, the two-dimensional smoothing function becomes

$$G(x, y) = 2 \sum_{n=0}^{N-1} \int_o^\infty s \cdot ds\, h(s) \cos[2\pi s(x \cos\varphi_n - y \sin\varphi_n)] \quad . \quad \text{(A-6)}$$

For the approximation of a Gaussian filtering characteristic, we find

$$h(s) = \exp[-2\pi^2 \Delta_g^2 s^2] \quad \text{(A-7)}$$

where Δ_g is the half-width of the filter.

Substituting this into Eq. (A-6) gives

$$G(x, y) = 2 \sum_{n=0}^{N-1} \int_o^\infty s\, ds\, e^{-as^2} \cos(2x_n s) \quad \text{(A-8)}$$

where

$$a = 2\pi^2 \Delta_g^2$$

$$x_n = \pi(x \cos\varphi_n - y \sin\varphi_n) \quad .$$

Equation (A-8) can be integrated and gives

$$G(x, y) = \frac{1}{2\pi^2 \Delta_g^2} \sum_{n=0}^{N-1} \left(1 - 2 \frac{x_n}{\sqrt{a}} \exp[-x_n^2/a] \int_o^{x_n/\sqrt{a}} e^{t^2}\, dt\right) \quad . \quad \text{(A-9)}$$

The function $f(y) = 1 - 2y \exp[-y^2] \int_o^y \exp[t^2]\, dt$ is shown in Fig. A-1. We see from this that the contribution to G(x, y) from a particular run corresponding to the angle φ_m is unity when $x_m = 0$, i.e., along a direction perpendicular to the baseline of run m. From this, it follows that the sidelobe rejection is directly proportional to the number of runs, or to the number of discrete baseline directions.

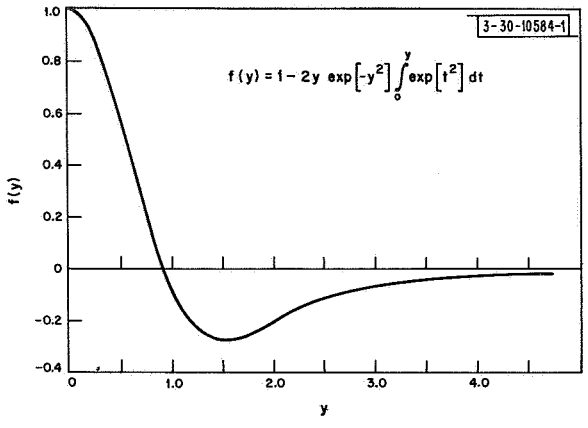

Fig. A-1. Plot of function f(y) (see text).

Next, consider the even more realistic case where the angle φ is allowed to vary continuously during each observation so that the value of the correlation function actually derived corresponds to the mean of a range of angles from $\varphi_m - \Delta\varphi/2$ to $\varphi_m + \Delta\varphi/2$. This averaging or smearing of the data occurs, of course, while the instantaneous rotation axis of the target is changing direction during a run.

When the smearing of the visibility function is caused by a rotation of the axis of the target, the modified visibility function for a particular run m becomes

$$\rho_a(s\cos\varphi_m;\ -s\sin\varphi_m) = \iint P(\xi',\eta')\,d\xi'\,d\eta'\,\frac{1}{\Delta\varphi}\int_{\varphi_m-\Delta\varphi/2}^{\varphi_m+\Delta\varphi/2} d\varphi$$

$$\times \exp[-2\pi i s(\xi'\cos\varphi - \eta'\sin\varphi)]$$

$$= \iint P(\xi',\eta')\,d\xi'\,d\eta'\left\{\frac{\sin[\pi s(\xi'\sin\varphi_m + \eta'\cos\varphi_m)\,\Delta\varphi]}{s\pi(\xi'\sin\varphi_m + \eta'\cos\varphi_m)\,\Delta\varphi}\right\}$$

$$\times \exp[-2\pi i s(\xi'\cos\varphi_m - \eta'\sin\varphi_m)] \quad . \tag{A-10}$$

Introducing

$$x_n = \pi\,[(\xi' - x')\cos\varphi_n - (\eta' - y')\sin\varphi_n]$$

$$y_n = \pi(\xi'\sin\varphi_n + \eta'\cos\varphi_n)\,\Delta\varphi$$

one obtains

$$G(x-\xi';\ y-\eta';\ \xi',\eta') = \sum_{n=0}^{N-1}(1/y_n)\int_0^\infty ds\ h(s)\,\{\sin[2s(x_n - y_n/2)]$$

$$- \sin[2s(x_n + y_n/2)]\} \tag{A-12}$$

and the smearing of the true distribution is no longer a true convolution. To second order in y_n,

$$G = 2\sum_{n=0}^{N-1}\int_0^\infty s\,ds\cdot h(s)\cdot\cos(2x_n s)\,(1 - s^2 y_n^2/6) \quad . \tag{A-13}$$

The condition that the angular smearing of the correlation function is not to influence the data appreciably corresponds to requiring $sy_n < 1$ for all values of s for which h(s) is not close to zero. In the Gaussian case, h(s) is close to zero whenever $s > 1/\pi\cdot\Delta_g\sqrt{2}$. If r_o measured in the same units as Δ_g denotes the largest value of $\sqrt{x^2+y^2}$ in P(x, y) for which a signal is present, we conclude that the smearing is important whenever

$$\Delta\varphi < \sqrt{2}\Delta_g/r_o \quad . \tag{A-14}$$

Comparison of the filter function for a Gaussian shape [Eq. (11a) of Sec. II-A and Eq. (A-7) above], against that given in Eq. (A-2) above, shows that

$$\Delta_g = \Delta_f\,\frac{3}{\pi} = 0.955\,\Delta_f \quad . \tag{A-15}$$

As explained in Sec. IV-B of the text, the width of the actual analyzing filter was $\Delta_f = r_o/25$, where r_o now is the lunar radius. Substitution of this into condition (A-14) shows that

$$\Delta\varphi < \sqrt{2}\cdot 0.955/25 = 0.054 \text{ radian} = 3.1^\circ \quad . \tag{A-16}$$

This is certainly <u>not</u> fulfilled in the runs analyzed in Sec. IV-B, where $\Delta\varphi$ in some instances was 4° It may be expected that the condition (A-14) can also be applied as a measure of the importance of the angular sampling if $\Delta\varphi$ is interpreted as the angle between the libration axes for consecutive runs. In the data analyzed, this interval was on occasion as large as 10°, which may

explain why it was necessary to apply smoothing to the data in order to obtain a reasonable map. The contour map presented as Fig. 7 was obtained with the equivalent of only 17 filters across the diameter of the moon. This sets the corresponding limit on the right-hand side of Eq. (A-16) at 9.3°, and satisfies the "smearing condition" as well as the "angular jump" conditions nearly throughout.

It should be noted that higher resolution can be achieved near the center of the moon. If we concentrate our attention only on the central disk ($r_o = 1/2$), then condition (A-14) can be satisfied for larger values of $\Delta\varphi$. This situation can be easily seen in Fig. 8, where the equivalent of 31 filters has been preserved across the lunar diameter. The sidelobe level along the edges is very prominent, as the above analysis predicts. However, it appears that the resolution is considerably increased near the center.

II. RANDOM ERRORS

Random errors in the estimate of the reflectivity in the maps arise either because there is an appreciable amount of random additive noise superimposed on the signal, or because the signal itself fades so that the mean signal power even in the absence of additive noise may only be significant after a considerable amount of signal integration. For most radar astronomy targets, except for the moon, additive noise is of greatest importance. When the most sensitive radar systems are applied to the study of the moon, however, the returns are so strong that additive noise is not limiting. Here, then, we shall be primarily concerned with the latter case.

It is difficult to give a completely general discussion of the computation of the random errors covering all experimental situations. Thus, we shall consider the particular experimental situation which arises in lunar observations where, as an approximation, one may regard the projection of the instantaneous apparent axis to change its direction at a constant angular velocity $\dot{\varphi}$. We shall also assume that the magnitude of the rotation rate (and hence the center-to-limb doppler) remains constant. The observations will be assumed to be carried out continuously, so that problems in connection with discrete angular sampling do not arise. (The experiment is therefore highly idealized.) The angle φ is replaced by $\dot{\varphi}t$, where t is the time, and the variable s [e.g., see Eq. (A-4)] will be replaced by $2\tau\Omega_{||}/\lambda$, where τ is the time shift in the correlation function, and $\Omega_{||}$ is the projection of the apparent angular velocity on the x, y plane. For the time-varying autocorrelation function at time t and delay τ, one obtains

$$\rho(\tau, t) = \iint dx\, dy\, P(x, y) \exp\{-4\pi i \frac{\tau}{\lambda} \Omega_{||} [x(\cos\dot{\varphi}t - \frac{\dot{\varphi}\tau}{2} \sin\dot{\varphi}t) - y(\sin\dot{\varphi}t + \frac{\dot{\varphi}\tau}{2} \cos\dot{\varphi}t)]\} \quad . \tag{A-17}$$

As explained previously, this ideal correlation function must be multiplied by a weight function $h(\tau)$ in order to achieve some filtering of the data. Furthermore, we cannot arrive at an estimate of the instantaneous correlation function at time t. In practice, we must make an estimate by taking a time average. Therefore, the correlation function available for transformation will be a random variable having a mean value given by

$$\rho_m(\tau, t) = h(\tau) \int_{-\infty}^{+\infty} \rho(\tau, t')\, g(t - t')\, dt' \tag{A-18}$$

where g(t) is a time-averaging function. The estimate of the filtered brightness over the target disk is

$$P_m(x, y) = \kappa \iint d\tau\ dt\ \tau \rho_m(\tau, t) \exp[4\pi i \frac{\tau}{\lambda} \Omega_{||}(x \cos \dot{\varphi} t - y \sin \dot{\varphi} t)] \qquad (A\text{-}19)$$

where κ is a constant of proportionality. Here, $\rho_m(\tau, t)$ is to be considered the mean value of the random variable $\rho^i_m(\tau, t)$; hence,

$$\rho_m(\tau, t) = \langle \rho^i_m(\tau, t) \rangle \quad .$$

The deviation or uncertainty in $P_m(x, y)$ is given by

$$\delta P^i_m(x, y) = \kappa \iint d\tau\ dt\ \tau(\rho^i_m - \rho_m) \exp[4\pi i \frac{\tau}{\lambda} \Omega_{||}(x \cos \dot{\varphi} t - y \sin \dot{\varphi} t)] \qquad (A\text{-}20)$$

and the mean-square uncertainty becomes

$$\delta P_m(x, y)^2 = \langle \delta P^i_m(x, y)^2 \rangle = \kappa^2 \iiiint d\tau\ dt\ d\tau'\ dt'\ (\langle \rho^i_m \rho^{i*\prime}_m \rangle - \rho_m \rho^{*\prime}_m)\ \tau\tau'$$

$$\times \exp\{\frac{4\pi i}{\lambda} \Omega_{||}\ [\tau(x \cos \dot{\varphi} t - y \sin \dot{\varphi} t) - \tau'(x \cos \dot{\varphi} t' - y \sin \dot{\varphi} t')]\} \qquad (A\text{-}21)$$

the primed functions having arguments τ' and t'. In order to compute the mean of the product of "instantaneous correlation functions" appearing under the integral sign, we proceed as follows:

$$\langle \rho^{i*}_m(\tau', t')\ \rho^i_m(\tau, t) \rangle = h(\tau)\ h(\tau') \iint dt''\ dt'''\ g(t - t'')\ g(t' - t''')$$

$$\cdot \langle \rho^i(\tau, t'')\ \rho^{i*}(\tau', t''') \rangle \quad . \qquad (A\text{-}22)$$

Since the random variable $\rho^i(\tau, t)$ is defined as a simple product of two random variables which are nearly always Gaussian, we may express the mean of the product in Eq. (A-22) in terms of products of means

$$\begin{aligned}
\langle \rho^i(\tau, t'')\ \rho^{i*}(\tau', t''') \rangle &= \langle f^*(t'' + \tau)\ f(t'')\ f(t''' + \tau')\ f^*(t''') \rangle \\
&= \langle f^*(t'' + \tau)\ f(t'') \rangle \langle f(t''' + \tau')\ f^*(t''') \rangle + \langle f^*(t'' + \tau)\ f(t''' + \tau') \rangle \\
&\quad \cdot \langle f(t'')\ f^*(t'') \rangle \\
&= \rho(\tau, t'')\ \rho^*(\tau', t''') + \rho^*(\tau' - \tau + t''' - t''; t'' + \tau) \\
&\quad \times \rho(t''' - t''; t'') \quad . \qquad (A\text{-}23)
\end{aligned}$$

The former of these two terms cancels the product of the means in Eq. (A-21), and there remains

$$\delta P_m(x, y)^2 = \kappa^2 \int \cdots \int d\tau\ d\tau'\ dt\ dt'\ \tau\tau' \exp\{\frac{4\pi i}{\lambda} \Omega_{||}\ [\tau(x \cos \dot{\varphi} t - y \sin \dot{\varphi} t)$$

$$- \tau'(x \cos \dot{\varphi} t' - y \sin \dot{\varphi} t')]\} \times h(\tau)\ h(\tau') \iint dt''\ dt'''\ g(t - t'')$$

$$\times g(t' - t''')\ \rho^*(\tau' - \tau + t''' - t''; t'' + \tau)\ \rho(t''' - t''; t'') \quad . \qquad (A\text{-}24)$$

This expression is so complex that general conclusions cannot easily be drawn regarding the relative uncertainty in the reflectivity determinations. Under these circumstances, the best one can probably accomplish is to construct an example which is simple enough for the computations to be carried through, yet complex enough to convey information of general validity. It appears that the following distribution is of such a nature:

$$P(x, y) = \exp[-(x^2 + y^2)/2a^2] \tag{A-25}$$

where a is a measure of the extent of the moon. From Eq. (A-17), it follows that

$$\rho(\tau, t) = \exp\{-2\pi^2(\tau f_L)^2\,[1 + (\dot{\varphi}\tau/2)^2]\} \approx \exp[-2\pi^2(\tau f_L)^2] \quad . \tag{A-26}$$

Here, we have introduced $f_L = 2a\Omega_{||}/\lambda$, which corresponds to the center-to-limb Doppler shift for a planet of radius a. Since $\rho(\tau, t)$ is not dependent on t, the convolution with $g(t - t')$ in Eq. (A-18) has no effect. Using a Gaussian weight factor $h(\tau)$ as in Eq. (A-7), one obtains

$$\rho_m(\tau, t) = \exp\{-2\pi^2(f_L\tau)^2\,[1 + (\Delta_g/f_L)^2]\} \cong e^{-\beta^2\tau^2} \quad . \tag{A-27}$$

Substituting this into Eq. (A-19) gives

$$\begin{aligned} P_m(x, y) &= \frac{\kappa}{\dot{\varphi}} \int_o^\infty \tau\, d\tau\, d^{-\beta^2\tau^2} \int_o^\pi d\psi\, \exp[4\pi i\, \frac{\tau}{\lambda}\, \Omega_{||}(x\cos\psi - y\sin\psi)] \\ &= \frac{\pi\nu}{\dot{\varphi}} \int_o^\infty \tau\, d\tau\, e^{-\beta^2\tau^2}\, J_o\left(4\pi\sqrt{x^2 + y^2}\, \frac{\tau}{\lambda}\, \Omega_{||}\right) \\ &= \frac{\kappa}{4\pi\dot{\varphi} f_L^2\,[1 + (\Delta_g^2/f_L^2)]} \exp\left\{-\frac{x^2 + y^2}{2a^2\,[1 + (\Delta_g^2/f_L^2)]}\right\} \quad . \end{aligned} \tag{A-28}$$

The mean observed distribution is therefore seen to closely resemble the original distribution as long as $\Delta_g \ll f_L$.

In order to compute the uncertainty $\delta P_m(x, y)$, we have to make the additional assumption that

$$g(t - t') = \frac{1}{\sqrt{2\pi}T_o} \exp[-(t - t')^2/2T_o^2] \quad . \tag{A-29}$$

With this assumption we find, after some considerable labor, that

$$\begin{aligned} \langle \rho_m^i \rho_m^{i*'} \rangle - \rho_m \rho_m^{*'} = {} & \frac{1}{\sqrt{3 + 2(2\beta T_o)^2}} \exp[-\alpha^2(\tau^2 + \tau'^2)] \cdot \exp[-(\beta/2)\,\Delta\tau^2] \\ & \cdot \exp\left\{-\frac{1}{2T_o^2}\left[\frac{2 + (2\beta T_o)^2}{3 + 2(2\beta T_o)^2}\right](t - t' - \frac{\Delta\tau}{2})^2\right\} \end{aligned} \tag{A-30}$$

where $\Delta\tau = \tau' - \tau$, and $\alpha = \sqrt{2\pi}\Delta_g$. We note that $\beta T_o \cong \sqrt{2\pi} f_L \cdot T_o$. The duration of a fading cycle is typically f_L^{-1}. Since T_o must include a great many fading cycles, we conclude that $\beta T_o \gg 1$. For the same reason, $\Delta\tau$ can be ignored in the last exponential factor by putting $\Delta\tau \doteq 0$. We also note that $\alpha \ll \beta$ for reasonable resolution to be obtained. It follows that, in the first exponential factor, one may put $\tau = \tau'$. With these simplifications, one obtains

$$\langle \rho_m^i \rho_m^{i*\prime} \rangle - \rho_m \rho_m^{*\prime} \approx \frac{1}{\sqrt{2}\, 2\beta T_o} \exp\left[-2\alpha^2 \tau^2 - \frac{\beta^2}{2} \Delta\tau^2 - \frac{1}{4T_o^2} \Delta t^2 \right] \qquad \text{(A-31)}$$

with $\Delta t = t' - t$.

When substituting into Eq. (A-21), we expand the exponent of the phase factor to first order in Δt about $\Delta t = 0$, and integrate with respect to t. The result is

$$\frac{\pi \kappa^2}{\sqrt{2}\, \dot{\varphi} \beta T_o} \int_o^\infty \tau \, d\tau \cdot e^{-\alpha^2 2\tau^2} \int_{-\tau}^\infty d(\Delta\tau)\, (\tau + \Delta\tau) \cdot e^{-\beta^2 \Delta\tau^2/2}$$

$$\cdot \int_{-\infty}^{+\infty} d(\Delta t) \cdot e^{-\Delta t^2/4T_o^2} \cdot J_o\left[2\pi f_L \frac{r}{a} \sqrt{\Delta\tau^2 + \tau^2 (\dot{\varphi} \Delta t)^2} \right] = \delta P_m(r)^2 \qquad \text{(A-32)}$$

where $r = \sqrt{x^2 + y^2}$. Since this is not easily integrable, we have to be content to find an upper bound to $\delta P_m(r)^2$ by computing the triple integral for $r = 0$ only. Making some further approximations which are all compatible with previous assumptions, we finally obtain

$$\delta P_m^2 \leqslant \frac{\pi}{4} \left(\frac{\pi}{2}\right)^{3/2} \frac{\kappa}{\dot{\varphi} \beta^2 \alpha^3} \quad . \qquad \text{(A-33)}$$

Substitution of $\dot{\varphi} = \pi/T$, where T is the total time of observation, and computation of the relative uncertainty gives for $r = 0$

$$\frac{\delta P_m^2}{P_m^2} \approx \frac{\sqrt{\pi}}{4} \cdot \frac{1}{T\Delta_g} \cdot \left(\frac{f_L}{\Delta_g}\right)^2 \quad . \qquad \text{(A-34)}$$

We note that this is independent of transmitter power because of the absence of additive noise. The uncertainty $\delta P_m / P_m$ is inversely proportional to the square root of observation time multiplied by the smoothing filter bandwidth, and directly proportional to linear resolution. For a given resolution, we see that the uncertainty is inversely proportional to the square root of the operating frequency since, for a given resolution, one must make Δ_g proportional to the operating frequency.

Suppose we desire to obtain reflectivity data to an accuracy of $\delta P_m / P_m = 0.25$. Let us determine, according to Eq. (A-34), to what resolution we can map. Taking 12 hours as a typical observing time and the center-limb doppler to be 10 Hz, we obtain

$$\frac{\Delta_g}{f_L} \geqslant 2.54 \cdot 10^{-2}$$

which corresponds to a resolution of 43 km on the moon. This appears to be the ultimate resolution which the method can yield at 23 cm using the Millstone antenna. At 3.8 cm, where the narrow antenna beam can be used to effectively reduce the apparent size of the moon, the achievable resolution for the same relative uncertainty should be about one-tenth of this, i.e., approximately 5 km. In view of the excellent resolution achieved – even near the subradar point – using the delay-doppler technique at 3.8 cm, it does not appear worthwhile to apply the supersynthesis technique for high-resolution mapping of the moon at 3.8 cm.

APPENDIX B
MAPPING ERRORS RESULTING FROM UNCERTAINTIES IN THE LUNAR RADIUS AND ROTATION

Inaccuracies in the knowledge of the lunar radius and apparent rotation can introduce mapping errors of several types. Since the reference for the determination of relative delay is τ_o, corresponding to the echo from the subradar point [see Eq. (14)], an error in the assumed radius ρ_o of the subradar point is reflected into determinations of all z through

$$\frac{\partial z}{\partial \rho_o} = \frac{1}{\rho} \quad . \tag{B-1}$$

Similarly, an error in the magnitude of the projected rotation ω_a gives rise to

$$\frac{\partial x}{\partial \omega_a} = -\frac{x}{\omega_a} \tag{B-2}$$

while an error in the value ρ of the radius for a particular point enters as

$$\frac{\partial x}{\partial \rho} = -\frac{x}{\rho}$$

$$\frac{\partial z}{\partial \rho} = -\frac{z}{\rho} \quad . \tag{B-3}$$

By combining these, it follows that

$$\Delta x = -x\left(\frac{\Delta \omega_a}{\omega_a} + \frac{\Delta \rho}{\rho}\right)$$

$$\Delta z = \frac{1}{\rho}\,(\Delta \rho_o - z\Delta \rho)$$

$$\Delta y = \frac{-1}{y}\,(x\Delta x + z\Delta z) \quad . \tag{B-4}$$

Equations (B-4) can be expressed in terms of selenographic coordinates through the use of

$$x = \cos\varphi\,\cos\delta\,\sin(\lambda - \lambda_o) - \sin\varphi\,\sin\delta\,\cos\delta_o + \sin\varphi\,\cos\delta\,\sin\delta_o\,\cos(\lambda - \lambda_o)$$

$$y = \sin\varphi\,\cos\delta\,\sin(\lambda - \lambda_o) + \cos\varphi\,\sin\delta\,\cos\delta_o - \cos\varphi\,\cos\delta\,\sin\delta_o\,\cos(\lambda - \lambda_o)$$

$$z = (1 - x^2 - y^2)^{1/2} \tag{B-5}$$

which are obtained from Eqs. (20) and (23). Note that only the positive branch of z need be considered since this corresponds to the visible hemisphere of the lunar surface.

Finally, we need the transformation of the errors to selenographic coordinates, which may be obtained by straightforward differentiation and combination of Eqs. (19), (21), and (22):

$$\Delta\delta = \frac{1}{\cos\delta}\,[(-\sin\varphi\,\cos\delta_o)\,\Delta x + (\cos\varphi\,\cos\delta_o)\,\Delta y + (\sin\delta_o)\,\Delta z]$$

$$-\cos\delta_o\,\sin(\lambda - \lambda_o)\,\Delta\varphi$$

$$\Delta\lambda = \frac{1}{\cos\delta}\{[\cos\varphi\cos(\lambda-\lambda_o) - \sin\varphi\sin\delta_o\sin(\lambda-\lambda_o)]\Delta x$$
$$+ [\cos\varphi\sin\delta_o\sin(\lambda-\lambda_o) + \sin\varphi\cos(\lambda-\lambda_o)]\Delta y$$
$$- [\cos\delta_o\sin(\lambda-\lambda_o)]\Delta z\} - [\sin\delta_o - \tan\delta\cos\delta_o\cos(\lambda-\lambda_o)]\Delta\varphi \qquad \text{(B-6)}$$

where the effects of an error in the doppler angle φ have been included.

APPENDIX C
GEOGRAPHIC TOPOCENTRIC POSITION OF THE MOON

The geocentric position of the moon is given in celestial coordinates as α_c (right ascension), δ_c (declination), and π (horizontal parallax). The "azimuthal" angle (referenced to the vernal equinox) is α_c measured in the plane of the equator, while δ_c is the "elevation" angle above the equatorial plane. The center-of-earth to center-of-moon distance R_c is found from π by

$$R_c = a/\sin(\pi) \tag{C-1}$$

where a is the equatorial radius of the earth. The problem considered here is the computation of the position of the moon with respect to the radar.

A geocentric Cartesian coordinate system oriented to the radar and equatorial plane of the earth is shown in Fig. C-1. The x-y plane coincides with the equatorial plane of the earth, while the radar lies in the y-z plane. Let O be the center of the earth, M the center of the moon, and S the position of the radar. The vector from the center of earth to the radar is: $\overrightarrow{OS} = (0;\ \rho_c \cos\varphi_c;\ \rho_c \sin\varphi_c)$, where ρ_c = geocentric radius, and φ_c = geocentric latitude at the radar position. The vector from the center of the earth to the center of the moon is

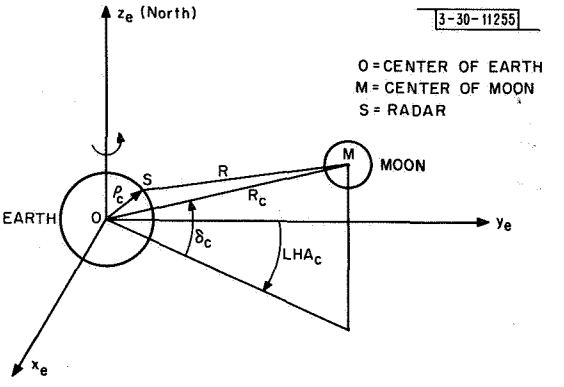

Fig. C-1. Geometry involved in topocentric reduction for use in preparing lunar ephemeris.

$$\overrightarrow{OM} = [R_c \sin(LHA_c)\cos(\delta_c);\ R_c \cos(LHA_c)\cos(\delta_c);\ R_c \sin(\delta_c)]$$

where

LHA_c = geocentric local hour angle of moon

= local sidereal time (LST) minus right ascension (α_c).

The vector from the radar to the center of the moon is found from the subtraction: $\overrightarrow{SM}(x_1, y_1, z_1) = \overrightarrow{OM} - \overrightarrow{OS}$, where $R = |\overrightarrow{SM}|$ and $R_c = |\overrightarrow{OM}|$. The components x_1, y_1, z_1 are related to the desired topocentric celestial coordinates through

$$x_1 = R \sin(LHA')\cos(\delta') = R_c \sin(LHA_c)\cos(\delta_c)$$

$$y_1 = R \cos(LHA')\cos(\delta') = R_c \cos(LHA_c)\cos(\delta_c) - \rho_c \cos(\varphi_c)$$

$$z_1 = R \sin(\delta') = R_c \sin(\delta_c) - \rho_c \sin(\varphi_c) \tag{C-2}$$

from which we derive

LHA' = topocentric local hour angle of the moon = $\arctan(x_1/y_1)$

α' = topocentric right ascension of the moon = LST − LHA'

δ' = topocentric declination of the moon = $\arctan\left(z_1 / \sqrt{x_1^2 + y_1^2}\right)$

$$R = \text{topocentric distance of the moon} = \sqrt{x_1^2 + y_1^2 + z_1^2} \tag{C-3}$$

the latter quantity may also be expressed as

$$R = \sqrt{R_c^2 + \rho_c^2 - 2\rho_c R_c \cos(\chi)} \tag{C-4}$$

where

$$\cos(\chi) = \sin(\delta_c) \sin(\varphi_c) + \cos(\varphi_c) \cos(\delta_c) \cos(\mathrm{LHA}_c) \tag{C-5}$$

The position angle of the projected polar axis is described by C', and is measured counterclockwise on the celestial sphere from the north part of the hour circle passing through the center of the disk to the direction of the north projected polar axis. The position of the radar with respect to the moon is described in terms of the selenographic longitude λ_o and latitude δ_o of the subradar point. These three angles are computed from Eqs. (13) to (17) of D.W.G. Arthur (1963) as

$$\cos(\text{☊}) \cos(\delta_o) = -\cos(\delta') \cos(\alpha' - \Omega')$$

$$\sin(\text{☊}) \cos(\delta_o) = -\cos(\delta') \cos(i) \sin(\alpha' - \Omega') - \sin(\delta') \sin(i)$$

$$\sin(\delta_o) = +\cos(\delta') \sin(i) \sin(\alpha' - \Omega') - \sin(\delta') \cos(i) \tag{C-6}$$

where

$$\text{☊} = \text{☾} + \lambda_o - \Omega + \Delta \tag{C-7}$$

and

$$\sin(C') = -\sin(i) \cos(\alpha' - \Omega') \sec(\delta_o)$$

$$= \sin(i) \cos(\text{☊}) \sec(\delta') \tag{C-8}$$

where

i = inclination of the moon's mean equator to the earth's true equator;

Δ = arc on the moon's mean equator from its ascending node on the earth's true equator to its ascending node on the ecliptic;

Ω' = arc in the earth's true equator from the true equinox to the ascending node of the moon's mean equator;

Ω = longitude of the ascending node of the moon's orbit on the ecliptic;

☾ = mean longitude of the moon, measured along the ecliptic from the mean equinox to the mean ascending node of the moon's orbit and then along the orbit.

These quantities are tabulated in the American Ephemeris and Nautical Almanac [U. S. Naval Observatory (1965)], α_c, δ_c, and π at hourly intervals and i, Δ, Ω', Ω, and ☾ at 10-day intervals. These time intervals are sufficiently close that the derivatives $\dot{R}$, $\dot{\lambda}_o$, and $\dot{\delta}_o$ can be obtained with no important loss in precision.

APPENDIX D
THE COOLEY-TUKEY ALGORITHM

The Cooley-Tukey algorithm has come into prominence only within the last few years, and has revolutionized signal processing of all kinds by vastly reducing calculation time. Samples of a complex waveform, equally spaced over a finite time interval, are Fourier transformed by

$$t_k = \sum_{j=0}^{N-1} d_j w^{jk} \quad , \quad k = 0, N-1 \tag{D-1}$$

where d_j are the samples in time (total number N), t_k are the transform values, and $w = e^{-2\pi i/N}$. The crucial point is that there are not N^2 independent values for w^{jk}, for each combination of j and k. Rather, since $w^N = 1$, w^{jk} takes on only N different values, namely, $w^0 (=1)$, $w, w^2, \ldots, w^{N-1}$. For example, suppose N = 6; then, $w^{3\cdot 5} = w^{15} = w^6 w^6 w^3 = w^3 = w^{3\cdot 1} = w^{3\cdot 3}$. It is this redundancy that the Cooley-Tukey method removes from the calculations.

A complete example will give a taste of the method. For N = 6, the transformation is written

$$\begin{aligned}
t_0 &= d_0 + d_1 + d_2 + d_3 + d_4 + d_5 \\
t_1 &= d_0 + wd_1 + w^2 d_2 + w^3 d_3 + w^4 d_4 + w^5 d_5 \\
t_2 &= d_0 + w^2 d_1 + w^4 d_2 + w^6 d_3 + w^8 d_4 + w^{10} d_5 \\
t_3 &= d_0 + w^3 d_1 + w^6 d_2 + w^9 d_3 + w^{12} d_4 + w^{15} d_5 \\
t_4 &= d_0 + w^4 d_1 + w^8 d_2 + w^{12} d_3 + w^{16} d_4 + w^{20} d_5 \\
t_5 &= d_0 + w^5 d_1 + w^{10} d_2 + w^{15} d_3 + w^{20} d_4 + w^{25} d_5
\end{aligned} \tag{D-2}$$

Naive calculation will take 25 complex multiplications and 30 complex additions. (Assume the w's have been precomputed and stored in a table.) Alternately, the calculations may be grouped as follows.

Let

$$\begin{aligned}
u_o &= d_0 + d_3 \\
u_1 &= d_0 - d_3 \\
u_2 &= d_1 + d_4 \\
u_3 &= d_1 - d_4 \\
u_4 &= d_2 + d_5 \\
u_5 &= d_2 - d_5
\end{aligned} \tag{D-3}$$

Then,

$$t_0 = u_0 + u_2 + u_4$$

$$t_1 = u_1 + wu_3 + w^2u_5$$

$$t_2 = u_0 + w^2u_2 + w^4u_4$$

$$t_3 = u_1 + w^3u_3 + w^6u_5$$

$$t_4 = u_0 + w^4u_2 + w^8u_4$$

$$t_5 = u_1 + w^5u_3 + w^{10}u_5 \qquad \text{(D-4)}$$

This formulation takes only 10 complex multiplications and 18 additions. In general, it can be shown that for N composed of factors (N = abc. . .) the total calculation can be reduced from about N^2 complex multiplications and additions to about N(a+b+c+. . .) [see IEEE Audio Transactions (June 1967)]. Powers of 2 run fastest of all; for $N = 2^k$, running time is proportional to Nk. Specifically, on the CDC 3300 computer, fixed-point calculation required about 60 Nk μsec per spectrum, or about 128 msec for N = 256 as used here.

One may note that if the time samples d_j are separated by Δt, the transform values t_k are separated by $\Delta f = 1/(N\Delta t)$. The zero coefficient t_o is the DC offset, while $t_{N/2}$ is at the Nyquist frequency. A listing of the Fortran statements, showing the logic of the programs, follows. The actual program used was written in CDC 3300 machine language and was found to run about 1.7 times faster than the Fortran version given here.

```
      SUBROUTINE FOUR1(DATA,NN,ISIGN)
C     THE COOLEY-TUKEY FAST FOURIER TRANSFORM IN USASI BASIC FORTRAN.
C     TRANSFORM(K) = SUM(DATA(J)*EXP(ISIGN*2*PI*SQRT(-1)*(J-1)*(K-1)
C     /NN)), SUMMED OVER ALL J AND K FROM 1 TO NN.  DATA IS A ONE-
C     DIMENSIONAL COMPLEX ARRAY (I.E., THE REAL AND IMAGINARY PARTS ARE
C     ADJACENT IN STORAGE, SUCH AS FORTRAN IV PLACES THEM) WHOSE LENGTH
C     NN=2**K, K.GE.0 (IF NECESSARY, APPEND ZEROES TO THE DATA).  ISIGN
C     IS +1 OR -1.  IF A -1 TRANSFORM IS FOLLOWED BY A +1 ONE (OR A +1
C     BY A -1) THE ORIGINAL DATA REAPPEAR, MULTIPLIED BY NN.  TRANSFORM
C     VALUES ARE RETURNED IN ARRAY DATA, REPLACING THE INPUT.  THE TIME
C     IS PROPORTIONAL TO NN*LOG2(NN), RATHER THAN THE NAIVE NN**2.
C     ACCURACY IS ALSO GREATLY IMPROVED, THE RMS RELATIVE ERROR BEING
C     BOUNDED BY 6*SQRT(2)*LOG2(NN)*2**(-B), WHERE B IS THE NUMBER OF
C     BITS IN THE FLOATING POINT FRACTION.  WRITTEN BY NORMAN BRENNER OF
C     MIT LINCOLN LABORATORY.  JULY 1967.  THIS IS THE SHORTEST VERSION
C     OF THE FFT KNOWN TO THE AUTHOR.  FASTER PROGRAMS FOUR2 AND FOURT
C     EXIST THAT OPERATE ON ARBITRARILY SIZED MULTIDIMENSIONAL ARRAYS.
C     SEE-- IEEE AUDIO TRANSACTIONS (JUNE 1967), SPECIAL ISSUE ON FFT.
      DIMENSION DATA(1)
      N=2*NN
      J=1
      DO 5 I=1,N,2
      IF(I-J)1,2,2
1     TEMPR=DATA(J)
      TEMPI=DATA(J+1)
      DATA(J)=DATA(I)
      DATA(J+1)=DATA(I+1)
      DATA(I)=TEMPR
      DATA(I+1)=TEMPI
2     M=N/2
3     IF(J-M)5,5,4
4     J=J-M
      M=M/2
      IF(M-2)5,3,3
5     J=J+M
      MMAX=2
6     IF(MMAX-N)7,10,10
7     ISTEP=2*MMAX
      THETA=6.283185307/FLOAT(ISIGN*MMAX)
      SINTH=SIN(THETA/2.)
      WSTPR=-2.*SINTH*SINTH
      WSTPI=SIN(THETA)
      WR=1.
      WI=0.
      DO 9 M=1,MMAX,2
      DO 8 I=M,N,ISTEP
      J=I+MMAX
      TEMPR=WR*DATA(J)-WI*DATA(J+1)
      TEMPI=WR*DATA(J+1)+WI*DATA(J)
      DATA(J)=DATA(I)-TEMPR
      DATA(J+1)=DATA(I+1)-TEMPI
      DATA(I)=DATA(I)+TEMPR
8     DATA(I+1)=DATA(I+1)+TEMPI
      TEMPR=WR
      WR=WR*WSTPR-WI*WSTPI+WR
9     WI=WI*WSTPR+TEMPR*WSTPI+WI
      MMAX=ISTEP
      GO TO 6
10    RETURN
      END
```

APPENDIX E
FORTRAN LISTING OF MAPPING PROGRAM

In addition to a direct reproduction of the annotated Fortran listing for the mapping program, an alphabetized list of definitions of the most commonly used program variables and constants is also included in this appendix.

Basic Variables

AA	The array describing the selenographic location (relative to map center) of each element of the map
AIPP	The interpulse period in milliseconds
BEAM DB BEAM FB BEAM YB	Location of the antenna beam center in relative delay-doppler coordinates
BRAD	Angular radius of antenna beam to half-power in arcmin (Θ_o in text)
DDELAY	The quantization (resolution) in delay; it is equal to the range gate separation
DEL LONG DEL LAT	Displacement of center of the antenna beam from map center in selenographic coordinates (Mercator projection)
DEL1	Distance from radar to center of the moon in milliseconds (R in text)
DELX, DELY	The increment between resolution elements in the directions x and y, respectively, given in arc-minutes in the Mercator projection and in fractions of the lunar radius in the orthographic projection
DFREQ	The quantization (resolution) in frequency
DØ	11.595 msec (radius of moon expressed as a two-way delay)
DXS, DYS, DZS	Matrix elements for transforming selenographic coordinates to range-doppler coordinates
FCL1	Center-limb maximum doppler frequency difference (f_{c1} in text)
FCLS	The lunar center-to-limb maximum doppler difference in hertz (f_{c1} in text)
FRES	Frequency resolution = DFREQ
FXS, FYS, FZS	Matrix elements for transforming selenographic coordinates to range-doppler coordinates
IADW, IADR	Disk writing and reading addresses
ICENFB	The midpoint frequency box
IEND	Control flag with value 1 normally, 2 when normal termination is required, and 3 when EOF on data or ephemeris tape is detected
IFB	The frequency box corresponding to the nominal map center (measured with respect to ICENFB)
IFBSHIFT	Parameter to center the frequency box data according to IFB
IH1	Libration tape start time in hours
IM1	Libration tape start time in minutes

INP	The array which accumulates the final output "mapped" power densities
IPOL	A flag whose value is 1 when polarized data are being treated, and 2 when depolarized data are being processed
IRB	The range box corresponding to the nominal map center
IRBSHIFT	Parameter to shift the range box data window (according to the number and position of boxes used in background noise measurements)
IRD	The array which receives the intermediate normalized delay-doppler power densities
ISCALE	Scaling factor used to scale down input radar data in order to avoid overflow
ITEST	Control flag
ITPUL	Pulse length in microseconds
LRB	Last range box containing lunar echo data
MAXFB	The number of frequency boxes with lunar data
MAXRB	The number of range boxes with usable lunar data
MODE	Flag whose value is 1 when a Mercator projection is desired, and 2 when an orthographic or direction-cosine projection is desired
NFB	Total number of frequency boxes = 256
NRB	Total number of range boxes = 200
NSUM	The count of the number of summations of data before libration changes require a termination; it is set to zero before a new set of summations is to begin
NTOTAL	The total number of summations over-all (equal to the sum of all intermediate NSUM's)
NX, NY	The number of mapped resolution intervals in the directions x and y, respectively
QD	0.01745329251 radians/degree
RBP1	Latitude of subradar point in radians (δ_o in text)
RCP	Center-limb maximum doppler frequency difference (f_{c1} in text)
RDA	Doppler angle in radians (φ in text)
RLP1	Longitude of subradar point in radians (λ_o in text)
SEMI	The square of the moon's angular semi-diameter, in radians squared
SYSNOISM	Average level of background noise (for frequencies $\neq 0$)
SYSNOSMØ	Average DC level of background noise
SYSTEMP	System temperature in degrees Kelvin
TIME	The time in seconds from 0^h UT to the start of the run
TPWR	Transmitter power in kilowatts
TSUM	The coherent integration period: 256.0* AIPP* 0.001 = TSUM = 1.0/DFREQ
XDB, YDB, ZDB	The delay-doppler coordinates of the center of the mapped region on the lunar surface

XOFF, YOFF, ZOFF	Displacement of center of the antenna beam from map center in selenographic coordinates (direction cosines)
XSB, YSB, ZSB	The selenographic direction cosines of the position of the beam center on the lunar surface (the surface is assumed spherical)
XX(1), YY(1)	Selenographic coordinates of the map center – given in longitude and latitude (radians) for Mercator projection, and in direction cosines for orthographic projection
XX(2), YY(2)	Easternmost and southernmost limits of the mapped region
XX(3), YY(3)	Westernmost and northernmost limits of the mapped region
Z OFFSET	An offset factor (varies from −1 to +1) which may be used to adjust the relative delay origin of the normalizing scattering law

```
      PROGRAM SUPER
C PROGRAM SUPER IS THE SUPERVISORY AND CALLING ROUTINE FOR THE OVERLAY-SEGMENT
C PROCEDURE.  THIS SCHEME ALLOWS SUB PROGRAMS TO BE RETRIEVED FROM MAGNETIC TAPE
C ONLY WHEN NEEDED THUS ALLOWING USE OF PROGRAMS OTHERWISE TOO LARGE FOR STORAGE
11    PAUSE 11
C MOUNT A RANGE-FREQUENCY DATA TAPE ON LU 8, OR, INSTEAD, IF A SHADED
C PLOT FROM A PREVIOUSLY PREPARED TAPE 20 IS DESIRED MOUNT THE TAPE 20
C ON LU 8 AND TURN SET SWITCH 4 ON.
      GO TO(55,1),SSWTCHF(4)
1     CALL OVERLAY(1,0,1)
C OVERLAY(1,0,1) IS PROGRAM MAIN AND IS A SUB-PROGRAM FOR EXECUTING THE LUNAR
C MAPPING COMPUTATIONS.
      PAUSE 22
C MOUNT A SCRATCH TAPE ON LU 8 IN ORDER TO GENERATE A TAPE FOR
C USE BY THE SHADED PLOT DISPLAY PROGRAM.
C TURN SW5 ON IF PRINTOUT OF POWER VERSUS SELENOGRAPHIC POSITION IS
C DESIRED.
      CALL OVERLAY(2,0,1)
C OVERLAY 2 IS THE TAPE HANDLING AND GENERATING ROUTINE.
      PAUSE 33
C TURN SW3 ON IF A SHADED PLOT IS TO BE OMITTED.
      GO TO (11,55),SSWTCHF(3)
55    PAUSE 44
C CLEAR ALL SWITCHES AND NOW CHOOSE ONLY THOSE SWITCHES APPROPRIATE TO
C CHOICES IN THE SHADED PLOT DISPLAY PROGRAM.
      CALL OVERLAY(3,0,1)
C OVERLAY 3 IS THE SHADED PLOT PROGRAM.
      GO TO 11
      END



      FUNCTION MOD(I,J)
C MODULO J ARITHMETIC PACKAGE.
C THIS IS LOADED PERMANENTLY IN CORE ALONG WITH PROGRAM SUPER.
      MOD=I-J*(I/J)
      RETURN
      END



      FUNCTION MODF(I,J)
C MODULO J ARITHMETIC PACKAGE WITH RANGE OF VALUES INCLUDING J BUT EXCLUDING
C ZERO.
C THIS IS LOADED PERMANENTLY IN CORE ALONG WITH PROGRAM SUPER.
      MOD=I-J*(I/J)
      IF(MOD)10,5,10
5     MOD = J
10    MODF = MOD
      RETURN
      END
```

```
      PROGRAM MAIN
C THIS IS OVERLAY(1,0,1). IT ACTS AS A SUB-SUPERVISORY PROGRAM BY BRINGING IN
C THE VARIOUS SUB-PROGRAMS (SEGMENTS) AS NEEDED FROM TAPE TO PERFORM THE ACTUAL
C ADJUSTING AND MAPPING OF THE RANGE-DOPPLER DATA.
      COMMON XSB, YSB, ZSB, FCLS, SEMI ,LRB,   IPOL
     1  ,IRB,IFB, DFREQ, DDELAY, TIME, NSUM, NTOTAL, TSUM,FRES,ISUB,
     1 ITITLE(18), MAXRB, MAXFB,  ICENFB ,
     2  MODE, XX(3), YY(3), NX, NY, DELX, DELY, QD, D0,NRB, NFB,
     3   XDB, YDB, ZDB,  IEND, FXS, FYS, FZS, DXS, DYS,DZS
     4  ,IH1,IM1,LT,DEL1,DOP,RLP1,RBP1,RCP,FCL1,RDA1,ZAZ,ZEL,RQ,RDP,RRAP
     5  ,TAPE1,TAPE2,SYSNOISM,SYSNOSM0,SYSTEMP,TPWR,ITPUL
     6  ,IFBSHIFT,IH2,IM2,DEL2,RLP2,RBP2,FCL2,RDA2
      COMMON IRBSHIFT,ITEST,IADW,IADR,ISCALE
      COMMON BRAD
      COMMON X OFF, Y OFF, Z OFF, Z OFF SET , BEAM FB, BEAM DB
10    REWIND 8
      REWIND 9
C LU 8 IS THE RANGE DOPPLER DATA TAPE.  LU 18 EQUALS LU 8. IT IS USED INSTEAD
C OF LU 8 WHENEVER BUFFER IN STATEMENTS ARE USED.
C LU 9 IS THE LIBRATION TAPE.
      READ(60,1) SYSNOISM,SYSNOSM0,SYSTEMP ,TPWR , ITPUL , NTOTLMAX
C CARD INPUT IS AVERAGE AND D.C. NOISE POWER, SYSTEM TEMPERATURE IN DEGREES
C KELVIN, TRANSMITTER POWER IN KILOWATTS, PULSE LENGTH IN MICROSECONDS AND
C THE UPPER BOUND ON THE NUMBER OF SUMMATIONS.
C
C
      READ(60,1) XX(1), YY(1), DELX, DELY, NX, NY, MODE,IPOL
1     FORMAT ( 4F10.3, 5I5 )
C CARD INPUT IS THE BEAM CENTER IN SELENOGRAPHIC COORDINATES, SELENOGRAPHIC
C GRID SUBDIVISION SIZE, THE NUMBER OF ELEMENTS IN THE SELENOGRAPHIC GRID,
C THE CARTOGRAPHIC PROJECTION SPECIFICATION AND THE POLARIZATION INDEX.
      GO TO (4,3),EOFCKF(60)
3     CONTINUE
      WRITE(61,7)SYSNOISM, SYSNOSM0, SYSTEMP, TPWR, ITPUL
7     FORMAT ( 1H0, 10X 28HNOISE LEVEL PER COHERENT SUM, F15.3,
     1  30H     DC LEVEL PER COHERENT SUM, F15.3,  //      11X
     2 18HSYSTEM TEMP(DEG-K), F15.3,19H     XMTR POWER(KW), F10.3 ,
     4   31H     XMTR PULSE LENGTH(MICROSC), I10 )
C   SEGMENT(1,1,1) IS SUBPROGRAM SETUP
      CALL SEGMENT(1,1,1)
```

```
C      TAPE 8 IS NOW SPACED JUST PAST ITS TITLE RECORD AND TAPE 9 IS JUST
C      PAST ITS TITLE RECORD AND FIRST DATA RECORD.
       GO TO ( 15,15,200 ) IEND
C    SEGMENT(1,2,1) IS SUBPROGRAM SELEN
15     CALL SEGMENT(1,2,1)
C    SEGMENT(1,3,1) IS SUBPROGRAM READIN
20     CALL SEGMENT(1,3,1)
       GO TO (30,30,200) IEND
C    SEGMENT(1,4,1) IS SUBPROGRAM NORMAL
30     CALL SEGMENT(1,4,1)
       IF(NTOTLMAX )4002,4002,4003
4003    IF(NTOTAL .GE. NTOTLMAX)4000,4002
4002   GO TO(4000,4001),SSWTCHF(2)
4000   IEND=2
       REWIND 18
4001   CONTINUE
C    SEGMENT(1,5,1) IS SUBPROGRAM READOUT
       CALL SEGMENT(1,5,1)
       GO TO ( 20,109,200 ) IEND
C
109    WRITE(61,121)
       WRITE(59,121)
121    FORMAT(26H    END OF MAPPING PROGRAM)
       PAUSE 2
        RETURN
C
C
200    WRITE(61,201)
       WRITE(59,201)
201    FORMAT(47H ERROR IN INPUT, PRESS RUN TO READ IN NEW INPUT)
       PAUSE
C PAUSE 1 = ERROR IN INPUT
       GO TO 10
4      WRITE(61,221)
221    FORMAT(54H PAUSE 2 *     END OF RUN                                  )
       END
```

```
      PROGRAM SETUP
C SETUP IS AN INITIALIZATION ROUTINE IN WHICH PARAMETERS USED LATER IN THE
C LUNAR MAPPING ARE DEFINED.
      COMMON XSB, YSB, ZSB, FCLS, SEMI ,LRB,    IPOL
     1  ,IRB,IFB, DFREQ, DDELAY, TIME, NSUM, NTOTAL, TSUM,FRES,ISUB,
     1 ITITLE(18), MAXRB, MAXFB,  ICENFB ,
     2  MODE, XX(3), YY(3), NX, NY, DELX, DELY, QD, D0,NRB, NFB,
     3   XDB, YDB, ZDB,  IEND, FXS, FYS, FZS, DXS, DYS,DZS
     4  ,IH1,IM1,LT,DEL1,DOP,RLP1,RBP1,RCP,FCL1,RDA1,ZAZ,ZEL,RQ,RDP,RRAP
     5  ,TAPE1,TAPE2,SYSNOISM,SYSNOSM0,SYSTEMP,TPWR,ITPUL
     6  ,IFBSHIFT,IH2,IM2,DEL2,RLP2,RBP2,FCL2,RDA2
      COMMON IRBSHIFT,ITEST,IADW,IADR,ISCALE
      COMMON BRAD
      COMMON X OFF, Y OFF, Z OFF, Z OFF SET , BEAM FB, BEAM DB
      COMMON INP(257)
      REAL NORTHLAT,IDELAY
C
C LOGICAL UNIT 8 IS RANGE-DOP DATA
C LOGICAL UNIT 9 IS LIB TAPE
C LU 18=LU 8.
C THE MASS STORAGE DEVICE IS REFERENCED BY THE CALL TO YYDISK.  YYWAIT IS
C THE CALL TO CHECK THE STATUS OF THE PREVIOUS CALL TO YYDISK.
      SETPTIME=CLOCK(0)
      NTOTAL = 0
      IEND = 1
      DEGREE=57.295779513
      QD=1.0/DEGREE
      ITEST =1
      D0 = 11.595
C READ RANGE-DOP TAPE FOR TAPE TITLE.
  151 BUFFER IN (18,1) (ITITLE(1),ITITLE(18))
  152 GO TO (152,154,155,153), UNITSTF(18)
  153 BACKSPACE 18
      GO TO 151
  155 WRITE (59,1536)
1536  FORMAT(50H END OF FILE ON LU 8. HIT RUN TO READ NEXT RECORD.     )
      PAUSE 20
      GO TO 151
  154 CONTINUE
      READ(60,6578)ND1,ND2,IRB,IFB,IDELAY,DFREQ,DTIME,ISTARTHR,ISTARTMN,
     $  ISTARTSC
 6578 FORMAT(4I5,3F7.0,6I5)
C ND1 AND ND2 ARE DUMMY VARIABLES TO COMPENSATE FOR DATA NO LONGER NECESSARY.
C IRB IS THE BEAM CENTER RANGE BOX, IFB IS THE BEAM CENTER FREQUENCY BOX
C OFFSET, IDELAY IS THE RANGE GATE SEPARATION IN MICROSECONDS, DFREQ IS THE
C SPECTRAL RESOLUTION, DTIME IS THE COHERENT INTEGRATION TIME, ISTARTHR,
C ISTARTMN, AND ISTARTSC IS THE START TIME OF THE EXPERIMENT.
      READ(60,6000)IRBSHIFT,ICENFB,MAXRB,MAXFB,ISCALE,BRAD,AIPP
6000  FORMAT(5I5,2F20.0)
```

```
C IRBSHIFT IS THE NUMBER OF RANGE BOXES RELEGATED TO NON LUNAR SIGNAL, ICENFB IS
C THE CENTRAL FREQUENCY BOX (ALWAYS 128 IN THESE SERIES OF RUNS), MAXRB IS THE
C MAXIMUM NUMBER OF RANGE BOXES WITH LUNAR SIGNAL, MAXFB IS THE MAXIMUM NUMBER
C OF AVAILABLE FREQUENCY BOXES, ISCALE IS A SCALE FACTOR APPLIED TO THE DATA IN
C ORDER TO AVOID OVERFLOWS DURING SUBSEQUENT COMPUTATIONS, BRAD IS THE ASSUMED
C RADAR BEAM RADIUS IN ARC MINUTES, AND AIPP IS THE INTERPULSE PERIOD IN MILLI-
C SECONDS.
      IF(BRAD .EQ. 0.0)6004,6005
6004  BRAD=2.20
6005  IF(ISCALE .EQ. 0)6002,6003
6002  ISCALE=1
6003  WRITE(61,6001)IRBSHIFT,ICENFB,MAXRB,MAXFB,ISCALE,BRAD
6001  FORMAT(/11H IRBSHIFT= I5, 8X 9H ICENFB= I5, 8X 8H MAXRB= I5, 8X
     1  8H MAXFB= I5, 8X 15HSCALE FACTOR=        I5//14H BEAM RADIUS= F5
     2  .2, 12H ARCMINUTES.  /)
      NRB=200
      NFB=256
      TIME=3600*ISTARTHR+60*ISTARTMN+ISTARTSC
C
      TSUM=DTIME
C     THE TIME PER COHERENT SUM
      FRES=1./TSUM
C     THE FREQUENCY RESOLUTION
      IF(AIPP .EQ. 0.0)5999,5998
5998  WRITE(61,5997)AIPP
5997  FORMAT(/42H THE INTERPULSE PERIOD IN MILLISECONDS IS F4.1/)
      TSUM=DTIME=AIPP*256.0 *0.001
      DFREQ=FRES=1.0/TSUM
5999  CONTINUE
      DDELAY=IDELAY/1000.
C     CONVERT DDELAY TO MILLISECONDS FROM MICROSECONDS
      IHS=ISTARTHR$  IMS=ISTARTMN$  ISS=ISTARTSC
C     THE STARTING TIME OF THE RANGE-DOPPLER DATA, IN HOURS, MINUTES AND
C     SECONDS.
      WRITE(61,7) (ITITLE(I),I=1,18)
7     FORMAT( 1H0  10X, 20HRANGE DOP MAP FOR    , 18A4 )
      WRITE(61,6) IHS, IMS, ISS, IRB, IFB, NRB,NFB,IDELAY,DFREQ,TSUM
6     FORMAT( 1H0, 10X, 16HSTART TIME (GMT),3I5, /,/,11X,
     1   21HBEAM CENTER RANGE BOX, I6, 25H     BEAM CENTER FREQ BOX,I6,
     4   18H      NUM RANGE BOX, I5, 17H      NUM FREQ BOX, I5,
     2   //    11X, 24HRANGE GATE SEP(MICROSEC),F7.3, 5X
     3   13HFREQ SEP(CPS), F10.3, 27H      COHERENT SUM TIME(SEC),F10.3)
      GO TO ( 118,119 ) IPOL
118   WRITE(61,8 )
8     FORMAT( 1H0, 10X, 19HPOLARIZED COMPONENT)
      GO TO 120
119   WRITE(61,9 )
9     FORMAT( 1H0, 10X, 21HDEPOLARIZED COMPONENT)
120   CONTINUE
      GO TO (19,20) MODE
19    WRITE(61,4) XX(1), YY(1), DELX, DELY,NX,NY
4     FORMAT( 1H0, 10X, 27HBEAM CENTER - SEL LONG(DEG), F10.3,
     1   17H      SEL LAT(DEG), F10.3, 20H      DELTA LONG(MIN), F10.3,
     2   18H    DELTA LAT(MIN), F10.3, //,25H            NUM DELTA LONG,
     4   I5, 18H      NUM DELTA LAT,I5 )
```

```
      XX(1) = QD*XX(1)
      YY(1) = YY(1)*QD
      DELX=( DELX*QD)/60.0
      DELY= ( DELY*QD )/60.0
      CLAT = COS( YY(1) )
      XSB = CLAT*SIN( XX(1) )
      YSB = SIN( YY(1) )
      ZSB = CLAT*COS( XX(1) )
      READ(60,7711)DEL LONG,DEL LAT,Z OFF SET
7711  FORMAT(3F20.0)
      WRITE(61,7712)DEL LONG,DEL LAT,Z OFF SET
7712  FORMAT(39H0BEAM CORRECTION FACTORS IN DEGREES ARE F9.4, 6H, AND
     1 F9.4, 1H./51H OFFSET IN DELAY FOR SCATTERING LAW COMPENSATION IS
     2 F9.6, 1H.)
      DEL LAT = DEL LAT * QD
      DEL LONG = DEL LONG * QD
      X OFF = COS(YY(1)+ DEL LAT)*SIN(XX(1)+DEL LONG)
      Y OFF = SIN(YY(1)+DEL LAT)
      Z OFF = SQRT(1.0-X OFF *X OFF - Y OFF *Y OFF)
      GO TO 21
20    WRITE(61,5)XX(1), YY(1), DELX, DELY, NX, NY
5     FORMAT( 1H0, 10X, 33HBEAM CENTER - DIRECTION COSINE XI, F10.3,
     1   8H      ETA, F10.3, /,/, 11X,  8HDELTA XI, F10.3,
     2   14H      DELTA ETA, F10.3, 17H      NUM DELTA XI, I5,
     3   18H      NUM DELTA ETA, I5 )
      XSB = XX(1)
      YSB = YY(1)
      ZSB = 1.0 - XSB*XSB - YSB*YSB
      IF (ZSB) 220,222,222
220   WRITE(59,221 )
       WRITE(61,221)
221   FORMAT( 25HERROR IN SELEN GRID INPUT)
      IEND = 3
      GO TO 50
222   ZSB = SQRT(ZSB)
C DEL XI AND DEL ETA ARE OFFSET FACTORS IN DIRECTION COSINES.
      READ(60,7711)DEL XI, DEL ETA, Z OFF SET
      WRITE(61,7718)DEL XI, DEL ETA, Z OFF SET
7718  FORMAT(50H0BEAM CORRECTION FACTORS IN DIRECTION COSINES ARE 2E10.3
     1 //51H OFFSET IN DELAY FOR SCATTERING LAW COMPENSATION IS  F9.6, 1
     2H.)
      X OFF = XX(1) + DEL XI
      Y OFF = YY(1) + DEL ETA
      ZEBRA = (1.0 - X OFF * X OFF - Y OFF * Y OFF )
      IF(ZEBRA)7713,7714,7714
7713  X OFF = XSB
      Y OFF = YSB
      Z OFF = ZSB
      GO TO 7715
```

```
 7714 Z OFF = SQRT(ZEBRA)
7715  CONTINUE
21    XX(2) = XX(1) - 0.5*NX*DELX
      XX(3)=XX(1)+0.5*NX*DELX
      GO TO(24,25),MODE
24    YY(2)=2.0*ATAN(EXP(-0.5*NY*DELY)*TANF(0.7853981634 +0.5*YY(1)))
     1  -1.570796329
      YY(3)=2.0*ATAN(EXP(+0.5*NY*DELY)*TANF(0.7853981634 +0.5*YY(1)))
     1  -1.570796329
      SOUTHLAT=YY(2)/QD
      CENTRLAT=YY(1)/QD
      NORTHLAT=YY(3)/QD
      WRITE (61,6006)SOUTHLAT,CENTRLAT,NORTHLAT
6006  FORMAT(/30H THE SOUTHERNMOST LATITUDE IS F10.5,
     1  25H THE CENTRAL LATITUDE IS F10.5,
     2 30H THE NORTHERNMOST LATITUDE IS F10.5/)
      GO TO 26
25    YY(2)=YY(1)-0.5*NY*DELY
      YY(3)=YY(1)+0.5*NY*DELY
      WRITE(61,130)YY(2),YY(1),YY(3)
130   FORMAT(14H0ETA SOUTH IS F7.4, 17H , ETA MIDDLE IS F7.4,
     1  20H , AND ETA NORTH IS F7.4)
26    NX=NX+1
      NY = NY+ 1
      INP(1) = IADD =0
      CALL MOVE(INP(1),INP(2))
      DO 23 I=1,NX
      CALL YYDISK( 0, 2, IADD, INP,201 )
      IADD = IADD + 256
23    CALL YYWAIT(0)
C READ LIBRATION TAPE TO GET LIB TAPE START TIME
      READ(9) IDAY, MON, IYR
      READ( 9) IH1,IM1, LT, DEL1, DOP, RLP1,RBP1,RCP, FCL1,RDA1,ZAZ, ZEL
     1     ,RQ, RDP, RRAP
      WRITE(61,80)IH1, IM1, IDAY, MON, IYR
80    FORMAT( 1H0, 10X, 31HFIRST TIME ON LIBRATION TAPE IS, 2I5, 5H   ON
     1  , 3I5 , 8H   (GMT))
      TAPE1 = IH1*3600.0 + IM1*60.0
      IH2=IH1
      IM2=IM1
      DEL2=DEL1
      RLP2=RLP1
      RBP2=RBP1
      FCL2=FCL1
      RDA2=RDA1
      TAPE2=TAPE1
C     THE STARTING TIME OF THE LIBRATION DATA.
      IRB=IRB-IRBSHIFT
      SETPTIME=CLOCK(0)-SETPTIME
      WRITE(61,30)SETPTIME
30    FORMAT ( 15H     SETUP TIME, F10.3 )
50    RETURN
      END
```

```
      PROGRAM SELEN
C COMPUTES AND WRITES ON MASS STORAGE THE QUANTITIES XS,YS,ZS AND OTHER
C QUANTITIES USED IN THE SUBROUTINE READOUT.
      COMMON XSB, YSB, ZSB, FCLS, SEMI ,           LRB,   IPOL
     1  ,IRB,IFB, DFREQ, DDELAY, TIME, NSUM, NTOTAL, TSUM,FRES,ISUB,
     1 ITITLE(18), MAXRB, MAXFB,  ICENFB ,
     2  MODE, XX(3), YY(3), NX, NY, DELX, DELY, QD, D0,NRB, NFB,
     3   XYB, YDB, ZDB,                IEND, FXS, FYS, FZS, DXS, DYS,DZS
     4  ,IH1,IM1,LT,DEL1,DOP,RLP1,RBP1,RCP,FCL1,RDA1,ZAZ,ZEL,RQ,RDP,RRAP
     5  ,TAPE1,TAPE2,SYSNOISM,SYSNOSM0,SYSTEMP,TPWR,ITPUL
     6  ,IFBSHIFT,IH2,IM2,DEL2,RLP2,RBP2,FCL2,RDA2
      COMMON IRBSHIFT,ITEST,IADW,IADR,ISCALE
      COMMON BRAD
      COMMON X OFF, Y OFF, Z OFF, Z OFF SET , BEAM FB, BEAM DB
      COMMON IDUMMY(2564)
      EQUIVALENCE (AA,IDUMMY)
      DIMENSION AA(3,201), YYY(201)
      SELNTIME=CLOCK(0.0)
      NWDS = 6*NY
      CALL PROJECTN(YYY)
      ITENP1=524288
      DO 100 I=1,NX
      X=XX(2)+(I-1)*DELX
      GO TO(2000,2001),MODE
2000  CLON=COS(X)
      SLON=SIN(X)
2001  DO 90 J=1,NY
      Y=YYY(J)
      GO TO(10,20),MODE
10    CLAT=COS(Y)
      SLAT=SIN(Y)
      XS=CLAT*SLON-XSB
      YS=SLAT-YSB
      ZS=CLAT*CLON-ZSB
      GO TO 901
20    XS=X
      YS=Y
      ZS=1.0-XS*XS-YS*YS
      IF(ZS)21,23,23
21    WRITE(59,22)
      WRITE(61,22)
22    FORMAT(26H ERROR IN SELEN GRID INPUT)
      IEND=3
      RETURN
23    ZS=SQRT(ZS)
      XS=XS-XSB
      YS=YS-YSB
      ZS=ZS-ZSB
901   AA(1,J)=XS
      AA(2,J)=YS
90    AA(3,J)=ZS
      CALL YYDISK(0,2,ITENP1,AA,NWDS)
      ITENP1 = ITENP1 + 1536
      CALL YYWAIT(0)
100   CONTINUE
      SELNTIME=CLOCK(0.0)-SELNTIME
      WRITE(61,101)SELNTIME
101   FORMAT(11H SELEN TIME     3F10.3)
      RETURN
      END
```

```
      SUBROUTINE PROJECTN(YYY)
C SUBROUTINE PROJECTN COMPUTES LATITUDES FOR EACH SELEN GRID LINE ACCORDING
C TO THE TYPE OF CARTOGRAPHIC PROJECTION DESIRED, AND RETURNS THESE RESULTS
C IN ARRAY YYY.
      COMMON XSB, YSB, ZSB, FCLS, SEMI ,           LRB,   IPOL
     1  ,IRB,IFB, DFREQ, DDELAY, TIME, NSUM, NTOTAL, TSUM,FRES,ISUB,
     1 ITITLE(18), MAXRB, MAXFB,  ICENFB ,
     2  MODE, XX(3), YY(3), NX, NY, DELX, DELY, QD, D0,NRB, NFB,
     3   XYB, YDB, ZDB,                IEND, FXS, FYS, FZS, DXS, DYS,DZS
     4  ,IH1,IM1,LT,DEL1,DOP,RLP1,RBP1,RCP,FCL1,RDA1,ZAZ,ZEL,RQ,RDP,RRAP
     5  ,TAPE1,TAPE2,SYSNOISM,SYSNOSM0,SYSTEMP,TPWR,ITPUL
     6  ,IFBSHIFT,IH2,IM2,DEL2,RLP2,RBP2,FCL2,RDA2
      COMMON IRBSHIFT,ITEST,IADW,IADR,ISCALE
      COMMON BRAD
      COMMON X OFF, Y OFF, Z OFF, Z OFF SET , BEAM FB, BEAM DB
      COMMON IDUMMY(2564)
      DIMENSION YYY(201)
      GO TO(1,2),MODE
C MERCATOR PROJECTION FOR MODE 1.
1     DO 3 J=1,NY
3     YYY(J)=2.0*(ATAN(EXP(DELY*FLOAT(J-1))*TANF(0.7853981634 +0.5*YY(2))))
     1     -1.570796329
      GO TO 5
C ORTHOGRAPHIC (DIRECTION COSINES) PROJECTION.
2     DO 4 J=1,NY
4     YYY(J)=YY(2)+(J-1)*DELY
5     WRITE(59,100)
100   FORMAT(61H TYPE A 1 IF PRINTOUT OF SELEN. LAT. IS DESIRED FOR THIS
     1 MAP.)
      READ(59,101)ANODE
101   FORMAT(E30.0)
      IF(ANODE .GT. 0.0)6,7
6     CALL SELENLAT(YYY)
7     RETURN
      END
```

```
      SUBROUTINE SELENLAT(YYY)
C SUBROUTINE SELENLAT PROVIDES PRINTOUT OF SELEN LATITUDES VERSUS
C SELENOGRAPGIC GRID LINES IF DESIRED.
      COMMON XSB, YSB, ZSB, FCLS, SEMI ,           LRB,   IPOL
     1  ,IRB,IFB, DFREQ, DDELAY, TIME, NSUM, NTOTAL, TSUM,FRES,ISUB,
     1 ITITLE(18), MAXRB, MAXFB,  ICENFB ,
     2  MODE, XX(3), YY(3), NX, NY, DELX, DELY, QD, D0,NRB, NFB,
     3   XDB, YDB, ZDB,              IEND, FXS, FYS, FZS, DXS, DYS,DZS
     4  ,IH1,IM1,LT,DEL1,DOP,RLP1,RBP1,RCP,FCL1,RDA1,ZAZ,ZEL,RQ,RDP,RRAP
     5  ,TAPE1,TAPE2,SYSNOISM,SYSNOSM0,SYSTEMP,TPWR,ITPUL
     6  ,IFBSHIFT,IH2,IM2,DEL2,RLP2,RBP2,FCL2,RDA2
      COMMON IRBSHIFT,ITEST,IADW,IADR,ISCALE
      COMMON BRAD
      COMMON X OFF, Y OFF, Z OFF, Z OFF SET , BEAM FB, BEAM DB
      COMMON IDUMMY(2564)
      DIMENSION YYY(201)
      DO 11 JJ=1,NY
      YSUBJ=YYY(JJ)/(0.01745329251*(2-MODE)+MODE-1)
      ISUBJ=JJ-1
      KM=ISUBJ-20*(JJ/20)
      IF(KM .EQ. 0)10,11
11    WRITE(61,104)ISUBJ,YSUBJ
104   FORMAT(      /I20,F40.4)
      WRITE(61,105)
105   FORMAT(1H1)
      RETURN
10    WRITE(61,100) (ITITLE(I),I=1,18)
100   FORMAT(30H1ORDINATE VALUES FOR LUNAR MAP /5X 5H FOR 18A4//)
      GO TO (1,2),MODE
1     WRITE(61,101)
101   FORMAT(5X 21H MERCATOR PROJECTION./ /         )
      GO TO 3
2     WRITE(61,102)
102   FORMAT(5X 45H ORTHOGRAPHIC (DIRECTION COSINES) PROJECTION./)
3     WRITE(61,103)
103   FORMAT(4X 28H LINEAR INCREMENT VERTICALLY 20X 8HORDINATE//)
      GO TO 11
      END
```

```
      PROGRAM READIN
C FORMS THE INCOHERENT SUM OF SPECTRA UNTIL LIBRATION CHANGES REQUIRE
C A NEW DELAY-FREQ TO SELEN POSITION TRANSFORMATION
      COMMON XSB, YSB, ZSB, FCLS, SEMI ,LRB,   IPOL
     1  ,IRB,IFB, DFREQ, DDELAY, TIME, NSUM, NTOTAL, TSUM,FRES,ISUB,
     1 ITITLE(18), MAXRB, MAXFB,  ICENFB ,
     2  MODE, XX(3), YY(3), NX, NY, DELX, DELY, QD, D0,NRB, NFB,
     3   XDB, YDB, ZDB,  IEND, FXS, FYS, FZS, DXS, DYS,DZS
     4  ,IH1,IM1,LT,DEL1,DOP,RLP1,RBP1,RCP,FCL1,RDA1,ZAZ,ZEL,RQ,RDP,RRAP
     5  ,TAPE1,TAPE2,SYSNOISM,SYSNOSM0,SYSTEMP,TPWR,ITPUL
     6  ,IFBSHIFT,IH2,IM2,DEL2,RLP2,RBP2,FCL2,RDA2
      COMMON IRBSHIFT,ITEST,IADW,IADR,ISCALE
      COMMON BRAD
      COMMON X OFF, Y OFF, Z OFF, Z OFF SET , BEAM FB, BEAM DB
      COMMON IRD(256,30), IDUMMY(2564)
      EQUIVALENCE (IZERO,IRD)
      DIMENSION IZERO(1)
      EQUIVALENCE(TTIME,IDUMMY(1)),(I1,IDUMMY(3)),(I2,IDUMMY(4))
     *  ,(INDATA,IDUMMY(5))
      DIMENSION D(3,3),F(3,3),INDATA(2560)
      READTIME=CLOCK(0)
      IAR=IADR=1048576
      IAW=IADW=1572864
      HALFDDLY=   DDELAY
      HALFDFRQ=   DFREQ
      LRB=NRB-IRBSHIFT
      MAXRB=LRB
      IF(ITEST .EQ. 1)20,44
20    IFBSHIFT=ICENFB-IFB -1
      ITEST=2
2     IF(IFBSHIFT .LT. 0)3,4
3     IFBSHIFT=IFBSHIFT+NFB
      GO TO 2
4     IFB=ICENFB
44    IFB0=MOD(1+IFBSHIFT,NFB)+1
      NSUM = 0
      IZERO(1)=0
      CALL MOVE(IZERO(1),IZERO(2))
      ITEM=IAR
      DO5I =1,MAXRB
      CALL YYWAIT(0)
      CALL YYDISK(0,2,ITEM,IZERO,256)
      ITEM = ITEM + 256
5     CONTINUE
C
1000  CALL YYWAIT(1)
      CALL YYWAIT(0)
      CALL YYDISK(0,1,IAR,IRD(1,1),5120)
      IOFF=0
      IWRT=1
      IWRD=21
      IAR=IAR+5120
      CALL YYWAIT(0)
```

```
C READ RANGE-DOP TAPE(LU8) FOR UNNORMALIZED SPECTRA FOR NRB RANGE GATES
      NPARERR=0
151   BUFFERIN(18,1)(IDUMMY(1),IDUMMY(2564))
C LUN 8 = LUN 18
152   GOTO (152,103,118,156),UNITSTF(18)
C     GO TO (INCOMPLETE,COMPLETE OK,COMPLETE EOF,COMPLETE PARITY ERROR)
C     IN CASE OF PARITY JUST DO NOT ADD IN THE OFFENDING DATA RECORD.
103   I1=MIN0(I1,NRB)
      I2=MIN0(I2,NRB)
      DO 99 JK=5,2564
99    IDUMMY(JK)=IDUMMY(JK)/ISCALE
C     DO NOT TRANSFER MORE THAN NRB RANGE GATES OFF THE INPUT TAPE.
      ICC = 0
      DO 105 I=I1,I2
C
C
      L = I - IRBSHIFT
      IF ( L .GE. 1 .AND. L.LE. MAXRB ) 1039,105
 1039 CONTINUE
      IF (L-LRB)  102,102,156
102   J1=(L-(I1-IRBSHIFT))*256+1
      J2 = J1+NFB-1
      L = MODF(L,10) + IOFF
      ICC = 1
      CALL COHERESM(J1,J2,IFBSHIFT,NFB,MAXFB,IRD(1,L),INDATA(1))
C COHERESM PROVIDES AN ASSEMBLY LANGUAGE IMPLEMENTATION OF THE
C FOLLOWING COMMANDS.
C     DO 1041  J=J1,J2
C     K=MOD(J+IFBSHIFT,NFB)+1
C     IF(K .GT. MAXFB)1041,104
C 104 IRD(K,L)=IRD(K,L)+INDATA(J)
C1041 CONTINUE
  105 CONTINUE
156   IF(I2-NRB) 1100,155,155
1100  IF(ICC)151,151,1200
1200  CALL YYWAIT(1)
      CALL YYDISK(1,2,IAW,IRD(1,IWRT),2560)
      CALL YYWAIT(0)
      CALL YYDISK(0,1,IAR,IRD(1,IWRD),2560)
      IAW = IAW + 2560
      IAR = IAR + 2560
      IOFF = MOD(IOFF+10,30)
      IWRT = MOD(IWRT+10,30)
      IWRD = MOD(IWRD+10,30)
      GO TO 151
```

```
155   NSUM=NSUM+1
      NTOTAL = NTOTAL + 1
      TIME = TIME + TSUM
      CALL LIBREAD( RLP,RBP,FCL, RDA, DEL )
      GO TO (40,120,120) IEND
40    CLP = COS(RLP)
      CALL YYWAIT(1)
      CALL YYDISK(1,2,IAW,IRD(1,IWRT),2560)
C
C     CHANGE DISK ADDRESS FOR READING AND WRITING
C
      ITEM = IADR
      IAR = IADR = IADW
      IAW = IADW = ITEM
      SLP = SIN(RLP)
      SBP = SIN(RBP)
      CBP = COS(RBP)
      SDA = SIN(RDA)
      CDA = COS(RDA)
      DX = SLP*CBP*D0
      DY = SBP*D0
      DZ = CBP*CLP*D0
      FX =  FCL*( CDA*CLP + SDA*SLP*SBP )
      FY =-FCL*SDA*CBP
      FZ =-FCL*( CDA*SLP - SDA*CLP*SBP )
      IF(NSUM .EQ. 1)451,452
451   BEAM FB = (FX * X OFF + FY * Y OFF +FZ * Z OFF)/FCL
      BEAM DB = (DX * X OFF + DY * Y OFF + DZ * Z OFF )/D0
452   CONTINUE
      DO 100 I = 1,3
      DO 100 J = 1,3
      IF (I.GT.1.AND.J.GT.1 .OR. I.EQ.1.AND.J.EQ.1) 45,100
45     GO TO (46,47 ) MODE
46    X = COS(YY(J))*SIN(XX(I))
      Y = SIN(YY(J))
      GO TO 48
47    X = XX(I)
      Y = YY(J)
48    Z = SQRT( 1.0 - X*X - Y*Y )
      DP = DX*X + DY*Y + DZ*Z
      FP = FX*X + FY*Y + FZ*Z
      IF (I.EQ.1.AND.J.EQ.1)50,55
50    D1 = DP
      F1 = FP
      IF(NSUM-1)51,51,100
```

```
C COMPUTE QUANTITIES TO BE USED IN SUBROUTINES NORMAL AND READOUT.
51     XDB= FP/FCL
       Y1 = X*( SDA*CLP - CDA*SLP*SBP )
       Y2 =  Y*CDA*CBP
       Y3 =-Z*( SDA*SLP + CDA*CLP*SBP )
       YDB = Y1 + Y2 + Y3
       ZDB = DP/D0
       SEMI =(695.4/( DEL*QD ) )**2
C      SEMI IS THE SQUARE OF THE MOON'S SEMI-DIAMETER (IN ARCMIN)
       FCLS = FCL
       FXS =-FX/DFREQ
       FYS =-FY/DFREQ
       FZS =-FZ/DFREQ
       DXS =-DX/DDELAY
       DYS =-DY/DDELAY
       DZS =-DZ/DDELAY
55     DD = DP - D1
       DF = FP - F1
       IF(NSUM-1)60,60,65
60     D(I,J) = DD
       F(I,J) =DF
       GO TO 100
65     IF(ABS(DD-D(I,J)) .LT. HALFDDLY) 70,66
66     WRITE(61,68) I,J,NSUM
68     FORMAT ( 1H0, 10X, 5HDELAY, 3I10 )
C DELAY VARIATION GREATER THAN 1/2 RANGE GATE SEPARATION
       GO TO 120
70     IF(ABS(DF-F(I,J)) .LT. HALFDFRQ) 100,75
75     WRITE( 61,76) I,J,NSUM
76     FORMAT( 1H0, 10X, 9HFREQUENCY,3I10 )
C FREQ VARIATION GREATER THAN 1/2 FREQ SEPARATION
       GO TO 120
100    CONTINUE
       GO TO 1000
C
C
118    WRITE(61,117)
117    FORMAT( 40H          EOF DETECTED ON RANGE-DOP TAPE)
       IEND = 2
       REWIND 18
120    READTIME=CLOCK(0)-READTIME
       WRITE(61,121)READTIME,NSUM
121    FORMAT( 16H     READIN TIME, F10.3, 9H     NSUM, I10 )
       RETURN
       END
```

```
      SUBROUTINE LIBREAD ( RLP, RBP, FCL, RDA, DEL )
C READS LIBRATION TAPE(LU9) FOR SUBRADAR POINT, CEN-LIMB FREQ, DOPPLER ANGLE
C AND DELAY
      COMMON XSB, YSB, ZSB, FCLS, SEMI ,LRB,   IPOL
     1  ,IRB,IFB, DFREQ, DDELAY, TIME, NSUM, NTOTAL, TSUM,FRES,ISUB,
     1 ITITLE(18), MAXRB, MAXFB,  ICENFB ,
     2  MODE, XX(3), YY(3), NX, NY, DELX, DELY, QD, D0,NRB, NFB,
     3   XDB, YDB, ZDB,  IEND, FXS, FYS, FZS, DXS, DYS,DZS
     4  ,IH1,IM1,LT,DEL1,DOP,RLP1,RBP1,RCP,FCL1,RDA1,ZAZ,ZEL,RQ,RDP,RRAP
     5  ,TAPE1,TAPE2,SYSNOISM,SYSNOSM0,SYSTEMP,TPWR,ITPUL
     6  ,IFBSHIFT,IH2,IM2,DEL2,RLP2,RBP2,FCL2,RDA2
      COMMON IRBSHIFT,ITEST,IADW,IADR,ISCALE
      COMMON BRAD
      COMMON X OFF, Y OFF, Z OFF, Z OFF SET , BEAM FB, BEAM DB
C     INITIALLY TAPE1=TAPE2 AND IH2, IM2, ETC. ALL EQUAL IH1, IM2, ETC.
15    IF( TIME - TAPE1 ) 16,20,20
20    DT = TIME - TAPE2
      IF(DT) 40,30,30
30    IH1 = IH2
      IM1 = IM2
      DEL1 = DEL2
      RLP1 = RLP2
      RBP1 = RBP2
      FCL1 = FCL2
      RDA1 = RDA2
      READ( 9) IH2,IM2,LT, DEL2,DOP, RLP2,RBP2,RCP, FCL2,RDA2,ZAZ,ZEL
     1     ,RQ, RDP, RRAP
      GO TO ( 115,11 ) EOFCKF(9)
11    IF( IH1 - IH2 ) 13,13,12
12    IH1=IH1-24
C     HAVE PASSED THRU 2400.
13    TAPE1 = IH1*3600.0 + IM1*60.0
      TAPE2 = IH2*3600.0 + IM2*60.0
      GO TO 15
C LINEAR INTERPOLATION FOR QUANTITES OF INTEREST
40    X = -DT/( TAPE2 - TAPE1 )
      Y = 1.0 - X
      RLP = X*RLP1 + Y*RLP2
      RBP = X*RBP1 + Y*RBP2
      FCL = X*FCL1 + Y*FCL2
      RDA = X*RDA1 + Y*RDA2
      DEL = DEL1
      RETURN
115   WRITE(61,116 )
116   FORMAT( 40H          EOF DETECTED ON LIBRATION TAPE)
      IEND = 2
      RETURN
16    WRITE(59,18) TIME,TAPE1,TAPE2
      WRITE(61,18) TIME,TAPE1,TAPE2
18    FORMAT( 1H0, 5X, 35HTIME CALLED ON LIB TAPE IS IN ERROR   /
     *  11H DATATIME=  F10.3,  12H  LIBTIMES=  2F10.3)
      IEND = 3
      RETURN
      END
```

```
      PROGRAM NORMAL
C
C NORMALIZE INCOHERENT SUM OF SUBROUTINE READIN( RANGE DOP DATA) FOR
C ANTENNA BEAM SHAPE( GAUSSIAN),SCATTERING AREA, AND MEAN SCATTERING LAW.
      COMMON XSB, YSB, ZSB, FCLS, SEMI ,LRB,   IPOL
     1  ,IRB,IFB, DFREQ, DDELAY, TIME, NSUM, NTOTAL, TSUM,FRES,ISUB,
     1 ITITLE(18), MAXRB, MAXFB,  ICENFB ,
     2  MODE, XX(3), YY(3), NX, NY, DELX, DELY, QD, D0,NRB, NFB,
     3   XDB, YDB, ZDB,  IEND, FXS, FYS, FZS, DXS, DYS,DZS
     4  ,IH1,IM1,LT,DEL1,DOP,RLP1,RBP1,RCP,FCL1,RDA1,ZAZ,ZEL,RQ,RDP,RRAP
     5  ,TAPE1,TAPE2,SYSNOISM,SYSNOSM0,SYSTEMP,TPWR,ITPUL
     6  ,IFBSHIFT,IH2,IM2,DEL2,RLP2,RBP2,FCL2,RDA2
      COMMON IRBSHIFT,ITEST,IADW,IADR,ISCALE
      COMMON BRAD
      COMMON X OFF, Y OFF, Z OFF, Z OFF SET , BEAM FB, BEAM DB
      COMMON IRD(256),INDATA(256),OUTDATA(256)
      INTEGER SYSNOISE,SYSNOIS0,OUTDATA
      REAL NORMTIME,NORMTIM1,NORMTIM2,NORMTIM3
      NORMTIME=CLOCK(0)
C
C  SU BTRACT NOISE FROM RANGE DOP DATA
C
C JFIX PROVIDES A CONVERSION FROM A FLOATING POINT NUMBER TO A FIXED POINT
C NUMBER WITH ROUND OFF.
      SYSNOISE=JFIX(SYSNOISM/FLOAT(ISCALE))*NSUM
      SYSNOIS0=JFIX(SYSNOSM0/FLOAT(ISCALE))*NSUM
      IREAD = IADR
      IWRITE = IADW
      CALL YYWAIT(0)
      CALL YYDISK(0,1,IREAD,INDATA,256)
      IFB0=MOD(1+IFBSHIFT,NFB)+1
      AF1 = 1.0/.35
      AF2 = 1.0/(0.295*0.295)
      AF3 = 1.0 - AF2
      DELTAX = DFREQ/FCLS
      DELZ = DDELAY/D0
      YDBS = YDB*YDB
      YDB2 = 0.5/YDB
      Z0 = ZDB + IRB * DELZ + Z OFF SET
      AJAX=1.0 - BEAM FB * BEAM FB - BEAM DB * BEAM DB
      IF(AJAX)271,271,270
270   BEAM YB = SQRT( AJAX )
      GO TO 272
271   BEAM YB = 0.0
272   RAN NORM4=(2500.0/DEL1)**4
      AMP1 = (2.0*FCLS)/( .3*1738.0*ITPUL*FRES)
      AMP2 = SYSTEMP/SYSNOISM
      AMP3 = 100.0/TPWR
      AMP = ( AMP1*AMP2*AMP3)/(            RANNORM4 )
      BL = 1.38629436
C
C
      SEMI = ( SEMI*BL)/( BRAD*BRAD )
      CHECK = BL/SEMI
      BL = 0.9*BL
      NORMTIM1=CLOCK(0)-NORMTIME
      DO 300 J = 1,LRB
      Z = Z0 - J*DELZ
      CALL YYWAIT(0)
      CALL MOVE(INDATA,IRD)
      IREAD = IREAD+256
      CALL YYDISK(0,1,IREAD,INDATA,256)
```

```
      IF(Z.LE. 0. .OR. Z .GT. 1.) 215,190
  190 ZS = Z*Z
      ZP = 1.0 - ZS - YDBS
      DX = ( IFB - 1 )*DELTAX
      GO TO ( 200,210 ) IPOL
C 200 IS POLARIZED COMPONENT AND 210 IS DEPOLARIZED COMPONENT
200   IF ( Z - .504 ) 206,  203, 203
C
203   ST = SQRT( 1.0 - Z*Z )
      F = Z + AF1*ST
      SL = ( AMP*F*F*F ) /Z
      GO TO 220
206   FS = AF2 + AF3*Z*Z
      F = SQRT(FS)
      SL = ( AMP*FS*F )/Z
      GO TO 220
210   SL=AMP/Z
  215 CONTINUE
220   DO 290 K = 1,MAXFB
      IF(K-IFB0)222,224,222
222   IRD(K) = IRD(K) - SYSNOISE
      GO TO 226
224   IRD(K) = IRD(K) - SYSNOIS0
226   IF(IRD(K))228,229,229
228   IRD(K) =0
229   IF(Z. LE. 0. .OR. Z. GT. 1.) 250,230
230   X = XDB - DX
      DY = ( ZP - X*X )*YDB2
      DY = DY*( 1.0 - DY*YDB2 )
      Y = YDB + DY
      AY = Y
      IF ( AY ) 240,240,245
240   AY = -AY
245   YC = -Y
      DX2 = DX*DX
      R = SEMI*( DX2 + DY*DY )
      DYC = YC - YDB
      RC = DX2 + DYC*DYC
      IF ( RC - CHECK ) 250,250,249
249   IF ( R - BL ) 260,250,250
C IRD LESS THAN ONE INDICATES RANGE-DOP POINT OUTSIDE OF ANTENNA BEAM OR
C REFLECTING AREA AND ITS CONJUGATE ARE WITHIN ANTENNA BEAM
250   IRD(K)=-1
      GO TO 290
260   DRY=BEAM YB - ABS(Y)
      DRX = BEAM FB - X
      ER=EXP(SEMI*(DRY*DRY+DRX*DRX))
C     ER IS A GAUSSIAN APPROXIMATION TO THE BEAM SHAPE
      IRD(K)=IRD(K)*ER*SL*AY
290   DX = DX - DELTAX
      CALL YYWAIT(1)
      CALL MOVE(IRD,OUTDATA)
      CALL YYDISK(1,2,IWRITE,OUTDATA,256)
      IWRITE = IWRITE + 256
300   CONTINUE
      NORMTIM2=CLOCK(0)-NORMTIME-NORMTIM1
      NORMTIM3=NORMTIM1+NORMTIM2
      WRITE(61,1)NORMTIM1,NORMTIM2,NORMTIM3
1     FORMAT( 16H     NORMAL TIME,3F10.3 )
      GO TO ( 320,310 ) IEND
310   REWIND 8
320   RETURN
      END
```

```
      PROGRAM READOUT
C FINDS NORMALIZED POWER VERSUS SELEN POSITION
      COMMON XSB, YSB, ZSB, FCLS, SEMI ,LRB,   IPOL
     1  ,IRB,IFB, DFREQ, DDELAY, TIME, NSUM, NTOTAL, TSUM,FRES,ISUB,
     1 ITITLE(18), MAXRB, MAXFB,  ICENFB ,
     2  MODE, XX(3), YY(3), NX, NY, DELX, DELY, QD, DO,NRB, NFB,
     3   XDB, YDB, ZDB,  IEND, FXS, FYS, FZS, DXS, DYS,DZS
     4  ,IH1,IM1,LT,DEL1,DOP,RLP1,RBP1,RCP,FCL1,RDA1,ZAZ,ZEL,RQ,RDP,RRAP
     5  ,TAPE1,TAPE2,SYSNOISM,SYSNOSM0,SYSTEMP,TPWR,ITPUL
     6  ,IFBSHIFT,IH2,IM2,DEL2,RLP2,RBP2,FCL2,RDA2
      COMMON IRBSHIFT,ITEST,IADR,IADW
      COMMON ISCALE,BRAD
      COMMON X OFF, Y OFF, Z OFF, Z OFF SET , BEAM FB, BEAM DB
      COMMON IRD(256,65),INPP(201,19),INP(256,19)
      EQUIVALENCE (INP,AA)
      DIMENSION AA(3,201)
      READTIME=CLOCK(0)
      INPMIN = 1000000
      INPMAX = -1000000
      RESCALE=FLOAT(ISCALE)/FLOAT(NTOTAL)
      ISET = 1
      CALL YYWAIT (1)
      CALL YYDISK(1,1,IADR,IRD,16640)
      NUM = 3
      XJ0 = FLOAT(IFB) + 0.5
      LMAX = 66
      XI0 = FLOAT(IRB) + 0.5
      NWDS = 6*NY
      IAD10 = 524288
      IADD = KRB = 0
      I10 = 19
      LMIN = 0
      IADQ = 16640
30    GO TO (35,250),ISET
35    CONTINUE
      CALL YYWAIT(1)
      CALL YYWAIT(0)
      CALL YYDISK(1,1,IAD10,AA,NWDS)
      IAD10 = IAD10 + 1536
      KRB = KRB + 19
      IF(KRB.GT.NX)40,50
40    I10 = NX - (KRB - 19)
      ISET = 2
50    CONTINUE
      DO 70 I = 1,I10
      CALL YYWAIT(1)
      DO 60 JJ = 1,NY
      XS = AA(1,JJ)
      YS = AA(2,JJ)
      ZS = AA(3,JJ)
      IA = JFIX(XI0 + DXS*XS + DYS*YS + DZS*ZS)
      JA = JFIX(XJ0 + FXS*XS + FYS*YS + FZS*ZS)
```

```
C PACK IA AND JA AS TWO TWELVE BIT WORDS INTO A 24 BIT WORD.
      INPP(JJ,I) = AND(IA,7777B) + AND(JA,7777B)*10000B
60    CONTINUE
      IF(I.EQ.19)70,65
65    CONTINUE
      CALL YYDISK(1,1,IAD10,AA,NWDS)
      IAD10 = IAD10 + 1536
70    CONTINUE
       READTIM1=CLOCK(0)-READTIME
      CALL YYWAIT(0)
      CALL YYDISK(0,1,IADD,INP,4864)
      DO 100 I=1,NUM
      CALL YYWAIT(1)
      CALL YYWAIT(0)
      DO 80 J=1,I10
C RETRIEVE IA AND JA. USE THEIR VALUES AS INDICES OF THE IRD ARRAY IN ORDER
C TO SELECT THE CORRECT VALUE FROM IRD FOR THE SUMMATION INTO INP.
      CALL SUM(INP(1,J),INPP(1,J),IRD,LMAX,LMIN,NX)
80    CONTINUE
      IF(I.EQ.NUM)100,90
90    IAD = IADR + IADQ
      CALL YYDISK(1,1,IAD,IRD,16640)
      LMIN = MOD(LMIN+65,195)
      IADQ = MOD(IADQ+16640,49920)
100   CONTINUE
      GO TO (130,110),IEND
110   DO 120  I=1,I10
      DO 120  J=1,NX
      INP(J,I)=JFIX(FLOAT(INP(J,I))*RESCALE)
      IF(INP(J,I))112,116,114
112   INP(J,I) = -1
      GO TO 120
114   INPMAX=MAX0(INPMAX,INP(J,I))
116   INPMIN=MIN0(INPMIN,INP(J,I))
120   CONTINUE
      LRB   = INPMIN
      IPOL  = INPMAX
130   CALL YYDISK(0,2,IADD,INP,4864)
      IADD=IADD+4864
      GO TO 30
250   READTIM2=CLOCK(0)-READTIME-READTIM1
      READTIM3=READTIM1+READTIM2
      WRITE(61,251)READTIM1,READTIM2,READTIM3
251   FORMAT(17H     READOUT TIME, 4F10.3 )
      RETURN
      END
```

```
      PROGRAM TAPEMAKE
C RETRIEVES MAPPED DATA FROM MASS STORAGE AND STORES IT ON THE OUTPUT TAPE
C (LU 8).  BY THE TIME THIS SUBROUTINE HAS BEEN REACHED THE DATA TAPE ON LU 8
C HAS BEEN REPLACED WITH A SCRATCH TAPE.
C THIS SUBROUTINE ALSO PROVIDES AN OPTIONAL PRINTOUT OF DATA.
      COMMON LQ(10),INPMIN,INPMAX,LZ(15),ITTLE(18),LW(3),MODE,XX(3),
     1 YY(3),NX,NY,DELX,DELY
      COMMON INP(201),INDATA(201)
      COMMON JNP(64,201)
      EQUIVALENCE (JNP,KNP)
      DIMENSION KNP(12864)
      ISKIP = ICOUNT =0
      I64=64
      REWIND 20
      IADD = 0
      GO TO (4,5),SSWTCHF(5)
4     CONTINUE
      WRITE(61,2)(ITTLE(J),J=1,18),INPMIN,INPMAX
    2 FORMAT(18A4,2F10.5)
5     CONTINUE
      PAUSE 20
      WRITE(8 )(ITTLE(J),J=1,40),INPMIN,INPMAX
      IF(NX.GT.101)200,100
100   CONTINUE
      CALL YYDISK(0,1,IADD,INDATA,NY)
      DO 50 J=1,NX
      CALL YYWAIT(0)
      CALL MOVE(INDATA,INP)
      IADD=IADD+256
      CALL YYDISK(0,1,IADD,INDATA,NY)
      GO TO (45,50),SSWTCHF(5)
45    CONTINUE
      WRITE(61,1)(J,(INP(L),L=1,NY))
    1 FORMAT(1H0,I10,/(10X,10I10) )
50    WRITE( 8)(INP(L),L=1,NY)
      RETURN
200   DO 320 I =1,4
      IADD = ISKIP
      DO 210 N=1,NX
      CALL YYWAIT(0)
      CALL YYDISK(0,1,IADD,JNP(1,N),64)
      IADD = IADD +256
210   CONTINUE
      IF(I.EQ.4)220,230
220   I64=9
230   CONTINUE
      GO TO (280,300), SSWTCHF(5)
280   DO 290 J=1,I64
      ICOUNT = ICOUNT + 1
      WRITE(61,1) (ICOUNT,(JNP(J,L),L=1,NY)     )
290   CONTINUE
300   DO 310 J=1,I64
      WRITE(8) (JNP(J,L),L=1,NY)
310   CONTINUE
      ISKIP=ISKIP+64
320   CONTINUE
      RETURN
      END
```

```
          IDENT     COHERESM
SAVE      MACRO     (NARG,RET)
          UJP       **
          STI       RET,1
          STI       RET+1,2
          STI       RET+2,3
          LDA       *-4
          INA       NARG
          SWA       RET+3
          LDI       *-7,1
          ENDM
RETURN    MACRO
          ENI       **,1
          ENI       **,2
          ENI       **,3
          UJP       **
          ENDM
          EJECT
          ENTRY     COHERESM
*
*      DO 1041 J=J1,J2
*
*C     SHIFT FREQUENCY BOX IFB (AS READ IN) TO FREQUENCY BOX NO. ICENFB
*
*      K = MOD(J+IFBSHIFT,NFB)+1
*      IF ( K .GT. MAXFB ) 1041,104
*
*
* 104 IRD(K,L) = IRD(K,L)+INDATA(J)
*1041 CONTINUE
*
COHERESM SAVE       (7,RET)
          LDA,I     0,1
          SWA       J1.1
          SWA       J1.2
          LDA,I     1,1
          SWA       J2.1
          LDA,I     2,1
          SWA       IFBSHF.1
          LDA,I     3,1
          SWA       NFB.1
          STA       NFB
          LDA,I     4,1
          SWA       MAXFB.1
          LDA       5,1
          SWA       IRD.1
          LDA       6,1
          SWA       INDATA.1
K         EQU       1
J         EQU       3
J1.1      ENI       **,J
          INI       -1,J
J1.2      ENA       **
IFBSHF.1  INA       **
          INA,S     -1
          SHAQ      -24
          DVA       NFB
          SHAQ      24
          TAI       K
S104      INI       1,K
NFB.1     ISG       **,K
          UJP       *+2
          ENI       0,K
MAXFB.1   ISG       **,K
          UJP       *+2
          UJP       S1041
INDATA.1  LDA       **,J
IRD.1     RAD       **,K
S1041     INI       1,J
J2.1      ISG       **,J
          UJP       S104
RET       RETURN
NFB       BSS       1
          END
```

```
          IDENT     SUM
SAVE      MACRO     (NARG,RET)
          UJP       **
          STI       RET,1
          STI       RET+1,2
          STI       RET+2,3
          LDA       *-4
          INA       NARG
          SWA       RET+3
          LDI       *-7,1
          ENDM
RETURN    MACRO
          ENI       **,1
          ENI       **,2
          ENI       **,3
          UJP       **
          ENDM
          EJECT
*
*     CALL SUM(INP(1,J),INPP(1,J),IRD,LMAX,LMIN,NX)
*
          ENTRY     SUM
SUM       SAVE      (6,RET)
          LDA       0,1
          SWA       INP.1
          SWA       INP.2
          SWA       INP.3
          LDA       1,1
          SWA       INPP.1
          LDA       2,1
          SWA       IRD.1
          LDA,I     3,1
          SWA       LMAX.1              LMAX.1 IS THE MAX SIZE OF
*                                        IRD(1,LMAX)
          LDA,I     4,1
          SWA       LMIN.1
          LDA,I     5,1
          SWA       NX.1
          LDA       MAXRB
          INA       1
          SWA       MAXR.1
          LDA       MAXFB
          INA       1
          SWA       MAXF.1
*
L         EQU       1
K         EQU       2
*
          ENI       0,L
INP.1     LDA       **,L
INPP.1    LDQ       **,L                (PACKED JA IA)
          ENA,S     0
          SHAQ      12
          ASG       1
          UJP       NEG
MAXF.1    ASG       **
          UJP       *+2
          UJP       NEG
          SWA       JA.1
          ENA,S     0
```

```
          SHAQ      12
          ASG       1
          UJP       NEG
MAXR.1    ASG       **
          UJP       *+2
          UJP       NEG
          SBA       LMIN.1
          ASG,S     1
          UJP       S100
          LDQ       LMAX.1
          AQJ,GE    S100
          INA,S     -1
          MUA       =D256
JA.1      INA       **
          TAI       K
          INI       -1,K
IRD.1     LDA       **,K
INP.2     RAD       **,L
          UJP       *+3
NEG       LDA       N.30
INP.3     STA       **,L
S100      INI       1,L
NX.1      ISG       **,L
          UJP       INP.1
RET       RETURN
LMIN.1    00
LMAX.1    00
N.30      DEC       -30000
          COMMON
          ORGR      0
          BSS       45
MAXRB     BSS       1
MAXFB     BSS       1
          END
```

```
          IDENT     MOVE
          ENTRY     MOVE
MOVE      UJP       **
          STI       REST,1
          LDI       MOVE,1
          LDA       0,1
          LDQ       1,1
          INI       2,1
          STI       MOVE,1
          ENI       0,1
          ANA       77777B
          ANQ       77777B
          SHAQ      2
          SCHA      MOV+1
          SHAQ      24
          SCHA      MOV
MOV       MOVE      128,**,**
          UJP       *-2
LOOP      ENA       200B
          RAD       MOV
          RAD       MOV+1
          INI       3,1
          ISG       24,1
          UJP       MOV
REST      ENI       **,1
          UJP,I     MOVE
          END
```

ACKNOWLEDGMENTS

The work reported in Vols. 1 and 2 of the Final Report, Radar Studies of the Moon, has been performed under the joint direction of J.V. Evans, T. Hagfors, and G.H. Pettengill. Largely responsible for the design of the computer analysis and ephemeris programs were T.W. Thompson and J.E. Moriello, while M.L. Stone, R.P. Ingalls, L.G. Kraft, J.I. Levine, and L.P. Rainville, among others, played a central role in the realization of the necessary instrumentation. The all-night operating vigils of L.G. Kraft during the data-taking phases deserve special mention. Thanks are due N. Brenner for his efficient coding of the Cooley-Tukey algorithm. We wish to note important contributions by F.S. Weinstein, and by R. Wells (of Adams Associates) in many of the computer programs. C.R. Smith and his colleagues, I.I. Shapiro and M. Ash, have been involved in the calculations pertaining to the basic lunar ephemeris and the observed doppler residuals.

The contribution of all members of Group 31, Surveillance Techniques, which operates the Millstone and Haystack radar systems under the leadership of P.B. Sebring, is gratefully acknowledged, as is also the support of the U.S. Air Force in the operation of these facilities.

REFERENCES

Arthur, D.W.G., "Selenography," Chap. 2 of The Moon, Meteorites and Comets, B.M. Middlehurst and J.P. Kuiper, editors (University of Chicago Press, Chicago, 1963), pp. 57 – 77.

Bracewell, R.W., "Radio Astronomy Techniques," in Handbuch der Physik, Vol. 54 (Springer-Verlag, Berlin, 1962), pp. 42 – 129.

Eckert, W.J., Walker, M.J., and Eckert, D., "The Transformation of the Lunar Coordinates and Orbital Parameters," Astron. J. 71, 314 – 332 (1966).

Hagfors, T., Nanni, B., and Stone, K., "Aperture Synthesis in Radar Astronomy and Some Applications to Lunar and Planetary Studies," Radio Science 3 (New Series), 491 – 509 (1968).

Leadabrand, R.L., Dyce, R.B., Fredriksen, A., Presnell, R.I., and Schlobohm, J.C., "Radio Frequency Scattering from the Surface of the Moon," Proc. IRE 48, 932 – 933 (1960).

Mulholland, J.D., and Block, N., "JPL Lunar Ephemeris No. 4," Technical Memorandum 33-346, Jet Propulsion Laboratory, California Institute of Technology (August 1967).

Pettengill, G.H., "Measurements of Lunar Reflectivity Using the Millstone Radar," Proc. IRE 48, 933 – 934 (1960).

Pettengill, G.H., and Henry, J.C., "Enhancement of Radar Reflectivity Associated with the Lunar Crater Tycho," J. Geophys. Res. 67, 4881 – 4885 (1962).

Pettengill, G.H., and Thompson, T.W., "A Radar Study of the Lunar Crater Tycho at 3.8 and 70 cm Wavelength," Icarus 8 (1968), in press.

Shapiro, A., Uliana, E.A., Yaplee, B.S., and Knowles, S.H., "Lunar Radius from Radar Measurements," paper presented to COSPAR, London, 17 – 19 July 1967.

Smith, C.R., Pettengill, G.H., Shapiro, I.I., and Weinstein, F.S., "Discrepancies between Radar Data and the Lunar Ephemeris," Science 160, 876 – 878 (1968).

Thomson, J.H., and Ponsonby, J.E.B., "Two-dimensional Aperture Synthesis in Lunar Radar Astronomy," Proc. Roy. Soc. A303, 477 – 491 (1968).

United States Naval Observatory, The American Ephemeris and Nautical Almanac for the Year 1967 (U.S. Government Printing Office, Washington, D.C., 1965).